

LEVEL II

12

5



AD A099161

SDTIC  
ELECTRONIC  
MAY 20 1981  
E

Approved for public release;  
distribution unlimited.

FILE COPY

**LEVEL II**

12

Final Interim Report [REDACTED]  
Contract [REDACTED] F49620-80 C-0007  
IITRI Project J6511

**INITIATION MECHANISMS OF SOLID  
ROCKET PROPELLANT DETONATION**

Submitted by

Engineering Research Division  
IIT Research Institute  
10 West 35th Street  
Chicago, Illinois 60616

**DTIC  
SELECTED  
MAY 20 1981**

Prepared by

A. N. Takata  
A. Wiedermann

Prepared for

Air Force Office of Scientific Research  
Bolling Air Force Base  
Washington, DC 20332

March 1981

**AIR FORCE OFFICE OF SCIENTIFIC RESEARCH (AFSO)  
NOTICE OF TRANSMITTAL TO DDC**  
This technical report has been reviewed and is  
approved for public release under AFM 190-12 (7)  
Distribution is unlimited.  
A. D. BLOSE  
Technical Information Officer

UNCLASSIFIED

SECURITY CLASSIFICATION OF THIS PAGE (When Data Entered)

1. REPORT DOCUMENTATION PAGE		READ INSTRUCTIONS BEFORE COMPLETING FORM	
2. REPORT NUMBER	4. GOVT ACCESSION NO.	3. RECIPIENT'S CATALOG NUMBER	
AFOSR-TR-81-0466	AD-A099161		
4. TITLE (and Subtitle)		5. TYPE OF REPORT & PERIOD COVERED	
INITIATION MECHANISMS OF SOLID ROCKET PROPELLANT DETONATION		Final Report, Oct 1975-Oct 1980	
7. AUTHOR(s)		6. PERFORMING ORG. REPORT NUMBER	
A. N. Takata / Wiedemann		J6352; J6511	
8. PERFORMING ORGANIZATION NAME AND ADDRESS		9. CONTRACT OR GRANT NUMBER(s)	
IIT Research Institute 10 West 35th Street Chicago IL 60616		F49620-80-C-0007	
10. PROGRAM ELEMENT, PROJECT, TASK AREA & WORK UNIT NUMBERS		11. REPORT DATE	
2308/A1 61102F		March 1981	
12. CONTROLLING OFFICE NAME AND ADDRESS		13. NUMBER OF PAGES	
Air Force Office of Scientific Research/NA Bolling AFB, DC 20332		107	
14. MONITORING AGENCY NAME AND ADDRESS (if different from Controlling Office)		15. SECURITY CLASS. (of this report)	
IITR-81-0466-FR IITR-81-0466-FR		Unclassified	
16. DISTRIBUTION STATEMENT (of this Report)		17. SECURITY CLASS. (of this report)	
Approved for public release; distribution unlimited.		Unclassified	
17. DISTRIBUTION STATEMENT (of the abstract entered in Block 20, if different from Report)		18. DECLASSIFICATION/DOWNGRADING SCHEDULE	
Approved for public release; distribution unlimited.			
18. SUPPLEMENTARY NOTES			
19. KEY WORDS (Continue on reverse side if necessary and identify by block number)			
DEFLAGRATION TO DETONATION (DDT) ROCKET MOTOR DETONATION NUMERICAL METHODS PROPELLANTS			
20. ABSTRACT (Continue on reverse side if necessary and identify by block number)			
The purpose of this study is to identify mechanisms responsible for several accidental detonations of high-energy solid rocket propellant motors. Simple models were used to predict transient gas pressures within burning propellant cracks following arrival of a stress wave. Stress waves are the consequence of cracks propagating into a cavity containing gas at much higher pressure than that initially within the crack. Two factors were found important in creating gas pressures of similar magnitude and duration as needed to			

DD FORM 1 JAN 73 1473

EDITION OF 1 NOV 66 IS OBSOLETE

175350

UNCLASSIFIED

SECURITY CLASSIFICATION OF THIS PAGE (When Data Entered)

UNCLASSIFIED

SECURITY CLASSIFICATION OF THIS PAGE(When Data Entered)

initiate propellants by impact. Namely, the generation of melt or foam that sustains accelerated burning; and the production of stress waves that accelerate the burning by partially collapsing cracks and subsequently lessen crack expansion while the pressures continue to rise before decaying. Experiments designed to achieve DDT were unsuccessful due to inadequate piston closure of the void space over burning propellant. It was suspected that inadequate closure was due to blow off of melt raising pressures sufficiently to stop the piston before adequate closure was achieved.



UNCLASSIFIED

SECURITY CLASSIFICATION OF THIS PAGE(When Data Entered)

FOREWORD

The objective of this project is the understanding of the mechanisms controlling the transition from deflagration to detonation in solid propellant rocket motors. This final report covers the period from October 1975 to October 1980. The study was sponsored by the Air Force Office of Scientific Research (AFOSR), Directorate of Aerospace Sciences, United States Air Force under Contract ~~XXXXXXXXXX~~ <sup>F49620-80-C-0007</sup>. The program was monitored by Captain R. Laurence, Dr. J. S. Masi, Captain R. F. Sperlein and Dr. R. Canveny of AFOSR.

IIT Research Institute personnel who contributed to this research are C. Foxx, H. S. Napadensky, A. N. Takata and A. H. Wiedermann.

Respectfully submitted,

IIT RESEARCH INSTITUTE

*A. N. Takata*

A. N. Takata  
Senior Research Engineer

*Kim R. Mignotti*

for A. Wiedermann

Approved

*H. S. Napadensky*  
H. S. Napadensky  
Manager

Fire and Safety Research

Accession For	
NTIS CRA&I	<input checked="" type="checkbox"/>
DTIC TAB	<input type="checkbox"/>
Unannounced	<input type="checkbox"/>
Justification	
By _____	
Distribution/	
Availability Codes	
Avail and/or	
Dist _____	
<b>A</b>	

IIT RESEARCH INSTITUTE

## CONTENTS

	<u>Page</u>
Foreword . . . . .	ii
1. INTRODUCTION . . . . .	1
2. ANALYTICAL PROCEDURES. . . . .	6
2.1 Propellant Heating and Burning. . . . .	6
2.1.1 Heat Fluxes. . . . .	7
2.1.2 Steady and Nonsteady Burn Rates. . . . .	11
2.1.3 From Heat, Mass and Temperature. . . . .	11
2.2 Gas Dynamics. . . . .	12
2.2.1 Two-Dimensional Model of Gases . . . . .	12
2.2.2 One-Dimensional Model of Gases . . . . .	13
2.3 Stress Wave Generation and Effects. . . . .	14
2.4 Computational Procedures. . . . .	15
2.5 Computational Procedures. . . . .	15
2.5.1 Burn Procedures. . . . .	15
2.5.2 Gas/Crack Procedures . . . . .	16
3. HMX FOAM MASSES. . . . .	17
3.1 Foam Masses During Steady Burning . . . . .	17
3.2 Experimental Verification of Foam Mass. . . . .	20
3.2.1 Heat Absorbed by Burning Propellant. . . . .	20
3.2.2 Heat in Solid Propellant During Burning. . . . .	22
3.2.3 Steady Foam Mass at 1 Atmosphere of Pressure . . . . .	23
4. MODEL PREDICTIONS. . . . .	26
4.1 Sensitivity Analyses. . . . .	26
4.2 Multiple Cracks . . . . .	38
4.3 Foam Masses Generated Within Cracks . . . . .	40
5. BURNING PROPELLANT EXPERIMENTS . . . . .	50
5.1 Experimental Procedure. . . . .	50
5.2 Analysis. . . . .	52
5.3 Experimental Results. . . . .	53
6. SUMMARY/CONCLUSIONS. . . . .	61
6.1 Analyses. . . . .	61
6.2 Experiments . . . . .	63
6.2.1 Melt Layer . . . . .	63
6.2.2 DDT Experiments. . . . .	63
6.2.3 Recommendations. . . . .	64
Appendix A--Method for Predicting Transient Temperature in Solid-Phase of Propellants . . . . .	66
Appendix B--Determination of Constants $c_1$ and $c_2$ for Heat-Transfer Coefficient $h$ . . . . .	77
Appendix C--Ignition Criteria. . . . .	80
Appendix D--Dynamic Regression Rates of Propellants Having No Foam Layer. . . . .	83
Appendix E--Fluid Dynamics and Stress Waves. . . . .	85
Appendix F--Nomenclature and HMX Property Data . . . . .	102

IIT RESEARCH INSTITUTE

## LIST OF FIGURES

<u>Number</u>		<u>Page</u>
1	Composition B fragments found in closed bomb following sudden pressure relief. . . . .	2
2a	Crack configuration treated by PROS two-dimensional model . .	4
2b	Crack configuration treated by PROS one-dimensional model . .	4
3	Principal variables used to predict proellant burning . . . .	7
4	Predicted HMX foam mass as function of pressure during steady burning. . . . .	18
5	Experimental setup from measuring heat absribed by propellant during steady burning. . . . .	21
6	Enthalpy of HMX versus temperature. . . . .	24
7	Impact results from Reference 6 for HMX-nylon explosion . . .	27
8	Transient predictions for normal conditions cited by Table 2 . . . . .	30
9	Consequences of varying internal heat ( $Q_s$ ). . . . .	31
10	Consequences of varying propellant impedances ( $I_o$ ). . . . .	32
11	Consequence of varying intitial pressure ( $P_o$ ) within crack. .	33
12	Consequences of varying amplitude (AP) of incident stress wave . . . . .	35
13	Consequences of varying initial crack width ( $c_{wo}$ ) . . . . .	36
14	Consequences of varying initial foam mass ( $M_{fo}$ ) . . . . .	36
15	Pressure transients for three crack conditions. . . . .	39
16	Multiple cracks (case 1). . . . .	41
16	Multiple cracks (case 1) concluded. . . . .	42
17	Multiple cracks (case 2). . . . .	43
18	Multiple cracks (case 3). . . . .	44
19	Consequence of sudden exposure to "open crack" to high pressure (8 bars) cavity. . . . .	46
20	Consequence of sudden exposure of "open crack" to high pressure (16 bars) cavity . . . . .	47
21	Consequence of sudden exposure of "open crack" to high pressure (68 bars) cavity . . . . .	48
22	Mean HMX foam mass within "open cracks" versus time . . . . .	49
23	Schematic of experimental setup . . . . .	51
24	Mcdivied piston and chamber used in Test 17 . . . . .	57
25	Modified chamber used in Test 18. . . . .	59

LIST OF TABLES

<u>Number</u>		<u>Page</u>
1	Steady Heat Fluxes ( $q_f$ ), Burn Rates ( $r_f$ ), Form Masses ( $M_f$ ), And Foam Temperatures ( $T_f$ ) During HMX Burning Versus Pressure (P). . . . .	19
2	Parametric Values Selected For Sensitivity Studies . . . . .	28
3	Parametric Values For Three Selected Crack Conditions. . . . .	38
4	Summary Of Test Results. . . . .	60

## 1. INTRODUCTION

In recent years high-energy propellants have been developed containing cyclotetramethylenetrinitramine (HMX) to improve the performance of rocket motors. In developing such propellants, several accidental explosions have occurred during rocket motor firings. The purpose of this study is to identify the causes of the explosions so that such occurrences may be prevented in the future. The problem selected for study was that of pressure build-ups within burning propellant cracks. This selection was based upon IIT Research Institute's (IITRI) experiments with burning secondary high explosives in closed bombs.<sup>1,2</sup> In these experiments Composition B and PBX 9404 undergo multiple cracking prior to a violent explosion or high-order detonation. Two facts support the presence of multiple burning cracks. The first is random firing of ionization probes placed within 4 x 4 inch cylinders of the two secondary explosives. Random firing commenced when the pressure reached about 70 bars. The second is fragments of Composition B (See Figure 1) found in the bomb following sudden venting of the bomb. Explosive fragments varied in dimension from about 1/10 inch to 1 inch. All fragment surfaces were covered with a "frozen" melt layer indicating that they were burning prior to sudden pressure relief.

The subject matter reported herein is directed at the three project objectives. In order of execution, these are:

- (1) Use of analysis to identify mechanisms and propellant properties causing pronounced pressure transients within burning propellant cracks.
- (2) Compare predicted pressure transients with shock wave pressures and durations known to initiate propellants.
- (3) Conduct experiments with which to complement and validate analytical predictions.

DDT was studied analytically in two phases. In the first phase, cracks were considered to propagate into a cavity of high-pressure high temperature gas such as the combustion chamber of a rocket motor. This problem is

IIT RESEARCH INSTITUTE



*Figure 1. Composition B fragments found in closed bomb following sudden pressure relief.*

IIT RESEARCH INSTITUTE

illustrated by Figure 2a. It was chosen in that sudden exposure of cracks to high pressure gases creates stress waves that subsequently act to compress cracks after being reflected from the motor case. In this study two-dimensional models were developed with which to predict gas pressures, velocities and temperatures within the crack, and the propellant response to the predicted gas conditions. Mechanical responses of cracks to reflected stress, waves and transient pressures of gases within cracks were included. This model allows one to examine the consequences of various cavity gas pressures, cavity temperatures, motor cases, crack dimensions and propellant properties upon pressure build-ups within cracks. This model provides efficient predictions of dynamic pressure build-ups to a few thousand atmospheres or bars. Above such pressures, variations of crack widths and burning rates along the length of crack became too great to afford efficient computations. The models greatest value is in establishing crack/propellant conditions caused by sudden exposure of cracks to high-pressure high-temperature gases that may subsequently promote extremely rapid and pronounced pressure rises needed to cause detonation. Among these conditions are substantial melt formation over the burning propellant crack surfaces, minimal crack widths, and the presence of high-amplitude stress waves.

The second analytical phase focused upon those portions of the crack with conditions most likely to lead to rapid pronounced pressure transients. An illustration of this problem is provided by Figure 2b. Gas, propellant and crack conditions are considered uniform along the length of the crack element. The latter implies negligible gas escape from the crack element. Neglect of gas loss is predicated upon occurrence of extremely transient pressures within a few tenths of a millisecond or less. During such periods gas disturbances travel less than 10 cm. This model was computerized and used to determine values of the stress wave amplitudes, amounts of melt, and crack widths needed to generate pressures of the order to tens of K bars. The two-dimensional model serves to indicate the validity of the above values used in the one-dimensional model.

Predicted pressures transients varied widely with the propellant/crack/stress wave values used in the one-dimensional model. These studies identified conditions needed to generating pressures of the order to 10 K bars

IIT RESEARCH INSTITUTE

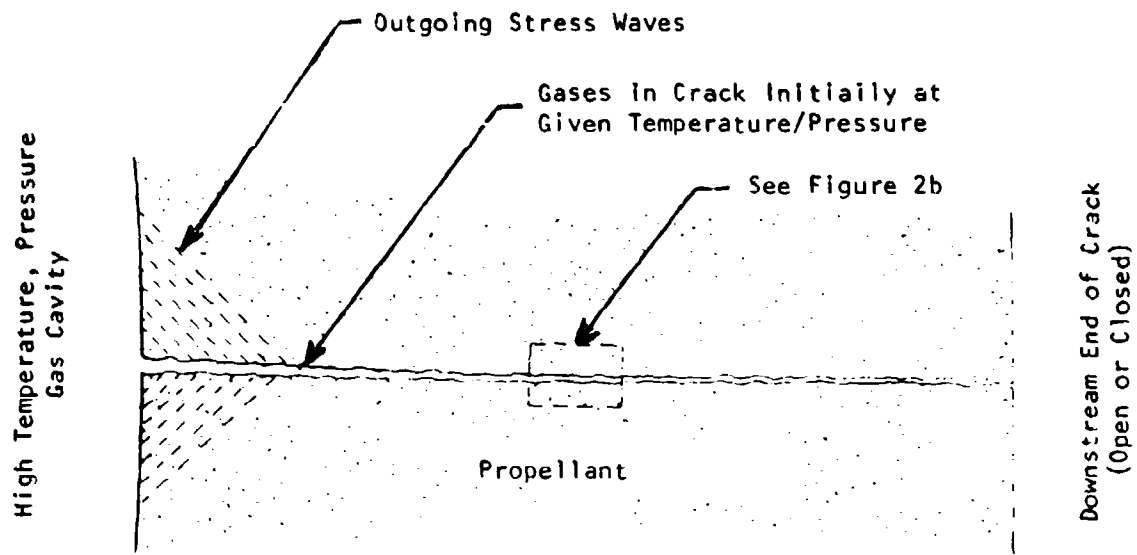


Figure 2a. Crack configuration treated by PROS two-dimensional model.

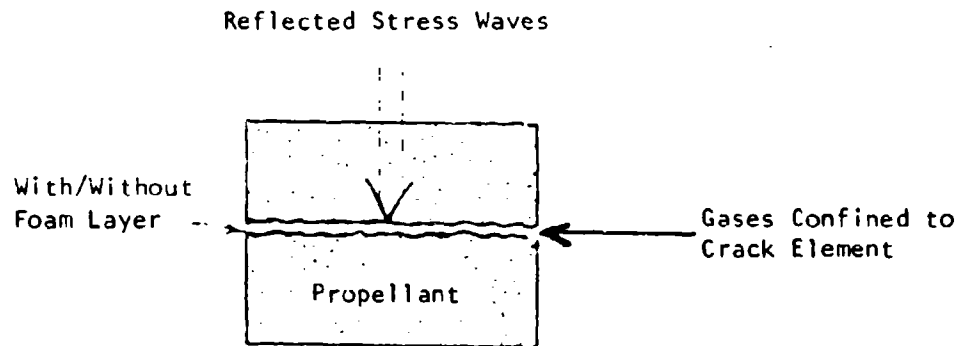


Figure 2b. Crack configuration treated by PROS one-dimensional model.

within a few tenths of a microsecond. Each of the above conditions involved applying high amplitude stress waves to relatively narrow crack elements containing substantial melt.

Validation of model DDT predictions was attempted experimentally. The experimental design simulates partial closure of a burning propellant crack caused by a stress wave. Unfortunately, DDT was not achieved due to inadequate of the void space over or between the burning propellant. Inadequate closure was attributed to more rapid acceleration of the burning than was expected. It is suspected that the rapid acceleration was caused by ejection of propellant melt or foams into the hot combustion gases by the rapid gas flow.

The remainder of this report contains analytical basis and predictions of the models, and conclusion drawn from the study insofar as DDT is concerned.

## 2. ANALYTICAL PROCEDURES

This section shall review means used to predict

- gas flows, gas pressures and gas temperatures produced within cracks suddenly exposed to high-pressure high-temperature cavities of gas
- stress wave amplitudes, deformation of cracks by the stress waves gas pressures
- heating and burning of propellant crack surfaces

Nomenclature is presented in Appendix F along with values used for the various parameters.

### 2.1 PROPELLANT HEATING AND BURNING

Propellant heating will, of course, vary depending upon whether or not the propellant is burning. Prior to ignition, the propellant will be heated connectively by the hot-gas stream and to a lesser extent by decomposition of heated propellant. The latter is termed internal heating. Following ignition, the internal heating increases and an additional heat source comes into being--namely conduction from the flames. For the above reasons each of the above periods will be discussed separately.

This section is primarily concerned with dynamic burning of propellants such as HMX with a melt or foam layer over the burning surface. The presence of a foam layer makes the analysis more complex than that of propellants without such a layer. After reviewing the equations used for propellants with a foam layer, we shall indicate revisions needed for propellants that burn without a foam or melt layer.

Figure 3 represents symbols used to represent various temperatures ( $T_f$ ,  $T_m$ ,  $T$ ), heat fluxes ( $q_f$ ,  $q_p$ ,  $q$ ) and regression rates ( $r_f$ ,  $r$ ) associated with the melt or foam layer and the two interfaces of the foam layer.

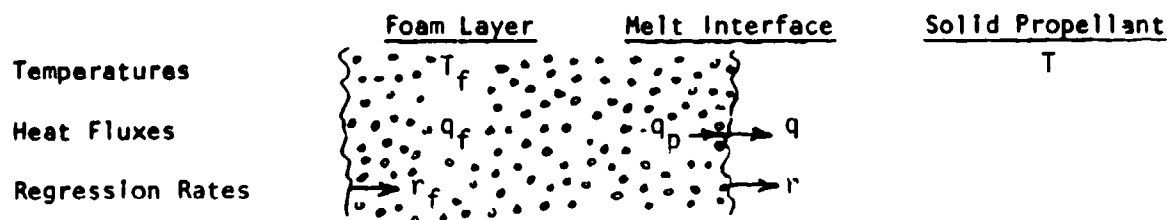


Figure 3. Principal variables used to predict propellant burning.

### 2.1.1 Heat Fluxes

#### Heat Flux Prior to Start of Melting

Prior to the start of melting, the convective heat-flux  $q$  equals that entering the solid propellant. It is described by the expression used by Kuo.<sup>3</sup> In terms of the gas temperature  $T_g$  and the temperature  $T_f$  of the propellant's surface, the convective heat flux  $q$  is

$$q = h_c (T_g - T_f) \quad (1)$$

while the heat transfer coefficient  $h_c$  is given by

$$h_c = \frac{0.547 C_p M_g^{0.1} (P_u)^{0.8}}{P_r^{0.6} R^{0.8} T_g^{0.67} (L C_w)^{0.1}} \quad (2)$$

#### Heat Fluxes During Melting Prior to Ignition

During melting, there are two sources by which the melt or foam layer is heated. The most obvious is by convection produced by the hot gas stream. This heat flux is described by Equation 1. Heat is also generated within the melt due to thermal decomposition. The latter heat flux is described by

$$Q \cdot M_f \cdot Z \cdot \exp(-E/T_f) \quad (3)$$

where  $M_f$  represents the mass of melt per unit area of surface. The expression  $Z \exp(-E/T_f)$  indicates the fractional rate of decomposition of the mass  $M_f$ . The constant of proportionality  $Q$  represents the quantity of heat transferred to the melt by the evolution of a unit mass of gas. Lacking experimental data we shall assume  $Q$  equals the internal heat  $Q_s$  transferred during burning.

During melting, the sum  $q_f$  of the fluxes entering the melt is

$$q_f = h_c (T_g - T_f) + Q_s \cdot M_f \cdot Z \exp(-E/T_f) \quad (4)$$

Part of the above flux acts to heat the foam, while the remainder is expended in melting the propellant and in heating the underlying solid propellant. The portion that acts to melt and heat the solid propellant is represented by  $q_p$ . In turn, the portion of  $q_p$  that is conducted into the solid propellant is represented by  $q$ . The difference between the heat fluxes  $q_p$  and  $q$  is expended in melting the propellant so

$$q_p - q = \rho r Q_m \quad (5)$$

where  $r$  represents the rate of melting of a propellant having a density  $\rho$  and a heat of fusion  $Q_m$ . Expressions for  $q_p$  and  $q$  are described below.

The heat flux  $q_p$  is described in terms of a heat-transfer coefficient  $h$  by

$$q_p = h(T_f - T_m) \quad (6)$$

Clearly  $h$  depends upon foam motions produced by escaping gases. For this reason  $h$  is considered to depend upon the rate of gasification in the following fashion:

$$h = c_1 \left[ \exp\left(-\frac{E}{T_f}\right) \right]^{c_2} \quad (7)$$

where  $c_1$  and  $c_2$  are constants which are evaluated in Appendix B for HMX.

Substitution of the above expression for  $h$  into Equation 6 yields the following expression for  $q_p$ .

$$q_p = c_1 \left[ \exp\left(-\frac{E}{T_f}\right) \right]^{c_2} (T_f - T_m) \quad (8)$$

At the solid propellant side of the melt interface, two conditions must be satisfied. The first expresses the rate of heat conduction  $q$  into the solid propellant as follows:

$$q = -k \frac{\partial T}{\partial x} \quad (9)$$

The second expresses the constant temperature at the melt interface as follows:

$$T = T_m \quad (10)$$

In view of the dependence of  $q$  upon temporal and spacial variations of the temperature within the solid propellant, the heat flux  $q$  is computed numerically. The procedure for computing the temperature  $T(x)$  of solid propellant is described in Appendix A for time-dependent fluxes  $q$ . The above procedure does not depend upon the presence of foam. However, foam will affect the fluxes  $q$ . When propellants melt  $q$  may be obtained from Equations 5 and 8; when propellants do not melt,  $q$  equals  $q_f$ . The above statements also apply after burning commences. In this regard, a discussion of propellant ignition is presented in Appendix C.

#### Heat Fluxes After Start of Burning

Once burning starts, the heat flux entering the propellant is

$$q_f = \frac{\rho_f \bar{r}_f^2}{r_f} [C_p (T_m - T_0) + C_m (\bar{T}_f - T_m) + Q_m - Q_s] + \rho r_f Q_s + \rho r_f (C_m - C_g) (T_f - T_f) + h_c (T_g - T_f) \exp\left(\frac{-B \rho r_f}{\rho_g \mu}\right) \quad (11)$$

Equation 11 includes a cross flow  $\rho_g \mu$ . When the cross flow is negligibly small, Equation 11 reduces to that developed by Krier,<sup>4</sup> namely

$$q_f = \frac{\rho \bar{r}_f^2}{r_f} [C_p (T_m - T_0) + C_m (\bar{T}_f - T_m) + Q_m - Q_s] + \rho r_f Q_s + \rho r_f (C_m - C_g) (T_f - \bar{T}_f) \quad (12)$$

Initial terms of Equations 11 and 12 account for heat feedback from the flame; the second term  $\rho r_f Q_s$  accounts for internal heating near the propellant surface; the third term corrects the previous flux when the specific heat  $C_m$  of the melt differs from that  $C_g$  of the gas; and the last term of Equation 11 accounts for heat fluxes produced by gas flowing laterally over the burning propellant surfaces.<sup>5</sup>

Bars over variables of Equations 11 and 12 indicate their values during steady burning at the pressure present. Heat fluxes depend upon the pressure  $p$ , burning rate  $r_f$  and cross flow  $\rho_g \mu$ . The importance of the three sources of fluxes changes as the burning becomes more dynamic. Pressure rises will accentuate heat feedback from the flame and erosive heating. More rapid burning diminished the latter fluxes and increases internal heating. As the burning becomes increasingly dynamic, internal heating becomes more and more dominant. In this regard over 90 percent of the heating can be due to internal heating during periods of highly dynamic burning needed to cause DDT.

In view of the importance of internal heating, it is wise to briefly examine assumptions implicate in the expression  $\rho r_f Q_s$  of Equations 11 and 12, and their consequences upon predicted burn rates. First of all, this expression indicates a linear dependence between the flux and the rate of gas evolution  $\rho r_f$ . Such a relationship presumes that the amount of heat transferred to the propellant is proportional to the amount of evolved gas regardless of its temperature or its residence time in the foam. In this regard, rapid pressure rises will act to compress gases within the foam, and thereby increases the period during which the gases undergo partial decomposition and transfer heat to the melt. For the above reason, it is believed that the

expression  $\rho r_f Q_s$  used for internal heating under estimates the internal heating during periods of rapid pressure buildup.

Another presumption of the expression  $\rho r_f Q_s$  is that the foam is not blown off into the flames by the rapid evolution of gas. This subject as well as the latter will be returned to in Section 6.

### 2.1.2 Steady and Nonsteady Burn Rates

Steady burning rates  $\bar{r}_f$  of Equations 11 and 12 are given as a function of pressure P by the conventional equation

$$\bar{r}_f = aP^n \quad (13)$$

where a and n are constants that are determined experimentally. Nonsteady burning rates  $r_f$  are a function of the foam mass  $M_f$  and temperature  $T_f$  as expressed by the following Arrhenius relationship

$$r_f = M_f Z \exp(-E/T_f) / \rho \quad (14)$$

where Z, E and  $\rho$  represent the frequency factor, activation energy and density of the propellant, respectively. The expression  $Z \exp(-E/T_f)$  represents the rate of gasification of the foam on a fractional basis at the temperature  $T_f$ . An expression for  $r_f$  is developed in Appendix D for propellants without a foam layer.

### 2.1.3 From Heat, Mass and Temperature

Here we shall represent the sensible heat within a unit surface area of foam by  $Q_f$  and reference it to the propellant melt temperature  $T_m$ . Rates of change of  $Q_f$  are given by

$$\dot{Q}_f = q_f - q_p - r_f C_m (T_f - T_m) \quad (15)$$

Here  $q_f - q_p$  represents the net heat flux to the foam while the last term represents the rate of heat carried away by the escaping gases.

Rates of change of the foam mass  $M_f$  are described by

$$\dot{M}_f = \rho(r-r_f) \quad (16)$$

When the sensible heat of the foam is referenced to its melt temperature  $T_m$ ,

$$Q_f = C_m M_f (T_f - T_m), \text{ and} \quad (17)$$

$$T_f = \frac{Q_f}{C_m M_f} + T_m \quad (18)$$

## 2.2 GAS DYNAMICS

As noted earlier, two computerized models were developed to study the behavior and effects of gases within propellant cracks. The first model is two-dimensional. It predicts the temperature, pressures, and velocities of the gases, crack deformations, heating and burning of the propellant surfaces, and the generation of stress waves. This model predicts special variations of the burning, crack widths and pressures along the length of cracks.

The second model focuses upon those portions of the crack with which appreciable pressures rises may occur. This model assumes uniform conditions along the length of the crack element and hence is one-dimensional.

The one-dimensional model serves to indicate crack/stress waves conditions needed for DDT; the two-dimensional model serves to identify conditions promoting DDT.

### 2.2.1 Two-Dimensional Model of Gases

Equations used to describe the flow and behavior of gases within cracks are presented in Appendix E. They are written with respect to an Eulerian frame of reference as functions of time and distance along the length of the crack. The equations conservation of mass, momentum, and energy as well as the effects of inertia, wall friction, crack deformations, and the addition of mass and energy from the burning propellant crack surfaces.

Rates of mass  $\dot{M}_g$  and energy  $\dot{Q}_g$  addition from the burning propellant are:

$$\dot{M}_g = 2f\rho r_f, \text{ and} \quad (19)$$

$$\dot{Q}_g = \dot{M}_g [Q_r + Q_m + C_p T_m + C_m (T_f - T_m)] - 2fq_f \quad (20)$$

The above equations apply to a unit length of crack. The factor  $f$  of the above equations represents the ratio of the area of the irregular crack surfaces to that of a planar surface, while the factor 2 accounts for the two crack surfaces.

For steady burning Equation 20 reduces as it should to:

$$\bar{Q}_g = \bar{M}_g u_r = 2f\rho r_f Q_r \quad (21)$$

Reactions of the evolved gases are assumed to be instantaneous.

### 2.2.2 One-Dimensional Model of Gases

The one-dimensional model assumes uniform gas/propellant conditions along a given length of burning crack. Rates of increase of the internal energy are described by

$$\frac{d\ell}{dt} = (\dot{Q}_g - P\dot{C}_w - \dot{M}_g) / (\rho_g C_w) \quad (22)$$

where  $\dot{M}_g$  and  $\dot{Q}_g$  are given by equations 19 and 20, respectively.

Combustion gases within the crack are assumed to obey the Nobel-Abel equation of state

$$P(1/\rho_g - b) = RT_g \quad (23)$$

where the internal energy  $\ell$  is

$$\ell = P(1/\rho_g - b) / (\gamma - 1) \quad (24)$$

where the ratio of the specific heats of the gas is assumed constant.

IIT RESEARCH INSTITUTE

Time-dependent pressure rises of the gas are described in terms of the interval energy by

$$P = (\gamma - 1) \rho / (1 / \rho_g - b) \quad (25)$$

### 2.3 STRESS WAVE GENERATION AND EFFECTS

Stress waves are generated by the sudden exposure of cracks to gas cavities with higher pressures than initially exist within the cracks. High-amplitude stress waves can also be generated by extremely rapid/pronounced pressure buildups due to burning. Analyses describing the generation, wave properties, reflection of stress waves from motor cases, and their effects upon cracks are described in Appendix E.

In the remainder of this section we shall present equations describing the consequences of stress waves of amplitude  $\Delta P$  upon the crack width  $C_w$ .

The velocities of the two crack walls will be distinguished by  $\dot{W}_1$  and  $\dot{W}_2$ , where  $\dot{W}_1$  equals the velocity of the crack wall upon which the stress wave is incident. Velocities  $\dot{W}_1$  and  $\dot{W}_2$  are considered positive when they act to increase the crack width  $C_w$  and negative otherwise. The velocity  $\dot{W}_1$  of the crack wall subjected to the stress wave is given by

$$\dot{W}_1 = r_f + \frac{P - P_0}{I(P)} \frac{2\Delta P}{P_0} \quad (26)$$

The velocity  $\dot{W}_2$  of the other crack wall is

$$\dot{W}_2 = r_f + \frac{P - P_0}{I(P)} \quad (27)$$

Notice that  $\dot{W}_1$  may be either positive or negative while  $\dot{W}_2$  is always positive. This, of course, is because the gas pressure and burning act to expand the crack, while the stress wave acts to contract the crack.

Rates of change of the crack width  $C_w$  are given by

$$\dot{C}_w = \dot{W}_1 + \dot{W}_2 \quad (28)$$

IIT RESEARCH INSTITUTE

Initially a stress wave contracts a crack; therefore the buildup pressure  $p$  within the crack causes the crack to expand. Gas pressure continues to buildup during crack expansion before decaying.

## 2.4 COMPUTATIONAL PROCEDURES

Three different predictive schemes are used to assess the effect of stress waves upon burning propellant cracks. These involve dynamic predictions of

- (1) gas behavior
- (2) crack deformations
- (3) burning propellant

Stable and accurate predictions require careful choice of time steps for each of the above predictions. In this regard, order of magnitude smaller time steps are usually needed for Items 1 and 2 than needed by Item 3. The latter is particularly true during the early stages of pressure buildup wherein the propellants response to the changing gas conditions is relatively slow. For the above reasons the modeling of Items 1 and 2 was treated separately from Item 3.

## 2.5 COMPUTATIONAL PROCEDURES

Predictions are made in a stepwise fashion with respect to time. Each model uses output supplied by the other. Burn predictions supply rates of energy and mass flows into the crack for the predictions; the gas/crack prediction supply gas pressures for the predictions.

### 2.5.1 Burn Procedures

Burn predictions require calculations of the following time-dependent terms:

- foam temperatures  $T_f$
- melt rates  $r$
- foam mass  $M_f$
- sensible heat  $Q_f$  in the foam following each time step

Time steps are calculated as follows

$$\Delta t_j = \text{minimum} \left[ \frac{4\alpha\beta^2}{r_j^2}, \frac{0.1\rho_f}{M_f} \right] \quad (29)$$

where  $r_j$  represents the mean melt velocity during  $\Delta t_j$ . The first expression is obtained using Equation A-8. It is arrived at by replacing  $x_j$  by  $r_j t_j$  and solving for  $\Delta t_j$ . The second expression is used to limit the fraction of the foam gasified during  $\Delta t_j$  to one-tenth.

Burn conditions are arrived at by means of successive approximations.

Each trial  $r_j$  is checked using the resultant values for the foam temperature  $T_f$  and the heat flux  $q_j$  or  $q$  conducted into the solid propellant. The trial  $r_j$  value is checked by first substituting  $T_f$  into Equation 8 to find  $q_D$ . Then the boundary condition given by Equation 5 is solved for  $r$ . If  $r$  does not agree with the trial value  $r_j$  within 0.3 percent,  $r_j$  is revised and the calculations repeated. Usually one to three trials are needed to achieve the above accuracy.

### 2.5.2 Gas/Crack Procedures

During each time step  $\Delta t_j$  the gas/crack predictions involve calculating the

- velocities  $\dot{W}_1, \dot{W}_2$  of the crack walls
- crack width  $C_w$
- gas density  $\rho_g$
- internal energy  $e$
- gas temperature  $T_g$
- gas velocity
- gas pressure  $P$

Velocities  $\dot{W}_1$  and  $\dot{W}_2$  of the crack walls are computed by substituting the burn velocity  $r_f$  and the pressure  $P$  into Equations 26 and 27. Changes of the crack width  $C_w$  are computed by substituting the velocities  $\dot{W}_1$  and  $\dot{W}_2$  into Equation 28 and multiplying by the time step.

### 3. HMX FOAM MASSES

#### 3.1 FOAM MASSES DURING STEADY BURNING

The heat-transfer constants  $c_1$  and  $c_2$ , presented in Appendix B may be used in conjunction with Equations 5 through 14 to predict the foam mass during steady burning as a function of the pressure  $P$ . Resultant foam masses are shown in Figure 4 in terms of  $g/cm^2$ . Table 1 provides tabular results for the predicted foam masses along with their associated steady heat fluxes  $\bar{q}_f$ , regression rates  $\bar{r}_f$ , and foam temperatures  $\bar{T}_f$ . Results presented in Figure 4 and Table 1 are predicted on negligible lateral gas flows across the burning propellant surfaces.

From Figure 4 it may be observed that the foam mass decreases with increased pressure. The latter is explained by the consequence of elevated pressures upon the rates of gasification of the foam and upon the rate of melting. When the pressure is suddenly increased to a fixed higher value, the heating of the foam will rise. Increased heating causes the rate of gasification to rise more rapidly than the rate of melting in that "excess foam" accentuates the rate of heating and temperature of the foam directly and subsequently the melting. Once sufficient foam is expended, the rate of gasification will slow while the entrance of relatively cool melt acts to stabilize the quantity of foam at a lower value.

From the above discussion, it should be clear that the shape as well as the magnitude of the curve of the steady foam mass versus pressure affects the quantity of "excess foam" following pressure rises. Rapid evolution of "excess foam" is believed to be the single most important factor responsible for the production of pronounced pressure transients needed to cause detonation. The latter, of course, remains to be proven.

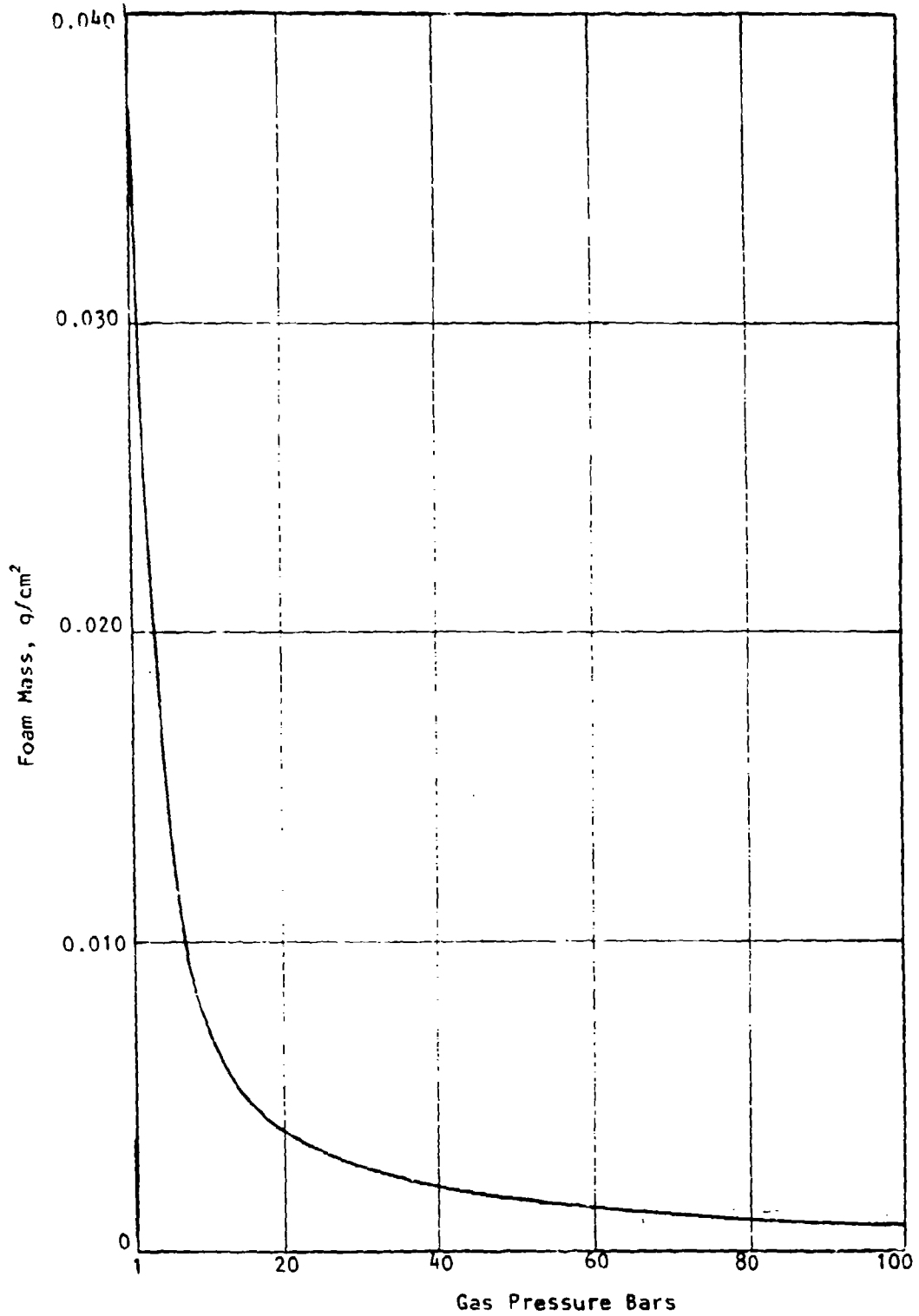


Figure 4. Predicted HMX foam mass as function of pressure during steady burning.

IIT RESEARCH INSTITUTE

TABLE 1. STEADY HEAT FLUXES ( $q_f$ ), BURN RATES ( $r_f$ ), FOAM MASSES ( $M_f$ ), AND FOAM TEMPERATURES ( $T_f$ ) DURING HMX BURNING VERSUS PRESSURE (P)

P, Bars	$q_f$ , cal/cm <sup>2</sup> -sec	$r_f$ , cm/sec	$M_f$ , g/cm <sup>2</sup>	$T_f$ , K
1	10.0	0.030	0.0367	601
2	19.0	0.055	0.0247	615
5	44.0	0.120	0.0132	635
10	34.0	0.217	0.0075	653
20	160.0	0.394	0.0039	673
30	233.0	0.559	0.0027	686
40	305.0	0.716	0.0021	695
50	376.0	0.867	0.0016	702
60	446.0	1.010	0.0014	709
70	515.0	1.160	0.0012	714
80	583.0	1.300	0.0010	719
90	652.0	1.440	0.0009	723
100	719.0	1.530	0.0008	727

At a pressure of 1 bar, the predicted HMX foam mass is roughly four times greater than those reported<sup>1</sup> for smaller types of secondary high explosives such as Composition B and PBX 9404. Foam masses for the above explosive materials are 0.010 and 0.008 g/cm<sup>2</sup>, respectively, during steady burning at 1 bar of pressure.

## 3.2 EXPERIMENTAL VERIFICATION OF FOAM MASS

A series of experiments was conducted to check the predicted foam mass of burning HMX at 1 atmosphere of pressure. These experiments used a HMX composite propellant described in Section 5. The foam mass was determined by measuring the quantity of sensible heat within the foam layer, and dividing the result by the product of the burn area and the enthalpy of foam during steady burning. The foam's heat was determined by first measuring the total sensible heat absorbed by burning propellant specimens, and then subtracting the experimentally determined heat within the solid portion of the propellant. A description of the experiments and results follows.

### 3.2.1 Heat Absorbed by Burning Propellant

Figure 5 illustrates the experimental setup. Burning was initiated by igniting a thin layer of ball powder sprinkled over the top propellant surface. An insulated steel tube was used to contain the resultant flames. Thermocouples (5 mil chromel-alumel) were imbedded at various depths in the upper half of the propellant. These thermocouples served to measure the rate of burning, and determine the temperature profile within the solid propellant. After steady burning was achieved, the remainder of the burning propellant disk was dropped into the water bath contained within the calorimeter. Burning ceased immediately upon entry of the disk into the water. Then the calorimeter was closed with a cork stopper housing a Berkman Thermometer. This thermometer measured the resultant temperature rise to within  $\pm 0.01^\circ\text{C}$ .

Next the total heat capacity  $H_c$  of the water bath, calorimeter and thermometer was measured by adding a known quantity of heat to the calorimeter, and observing the resultant temperature rise. In each test, the initial temperatures of all media were within  $0.5^\circ\text{C}$  of that of the environment.

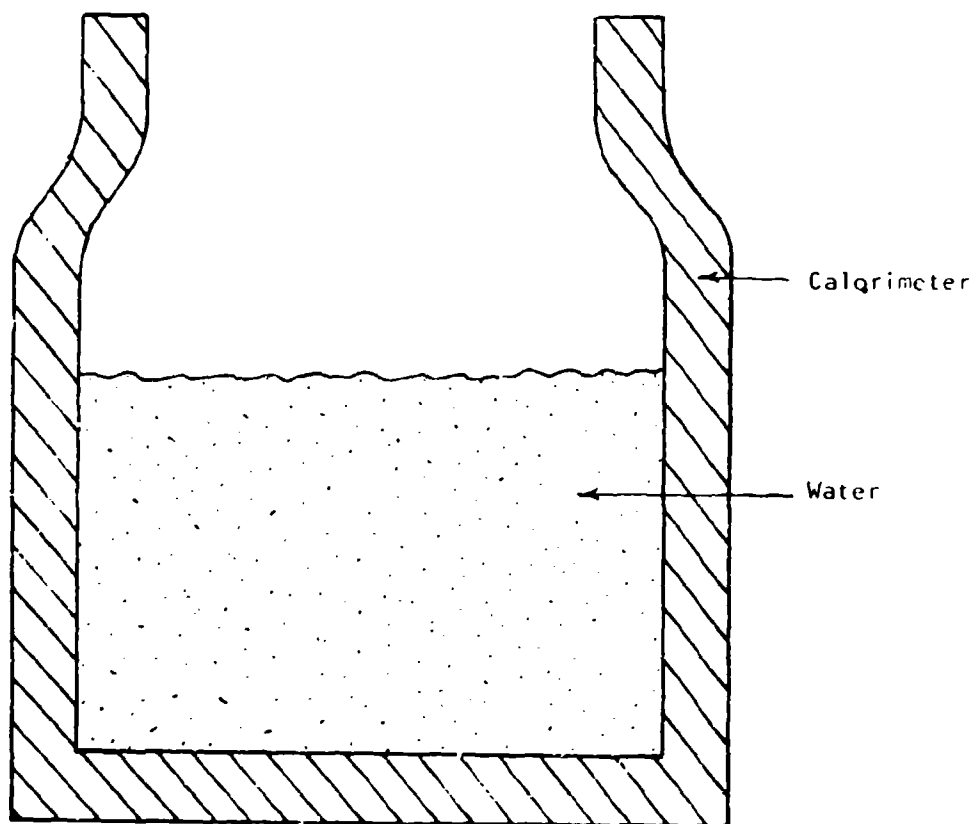
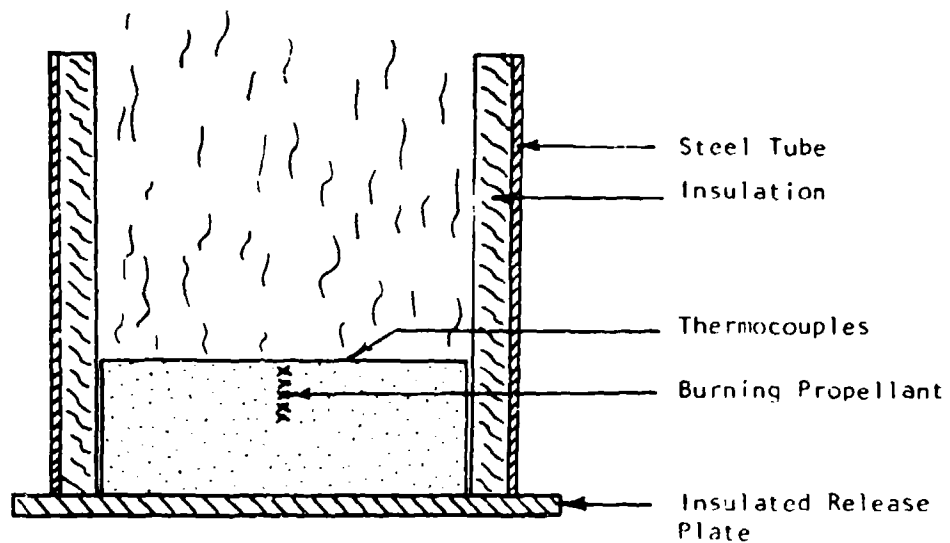


Figure 5. Experimental setup for measuring heat absorbed by propellant during steady burning.

IIT RESEARCH INSTITUTE

The total heat  $Q$  absorbed per unit area of burn propellant was determined by:

$$Q = [(H_c + M C_p) \Delta T - Q_f]/A \quad (30)$$

where:

$H_c$  = measured heat capacity of calorimeter plus water, cal/°C

$M$  = mass of propellant, g

$C_p$  = specific heat of propellant, cal/gm-°C

$\Delta T$  = temperature rise of calorimeter, °C

$Q_f$  = heat transferred to calorimeter during free-fall of burning propellant, cal

$A$  = area of propellant's burn surface, cm<sup>2</sup>

The specific heat  $C_p$  of the propellant was measured at a temperature of 24°C. It was 0.25 cal/g-°K. The quantity of heat  $Q_f$  transferred from flames to the calorimeter was found by dropping another burning propellant disk into an insulated vessel containing water which was partially submerged within the water bath of the calorimeter. The latter vessel was withdrawn along with the propellant's sensible test immediately after burning was extinguished by the water. Then the calorimeter was closed before observing the temperature rise of the calorimeter caused by the propellant flames. This heat equalled 6 percent of the total heat absorbed by the calorimeter when the propellant's heat was not withdrawn from the calorimeter.

The total heat  $Q$  absorbed by the propellant disk during steady burning at 1 atmosphere of pressure was 12.4 cal per cm<sup>2</sup> of burn surface. The latter represents the mean of 3 measurements given by 10.5, 11.7 and 15.1 cal/cm<sup>2</sup>. These measurements include sensible heats within the foam and underlying solid propellant. The burning rate was 0.3 cm/sec.

### 3.2.2 Heat in Solid Propellant During Burning

The sensible heat in the solid propellant, which is represented by  $\delta Q$ , was determined from the thermocouple measurements mentioned earlier. The thermocouples provided continuous temperature-time curves within the solid portion of the burning propellant as the burning approached steady velocities.

IIT RESEARCH INSTITUTE

Only those portions of the temperature-time curves associated with steady burning were used. The steady temperature profile  $T(x)$  versus propellant depth  $x$  was determined using the above temperature-time curve in conjunction with the rate of burning. The heat was determined in terms of the enthalpies  $H(T)$  corresponding to these temperatures  $T(x)$  as follows:

$$\delta Q = \rho \int_0^{\infty} H(T(x)) dx \quad (31)$$

The values of  $H(T)$  used in equation 31 are those for HMX shown in Figure 6. They were obtained from Reference 1.  $\delta Q$  was evaluated as 4.3 cal per cm of burn surface.

### 3.2.3 Steady Foam Mass at 1 Atmosphere of Pressure

The foam mass  $M_f$  was determined as follows:

$$M_f = \frac{(Q - \delta Q)}{H(T_f) - H(T_0)} \quad (32)$$

The foam temperature  $T_f$  cited above equals that to support the steady burning rate of HMX at 1 atmosphere. The latter temperature was predicated as 610°K from Table 1. The initial temperature  $T_0$  was 294 K. The enthalpies  $H$  are assumed equal to those of HMX shown in Figure 6.

The three mass determinations were 0.035, 0.042, and 0.062 g/cm<sup>2</sup>. The mean of the three values, namely 0.046 g/cm<sup>2</sup> is in rough agreement with the value 0.037 presented by Figure 4 for pure HMX at 1 bar of pressure. Thus the curve of Figure 4 roughly approximates three experimental points at 1, 34 and 68 bars.

Whether foam exists at pressures above 68 bars or sublimates away remains in question. In this regard foam can be generated within burning propellant cracks at pressures between 1 and 68 bars. Analysis presented in Section 4 indicates that rapid gasification of such foam can cause pronounced pressure rises within cracks; and lead to DDT provided sufficient foam is generated. Rapid sublimation of the foam at pressures above 68 bars would accentuate

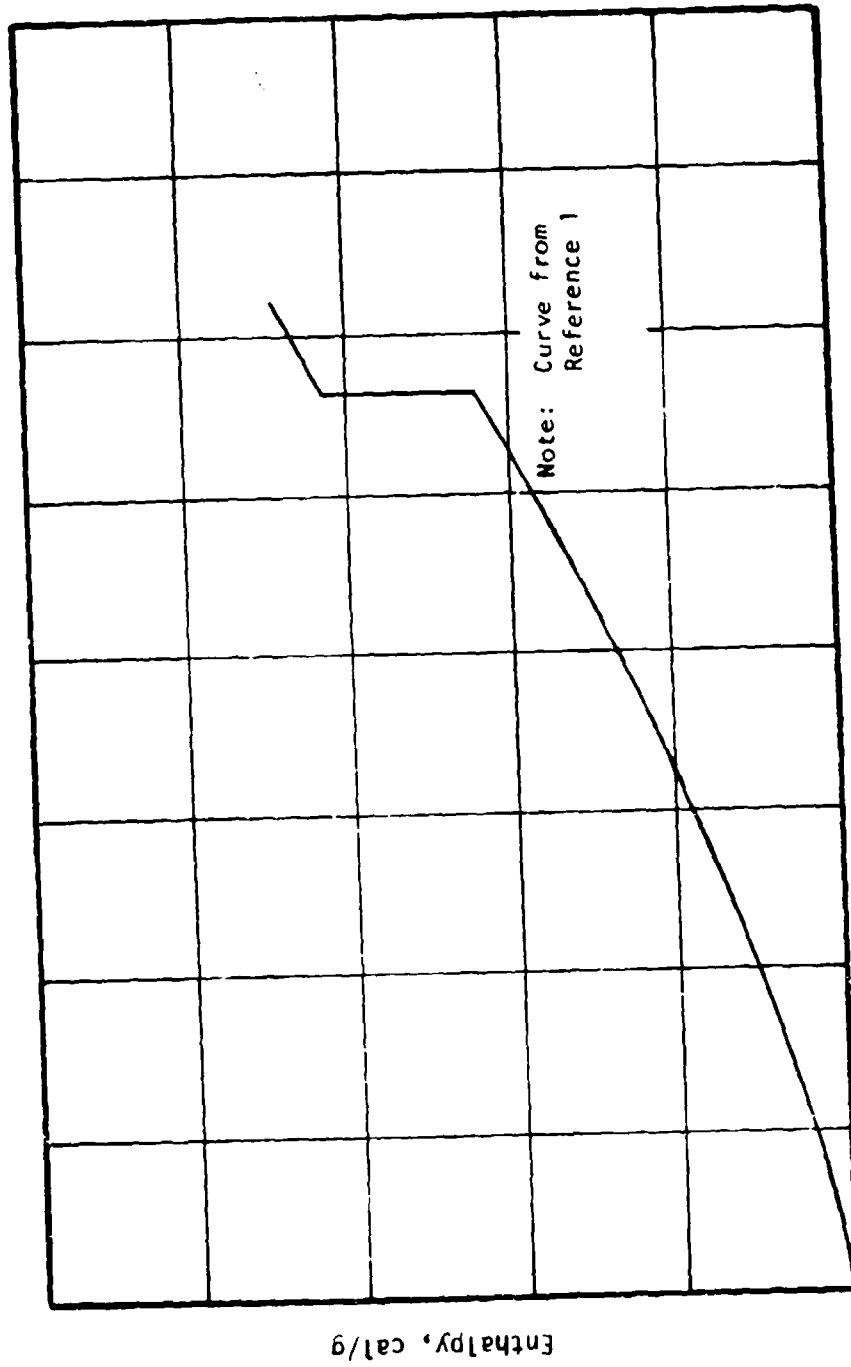


Figure 6. Enthalpy of RMX versus temperature.

the pressure rises and make DDT more likely. Therefore, in assuming the existence of foam at all pressures, we believe we are conservative insofar as DDT is concerned.

IIT RESEARCH INSTITUTE

## 4. MODEL PREDICTIONS

Before discussing model predictions it is important to appreciate the magnitudes, and durations of short wave pressures needed to cause DDT. In this regard de Longuville<sup>6</sup> presents threshold shock wave amplitudes (P) and durations (t) associated with the initiation of HMX-nylon by impact. His results are presented in Figure 7. The curve, which represents a constant weighted impulse  $P^2t$ , separates conditions in which detonation did and did not occur. Clearly weighted impulse has limited usefulness in that it applies to step-wise pressure waves and durations cited in the figure. Nevertheless de Longuville's results suggest DDT will require pressure rises of the order of tens of K bars or more within times of the order of a  $\mu$  sec or less. The more abrupt the pressure rise is and the slower its decay, the greater the likelihood of DDT is.

### 4.1 SENSITIVITY ANALYSES

Here we are concerned with examining the effect of various factors upon pressure transients produced in burning cracks. First the consequence of altering various propellant properties and crack conditions upon pressure transients within single cracks is examined. Then the consequence of applying pressure transients (or stress waves) from one crack to the next in a sequential fashion is determined. Table F-1 in the Appendix F describes property values used for the HMX propellant and combustion gases.

Six parameters were varied in this study. Two of the six parameters are propellant properties. These are:

- internal heat  $Q_s$
- propellant impedance  $I_0$  at ambient pressure

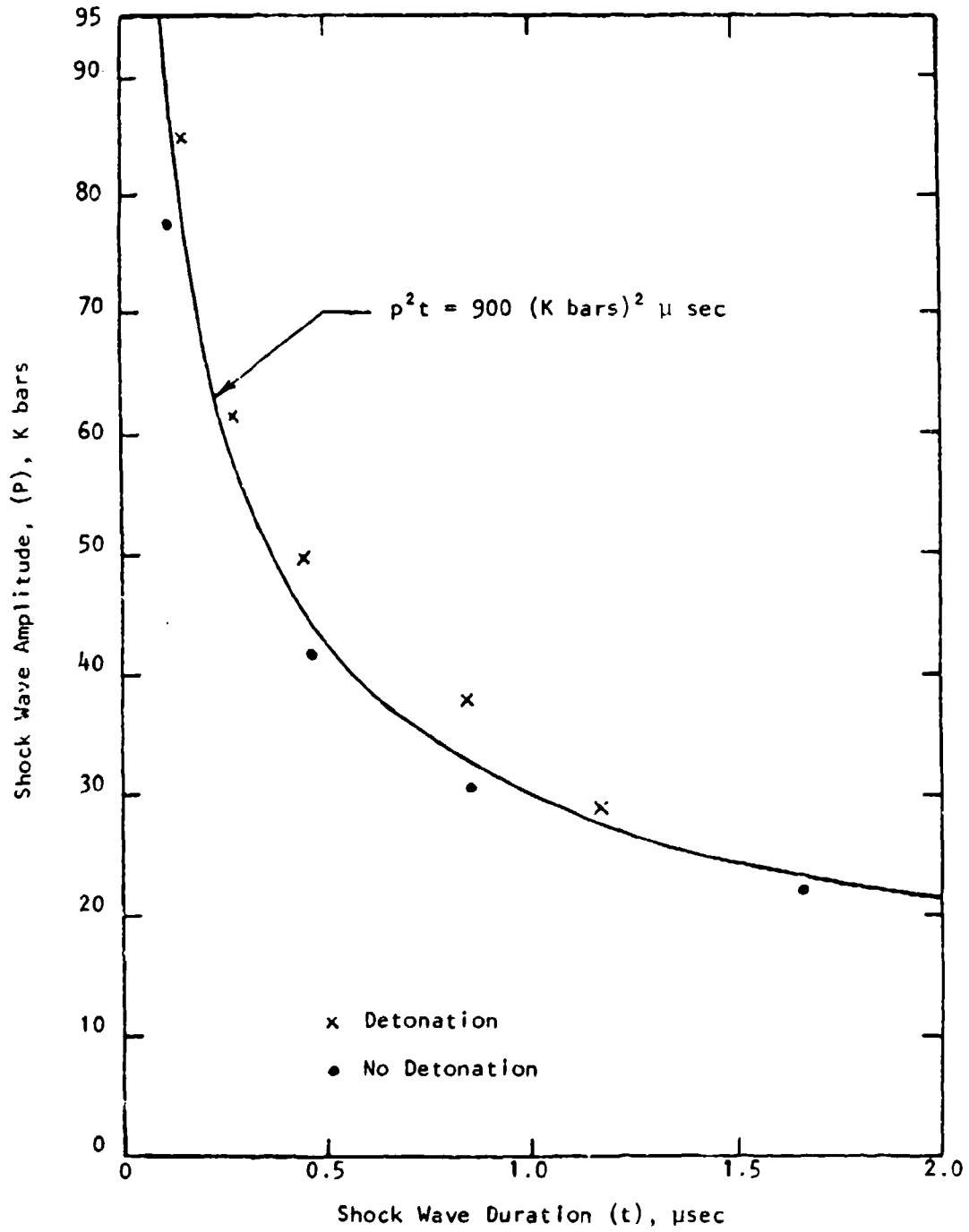


Figure 7. Impact results from Reference 6 for HMX-nylon explosion.

Remaining parameters are:

- initial crack width  $C_{w0}$
- initial gas pressure  $P_0$  (foam temperature adjusted accordingly)
- amplitude  $\Delta P$  of incident stress wave
- initial foam mass  $M_{f0}$

The adjective "initial" refers to values immediately before the stress wave arrives. Each of the latter parameters can vary widely from crack to crack depending upon how the crack develops, ignites and burns. Uncertainties also exist in the propellant properties. For these reasons, three values were chosen for each of the six parameters cited above. They are listed in Table 2. In each study the initial foam temperature was set equal to its value during steady burning at the initial pressure  $P_0$ .

TABLE 2. PARAMETRIC VALUES SELECTED FOR SENSITIVITY STUDIES

Parameter	Nominal value $\pm$ perturbations
$Q_s$	$150 \pm 50$ cal/g
$I_0^*$	$0.45 \pm 0.15$ bars sec/cm
$C_w$	$0.10 \pm 0.05$ cm
$P_0$	$34 \pm 17$ bars
$\Delta P$	$68 \pm 34$ bars
$M_{f0}$	$0.010 \pm 0.005$ g/cm <sup>2</sup>

\*Impedance  $I = I_0 (1 + 0.0002 P(\text{bars}))$

Values of the internal heat  $Q_s$  and propellant impedance  $I_0$  were estimated. The  $Q_s$  values are slightly smaller than cited in the literature<sup>7</sup> for HMX. The values for the initial gas pressure  $P_0$  and the amplitude  $\Delta P$  of the incident stress wave are considered typical of the magnitudes one may encounter in a crack. In this regard  $P_0$  varies with time and gas flow into a crack while  $\Delta P$  depends upon the cavity pressure and rocket motor geometries.

Foam masses  $M_{f0}$  presented in Table 2 are larger than the values presented in Figure 4 for steady burning at the pressure  $P_0$ . Implicit in this assumption is relatively low heating rates prior to ignition, or the cumulation of melt due to melt flow brought about by gas flows in the crack.

Figure 8 is presented to illustrate salient features of the problem. It presents transient crack widths, melt passes and pressures using the unperturbed values presented in Table 2. Time starts with the arrival of the given stress wave.

Initially the stress wave partially collapses the crack. The result is increased gas pressures which cause increased propellant heating (see Equations 11 and 13). The result is accelerated burning that supports progressive increases of the pressure.

Early during the pressure buildup the crack commences to expand in response to the elevated pressures. Pressures continue to rise during crack expansion until the "excess melt" is consumed by burning. The pressure spikes are due to the fact that much of the melt is consumed within short times of the order of a few  $\mu$  seconds. Thereafter the burning rates and pressures commence to decrease due to continued crack expansion.

Figure 9 indicates that higher internal heats  $Q_s$  promote higher pressures at earlier times. The latter is due to greater propellant heating with higher  $Q_s$  values. Figure 10 shows that higher propellant impedances  $I_0$  also cause higher pressures. In this case higher pressures are due to decreases in crack expansion.

In Figure 11 the initial pressure  $P_0$  and foam temperature were varied simultaneously. It shows that increased initial pressures and foam

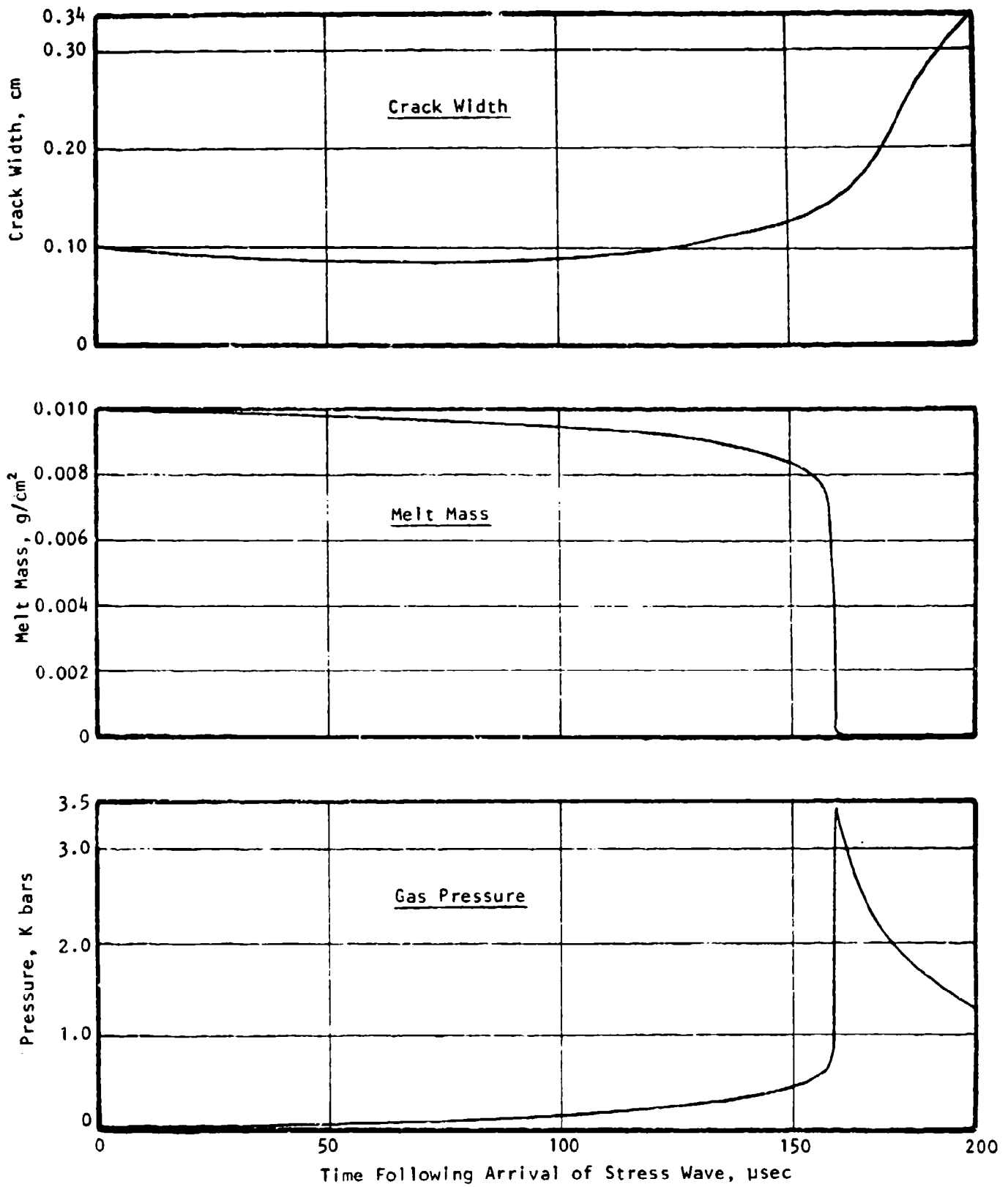


Figure 8. Transient predictions for normal conditions cited by Table 2.

IIT RESEARCH INSTITUTE

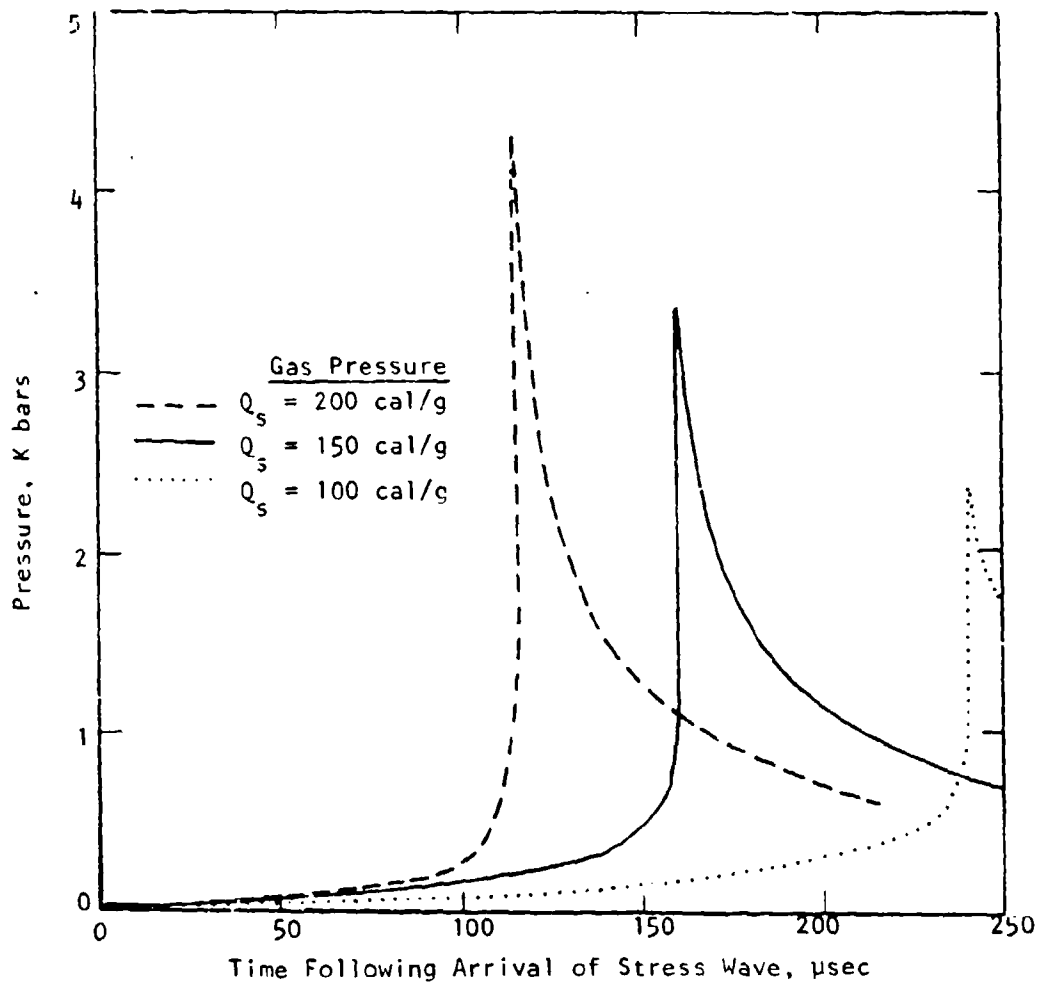
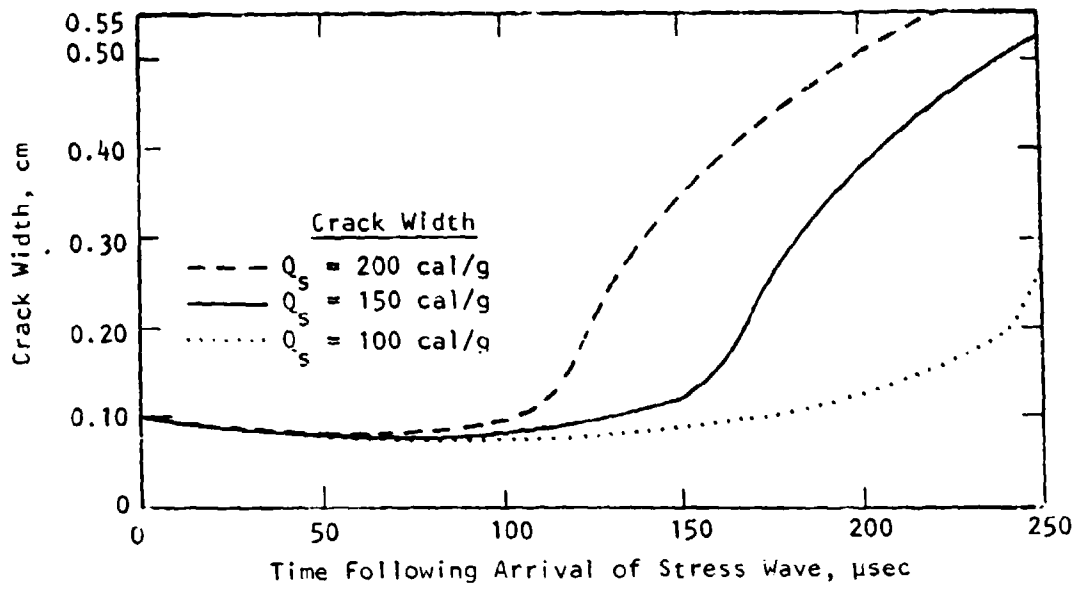


Figure 9. Consequences of varying internal heat ( $Q_s$ ).

IIT RESEARCH INSTITUTE

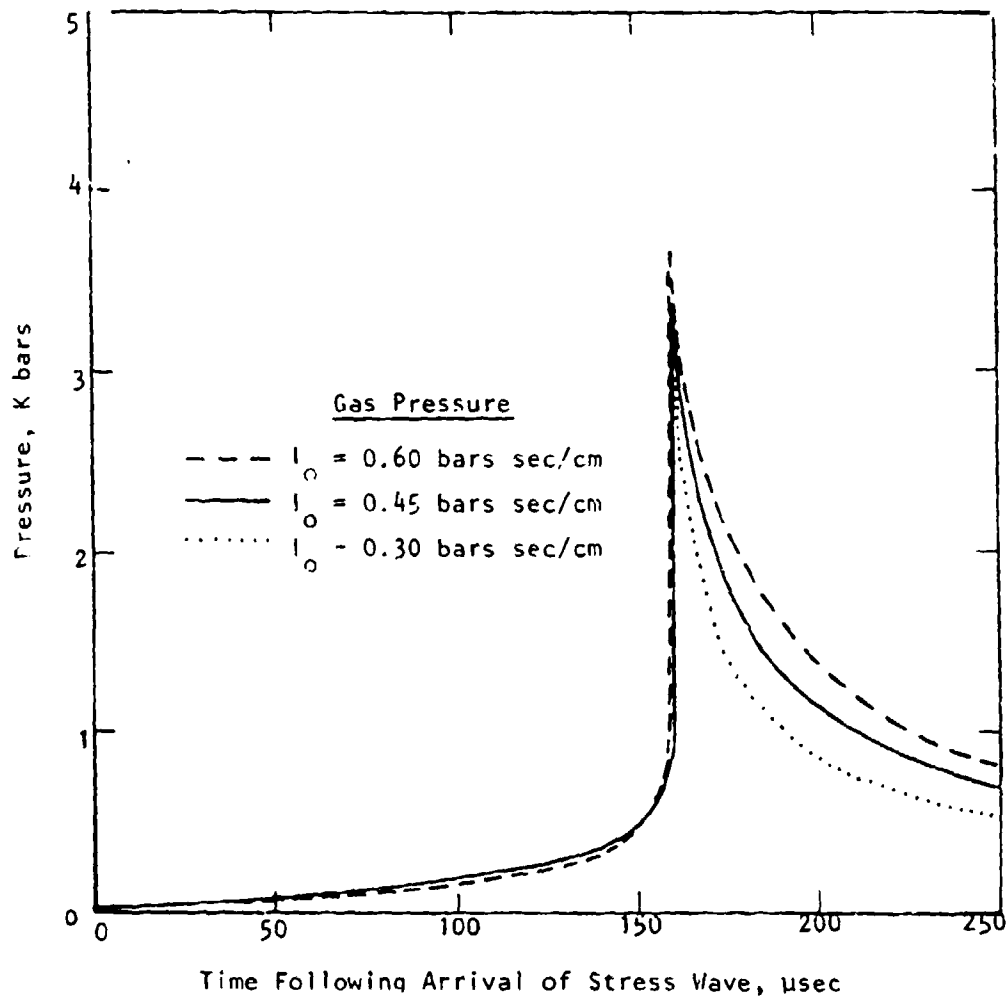
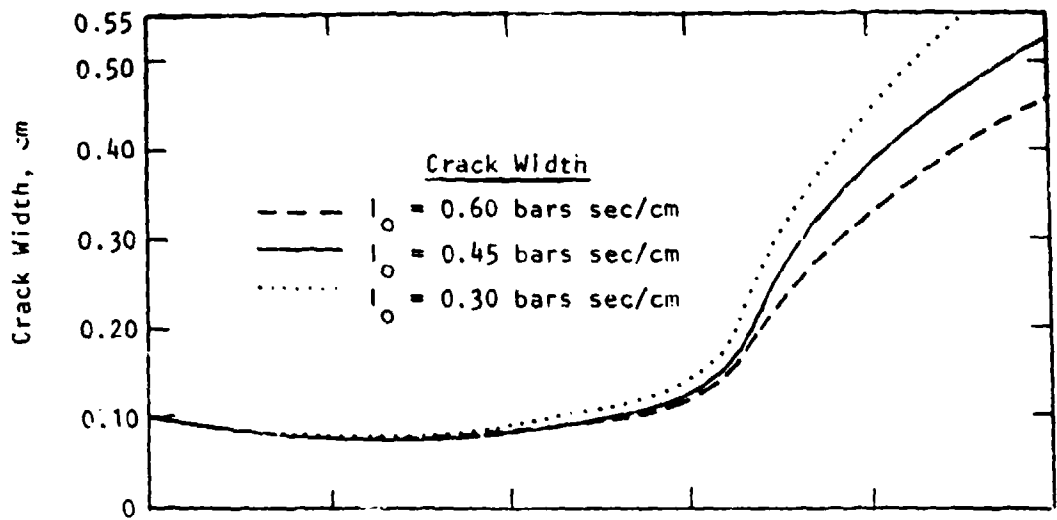


Figure 10. Consequences of varying propellant impedances ( $I_0$ ).

IIT RESEARCH INSTITUTE

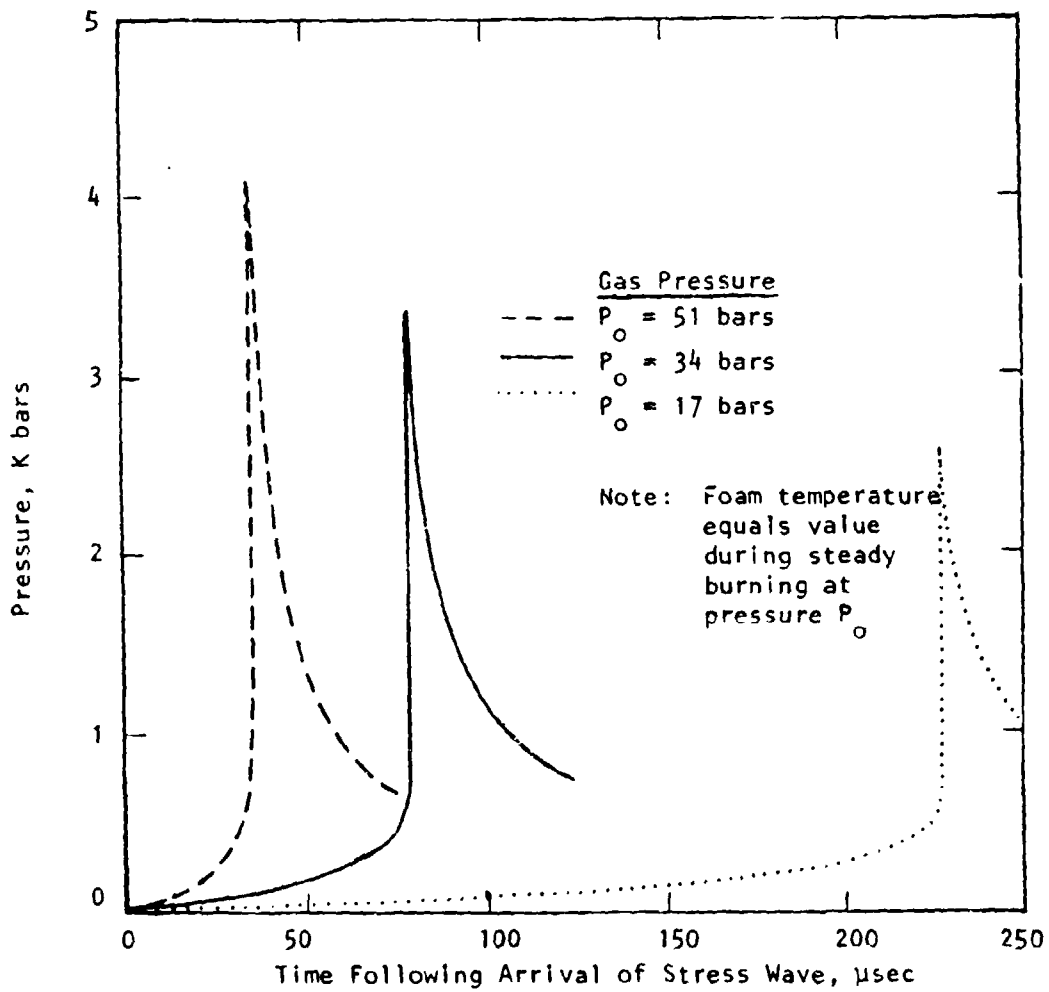
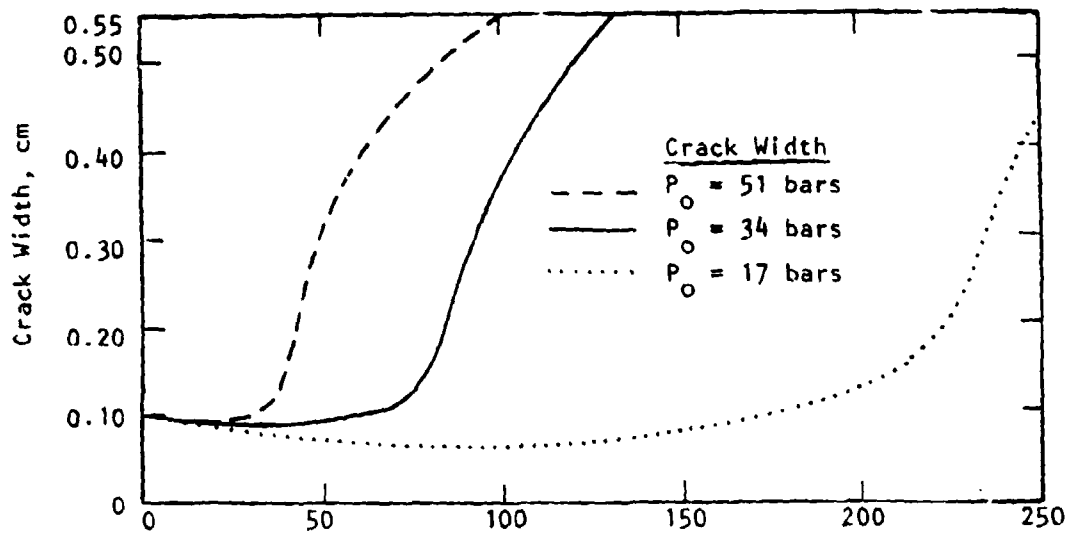


Figure 11. Consequence of varying initial pressure ( $P_o$ ) within crack.

IIT RESEARCH INSTITUTE

temperatures result in greater pressures at earlier times. Increased pressures are due to reductions in crack expansion caused by more rapid consumption of the "excess foam".

Smaller crack volumes can, of course, also be achieved by the application of higher amplitude stress waves or by starting with smaller cracks. Their effects are shown in Figures 12 and 13. Of the two, stress waves are considered more important in that it is possible to generate stress waves orders of magnitude greater than those cited in Figure 12. In addition it is difficult to maintain extremely small crack widths unless such stress waves are applied to counter crack expansion by the pressure buildup. Figure 13 shows that smaller cracks grow at significantly greater rate than larger cracks.

Figure 14 shows that larger initial foam masses  $M_{fo}$  produce pronounced increases of the pressures. There are two reasons for the higher pressures. The first is the larger amounts of gas evolved. The second is the more rapid gasification of the foam layer. The latter is explained by the cooling effects of the molten propellant entering the foam. Temperature rises are inhibited less by the incoming melt with larger foam masses. The result is more rapid gasification of the "excess foam". In turn rapid gasification yields less time for crack expansion and hence higher pressures.

Next let us select three sets of values for the six parameters presented in Table 2 to gain a better appreciation of the range of pressures that may be produced in cracks. The three sets of values are presented in Table 3.

The case 2 values represent nominal values presented in Table 2. The case 1 values are those that yielded the smallest pressures; the case 3 values are those that yielded the highest pressures.

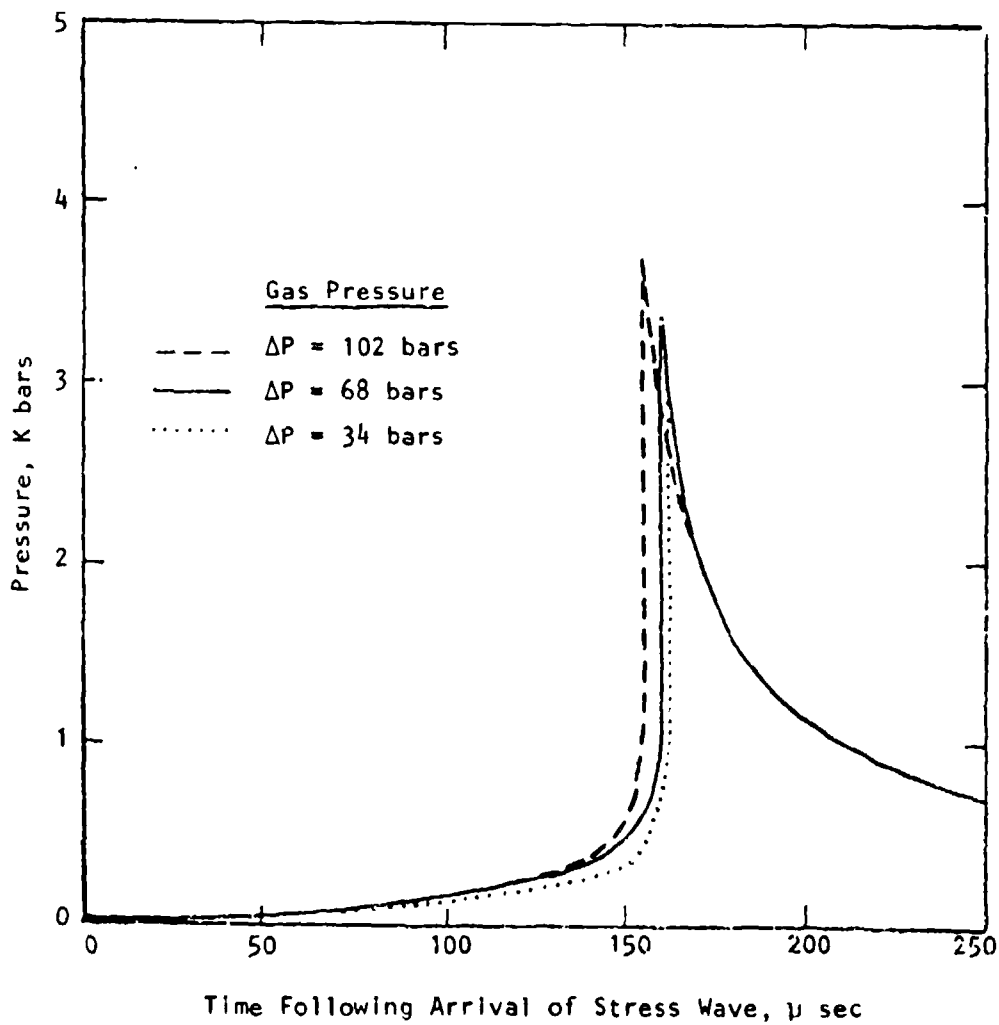
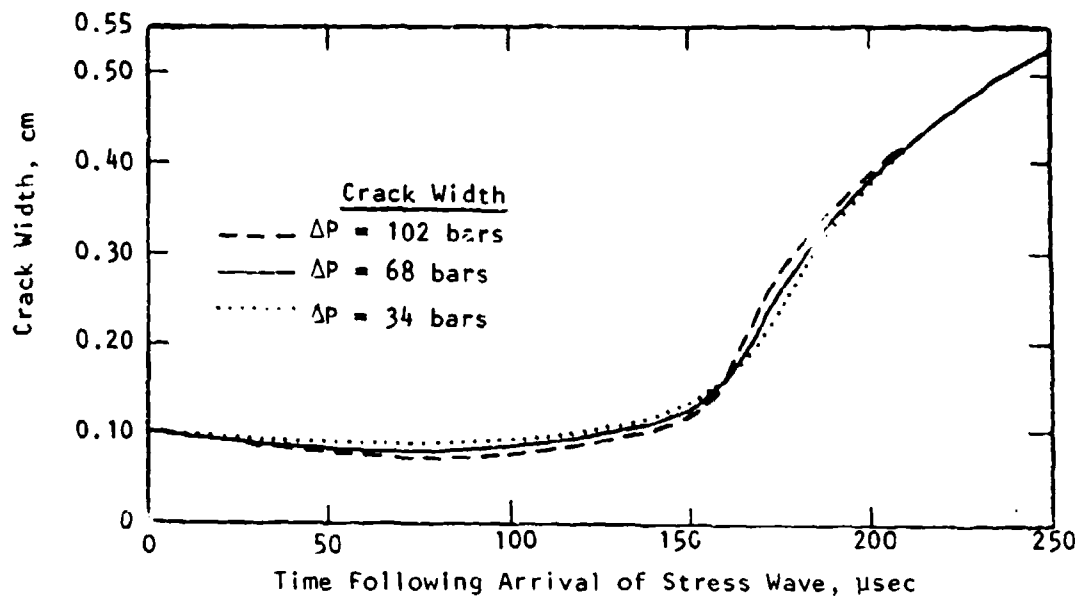


Figure 12. Consequences of varying amplitude ( $\Delta P$ ) of incident stress wave.

IIT RESEARCH INSTITUTE

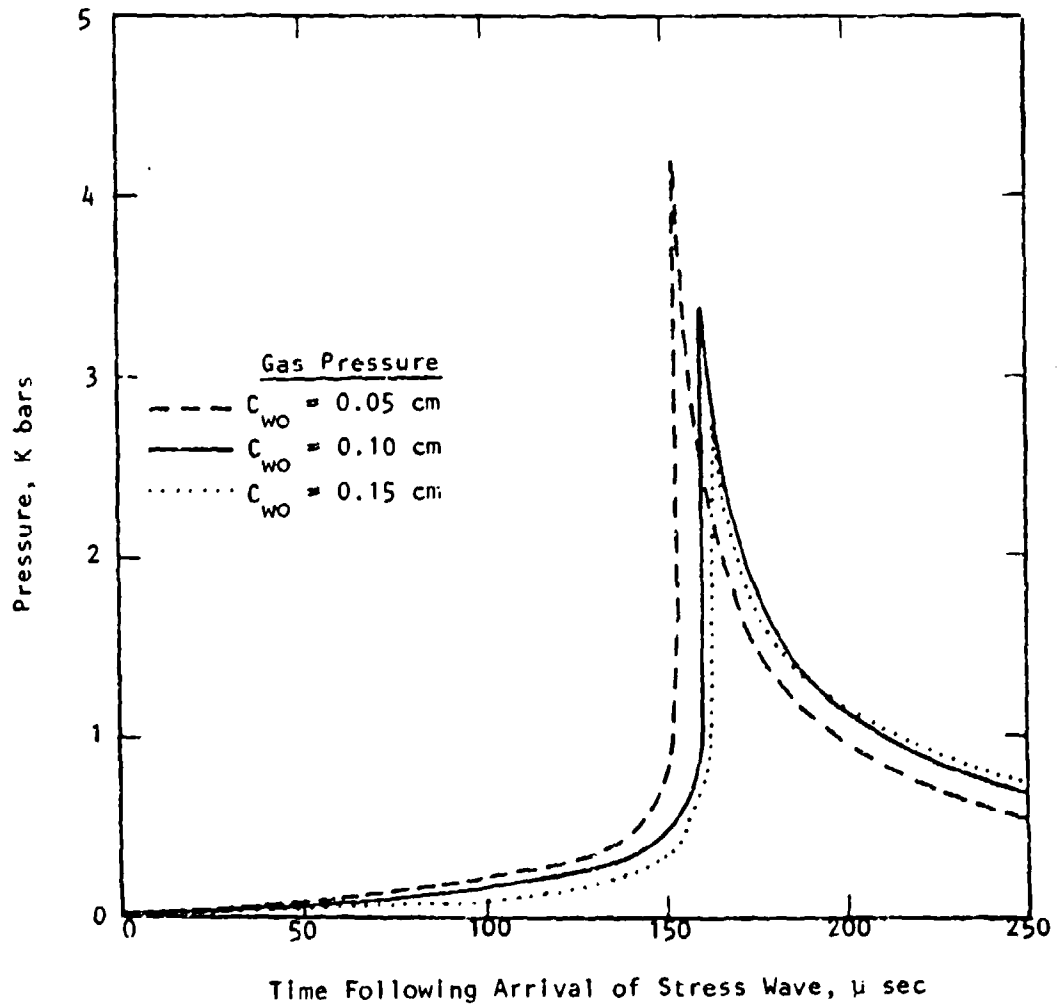
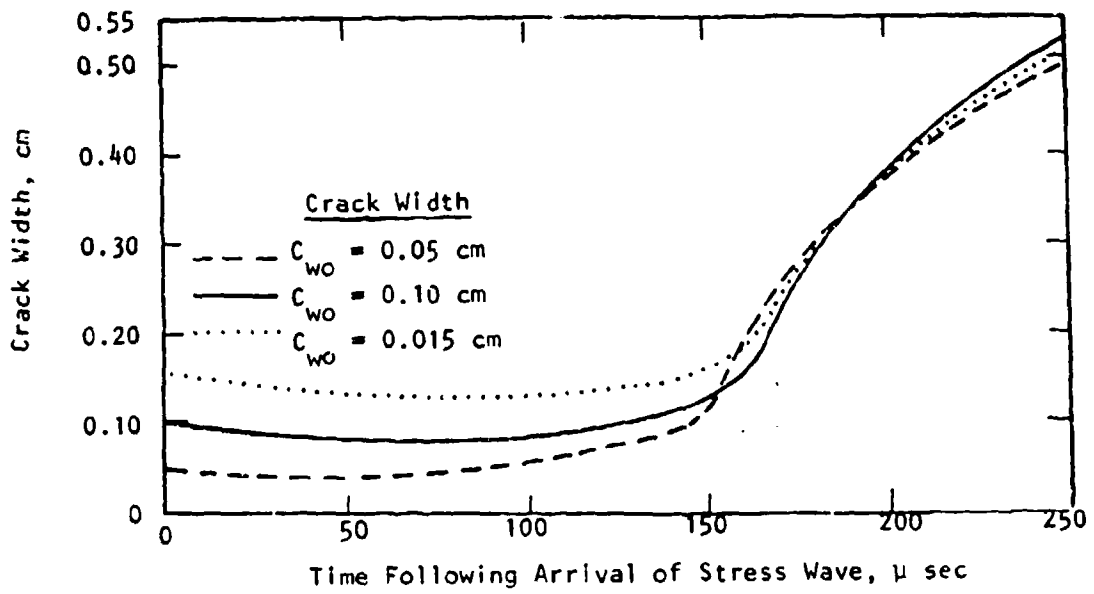


Figure 13. Consequences of varying initial crack width ( $C_{wo}$ ).

IIT RESEARCH INSTITUTE

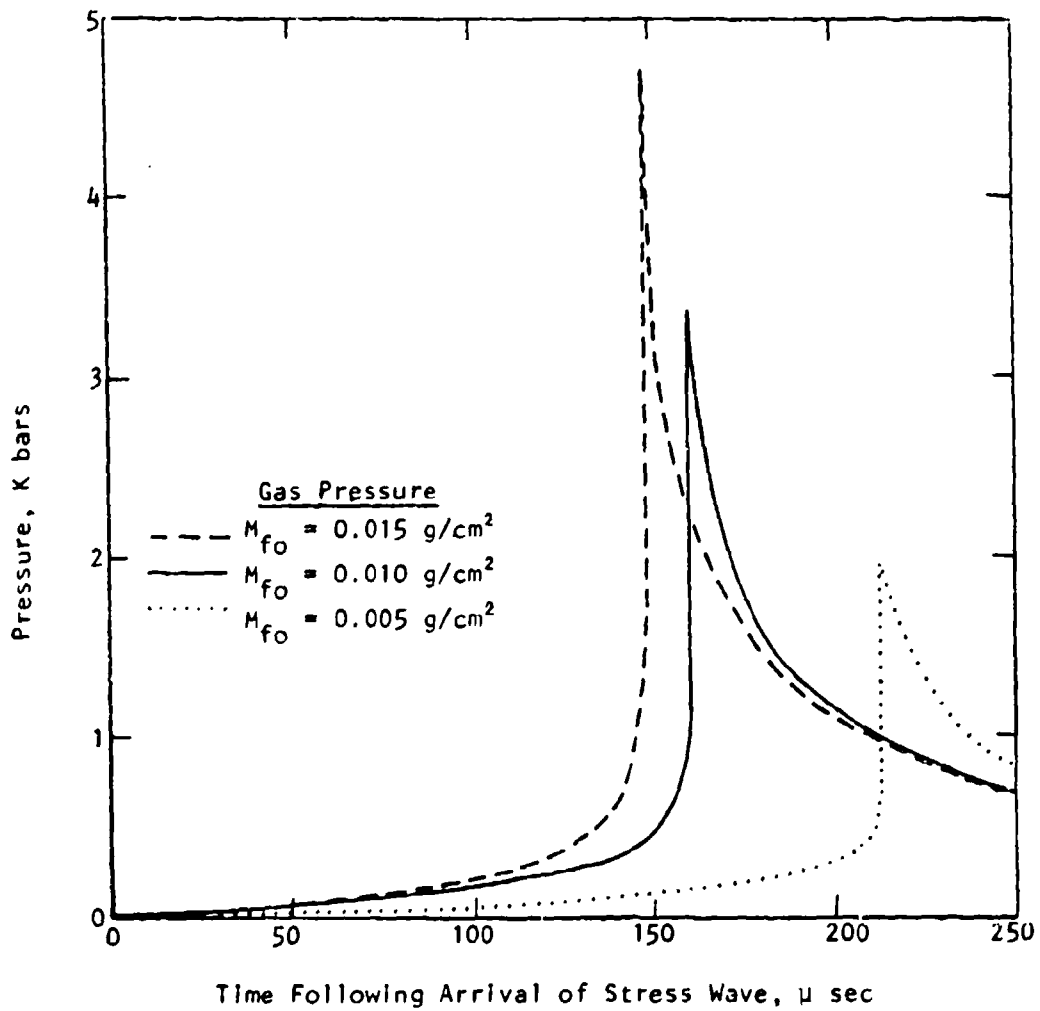
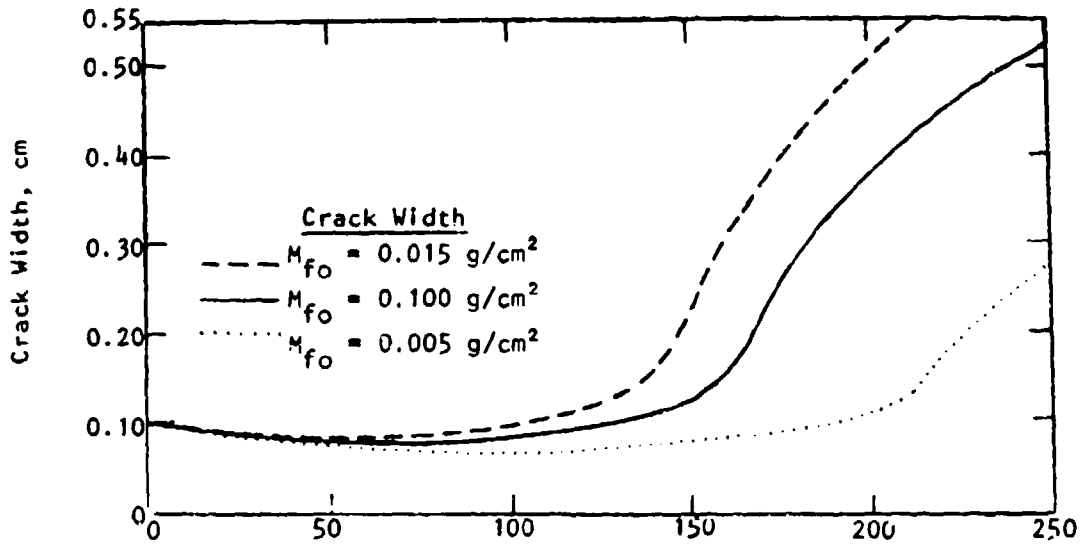


Figure 14. Consequences of varying initial foam mass ( $M_{fo}$ ).

IIT RESEARCH INSTITUTE

TABLE 3. PARAMETRIC VALUES FOR THREE SELECTED CRACK CONDITIONS

Parameter	Case 1 Values	Case 2 Values	Case 3 Values
$Q_s$	100 cal/g	150 cal/g	200 cal/g
$I_0^*$	0.30 bars sec/cm	0.45 bars sec/cm	0.60 bars sec/cm
$C_{wo}$	0.15 cm	0.10 cm	0.05 cm
$\Delta P$	34 bars	68 bars	102 bars
$P_0^\dagger$	17 bars	34 bars	51 bars
$M_{fo}$	0.005 g/cm <sup>2</sup>	0.010 g/cm <sup>2</sup>	0.015 g/cm <sup>2</sup>

\* Impedance  $I = I_0 (1 + 0.0002 P(\text{bars}))$

† Foam temperature and temperature distribution of solid propellant varied with  $P_0$  according to steady burning conditions

Resultant pressure transients are presented in Figure 15 for the three cases. Notice that peak pressures differ by an order of magnitude. It suggests that pressure transients will vary widely from crack to crack depending upon the propellant properties and how the crack develops, ignites and burns.

#### 4.2 MULTIPLE CRACKS

Multiple burning cracks are important in that the pressures produced by stress wave/crack interactions are greater than the applied stress wave. The result is an enhanced stress wave leaving cracks that can then act upon neighboring burning cracks. By this process progressively higher and steeper pressure transients can develop as stress waves move from crack to crack.

To better appreciate the problem consider three sets of identical parallel cracks. The cracks are identical to those considered earlier in the section. They are described by case 1, case 2, and case 3 in Table 3.

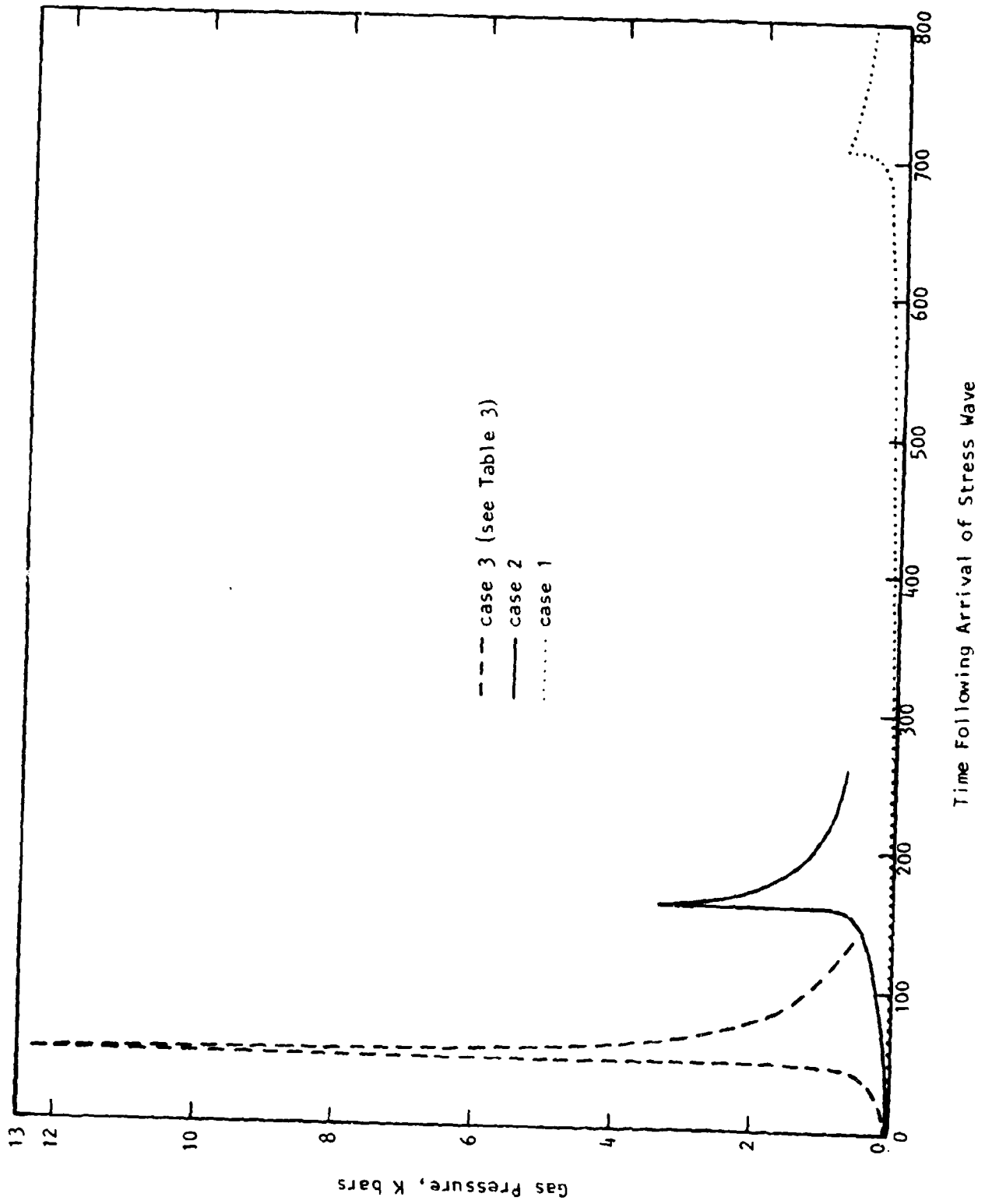


Figure 15. Pressure transients for three crack conditions.

Figure 16 illustrates the results for a series of identical case 1 cracks. Notice that the pressure transients become more pronounced with each succeeding crack. Much of the pressure increase is caused by progressive decreases of the crack width. At least seven cracks are needed to achieve pressures of the order of 10 k bars.

Figures 17 and 18 present similar results for case 2 and 3 cracks, respectively. In each of the above cracks, pressures rise more steeply to their peaks than the pressures produced by the case 1 cracks (see Figure 16). Steep pressure rises, are of course, more conducive to detonation. Also fewer cracks are needed to develop pressures of the order of tens of kbars with case 2 and 3 cracks than required with case 1 cracks.

The results of Figures 16, 17, and 18 suggest that multiple cracks may lead to detonation provided enough cracks are involved in the sequential fashion indicated. This hypothesis suggest that large propellant motors are more susceptible to detonation than small motors. It is consistent with unreported IITRI observations in which a few hundred pounds of secondary high explosives (HE) burned freely without event, while a few thousand pounds of the same HE detonated under similar burning conditions. Each test result was replicated four times.

#### 4.3 FOAM MASSES GENERATED WITHIN CRACKS

Propellant surfaces in cracks are exposed to cross gas flows that accentuate propellant heating and thereby lessen foam formation. In this section we shall present predicted foam masses generated in cracks that propagate into a cavity of high-temperature high-pressure gases. Initially the gases in the cracks are assumed to have a temperature of 294°K and a pressure of 1 bar. The downstream end of the crack is considered connected to a second cavity of gases held at the same temperature and pressure as the gases initially in the crack.

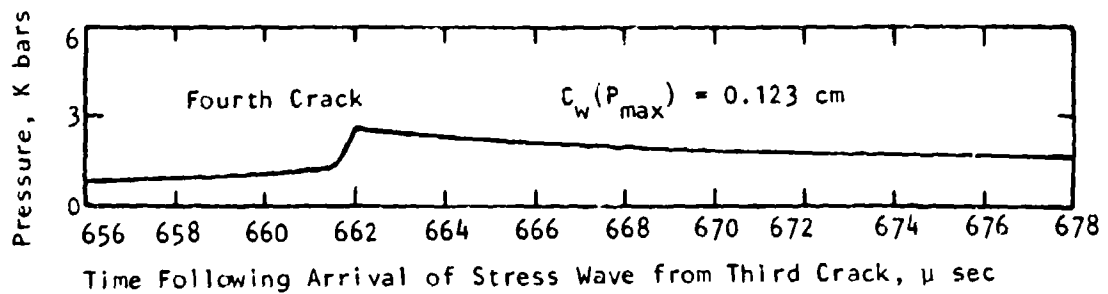
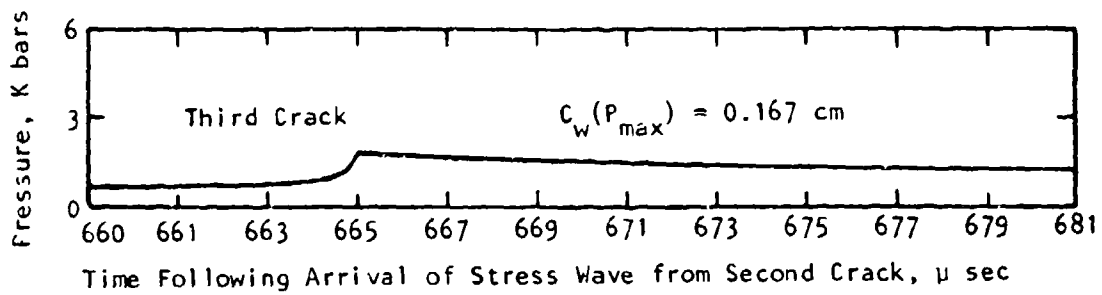
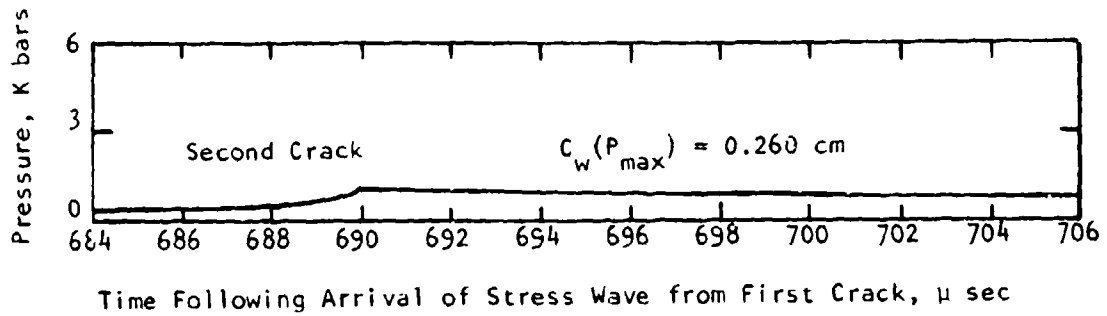
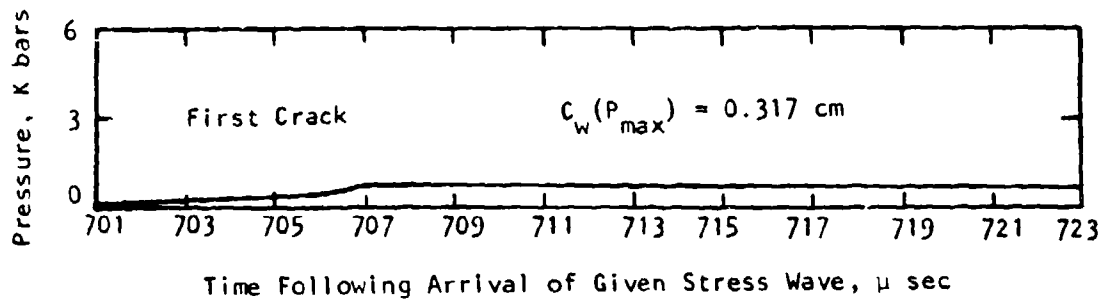


Figure 16. Multiple cracks (case 1).

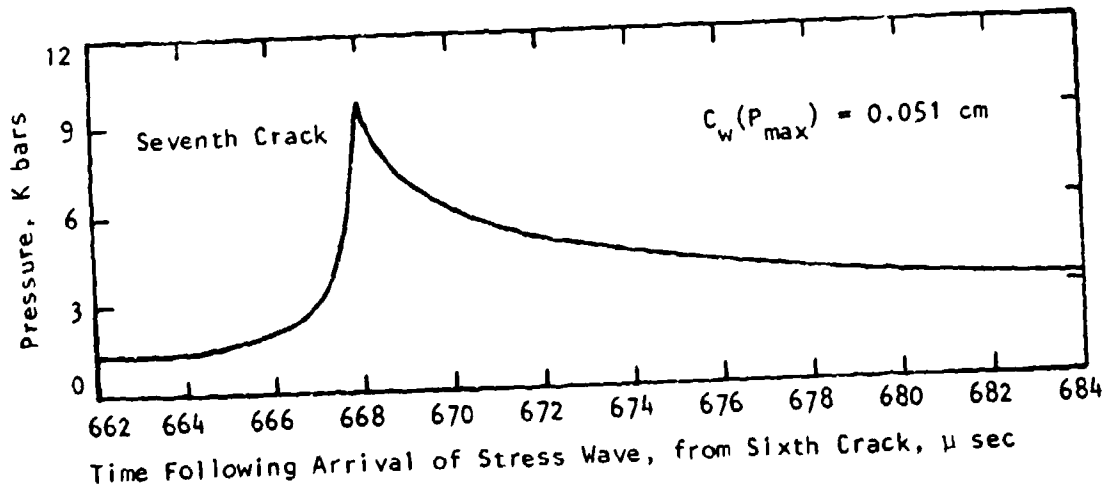
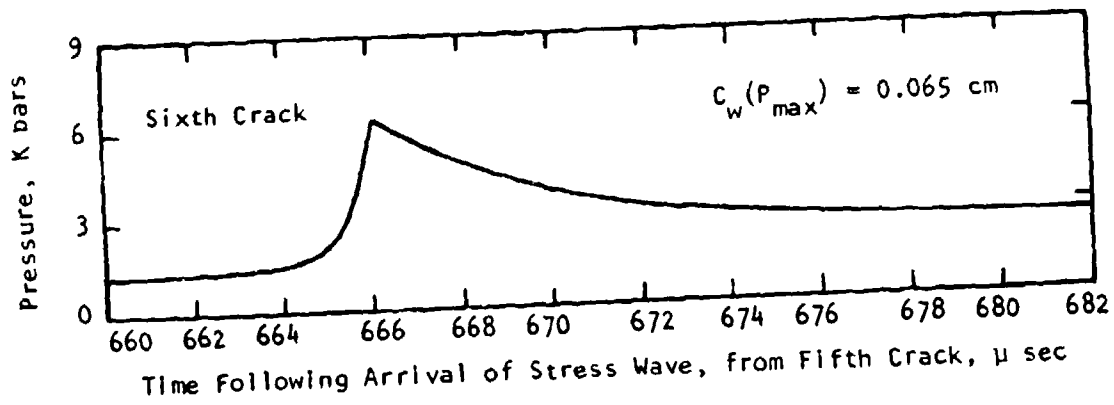
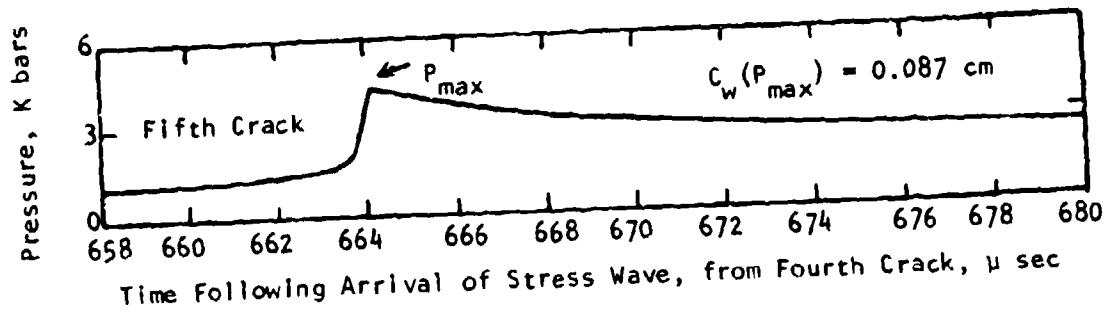


Figure 16. Multiple cracks (case 1) concluded.

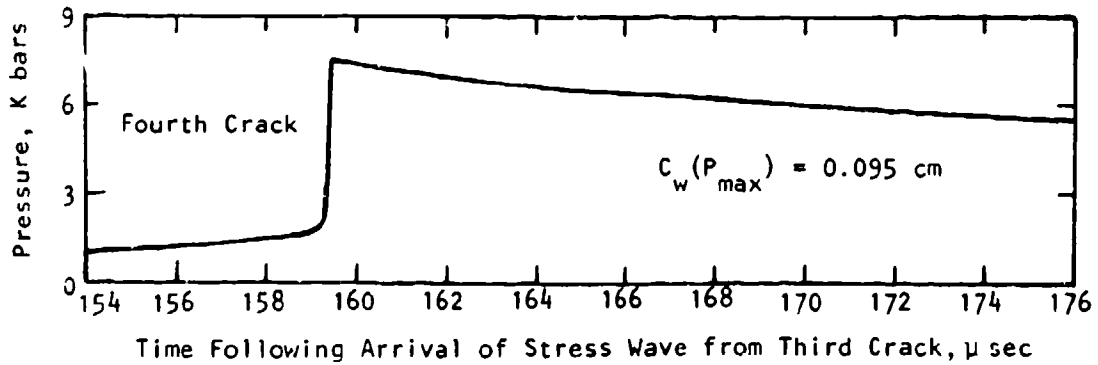
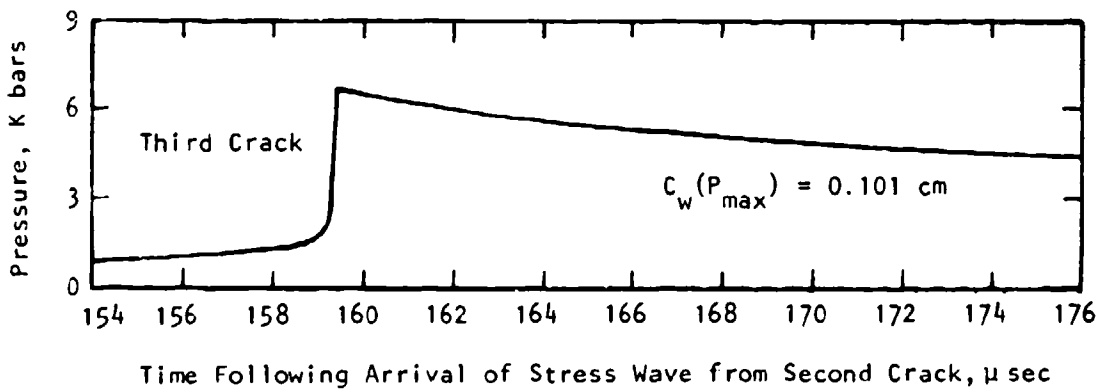
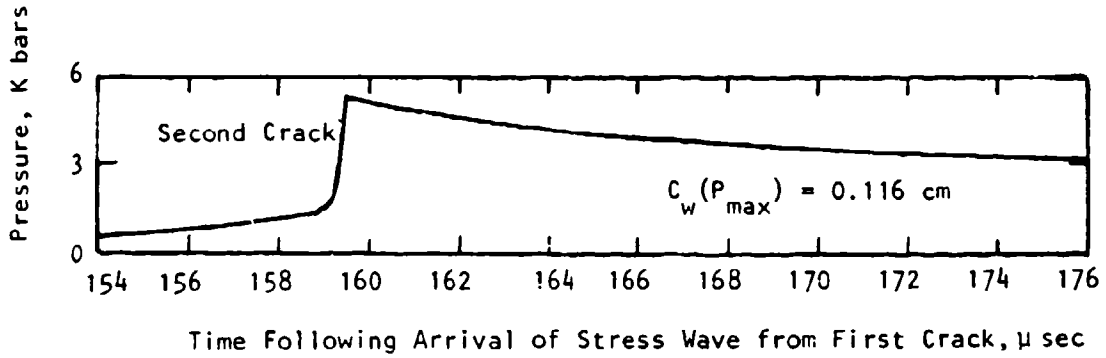
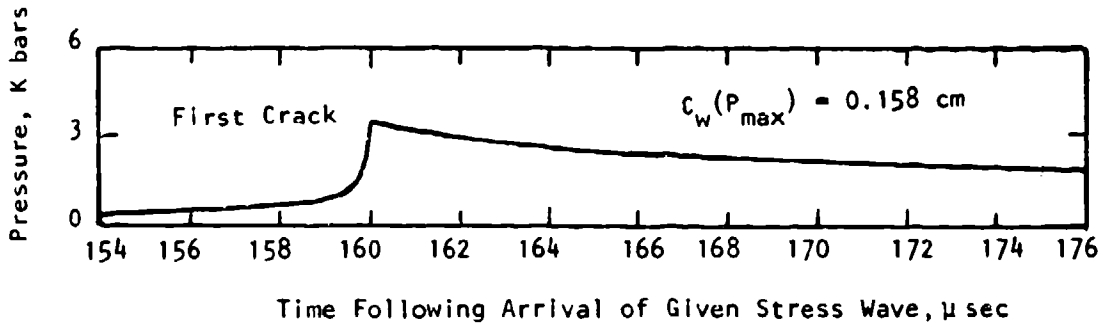


Figure 17. Multiple cracks (case two).

IIT RESEARCH INSTITUTE

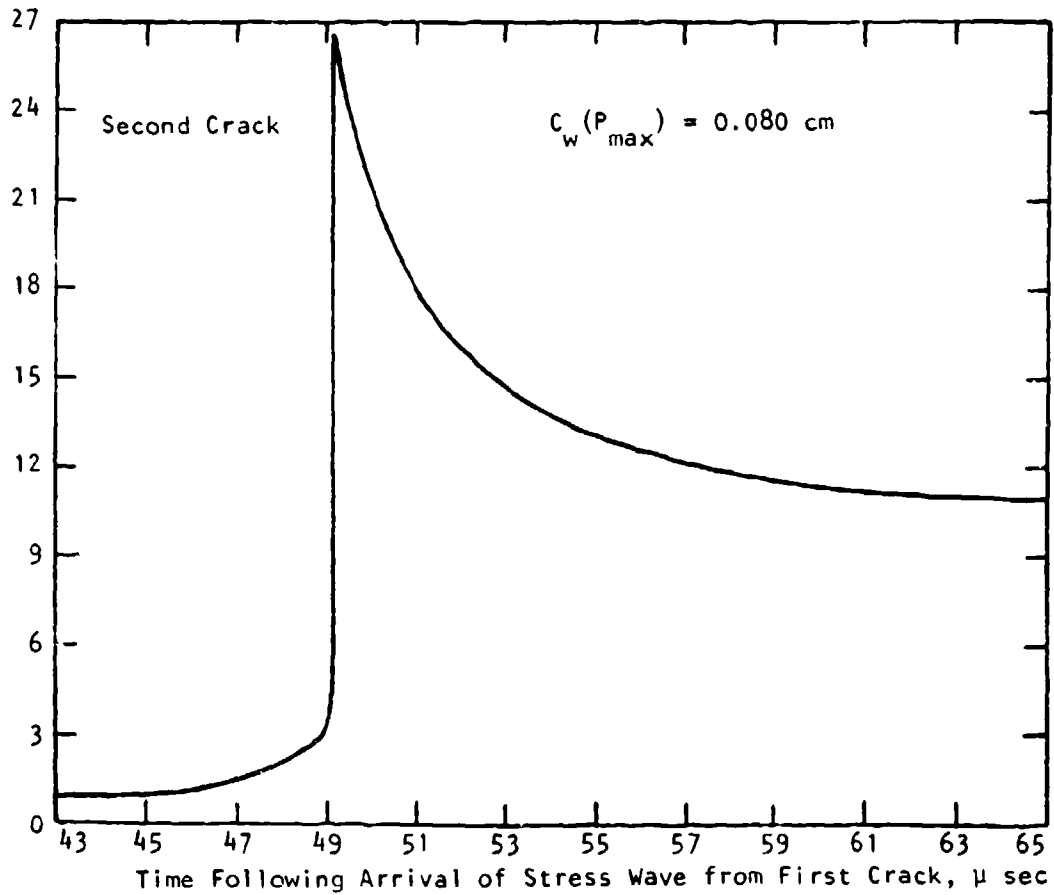
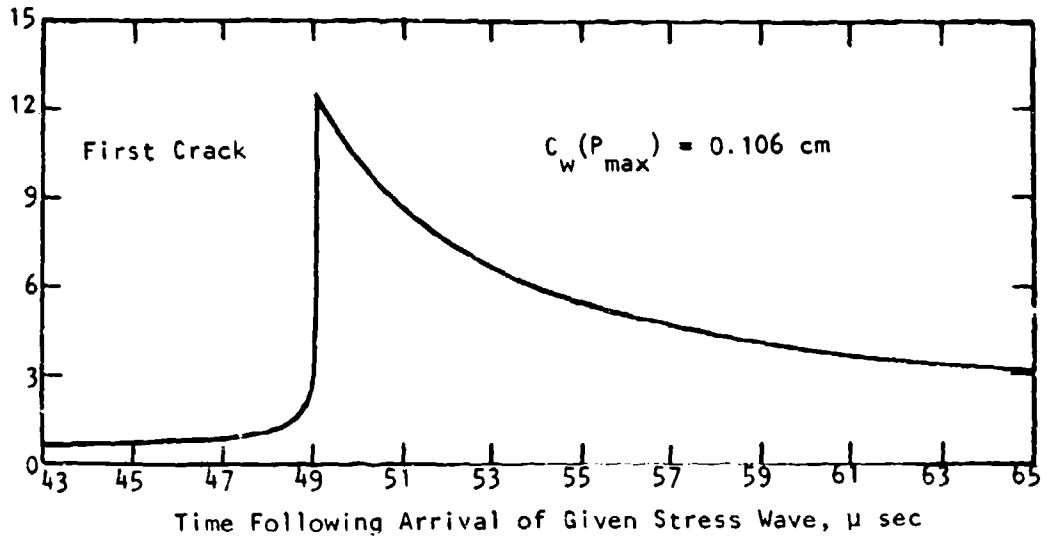


Figure 18. Multiple cracks (case three).

IIT RESEARCH INSTITUTE

Figures 19 through 21 present dynamic foam masses as well as gas velocities, cracks widths and gas pressures along the length of the crack for cavity pressures of 8, 16 and 68 bars, respectively. Conditions are presented for three times following exposure of the crack to the high-pressure cavity.

As one would expect, the foam mass is greatest initially at the high-pressure end of the crack. Thereafter, the greatest foam mass occurs at increasing crack depths before being found at the downstream end of the crack. The latter is due to the smaller downstream heat fluxes; i.e., the heat fluxes at the upstream end are relatively high. In this regard lower fluxes produce greater foam masses over longer periods of time.

Mean values of the foam masses within the crack are presented in Figure 22 as a function of time for each of the three cases illustrated in Figures 19 through 21. It may be observed that the mean foam mass asymptotically approaches values of approximately 0.0040, 0.0020, and 0.0005 g/cm<sup>2</sup> for cavity pressures of 8, 16, and 68 bars, respectively. These foam masses are roughly 40 percent of their steady-state values presented in Figure 4. Figure 22 indicates that greater amounts of foam require longer times to produce.

The relatively low foam masses cited above do not appear adequate to cause DDT unless extremely intense stress waves are generated say by multiple burning cracks. Two possibilities exist for foam enhancement. The first and most obvious is low gas pressures and propellant heating rates. This possibility does not appear likely. The second possibility is accumulation of melt at particular regions of a crack due to flow of melt caused by high velocity gases. This possibility is more likely in that mixing of relatively cool melt with hotter melt will lessen the net gasification of the melt, and thereby increase the total amount of melt present.

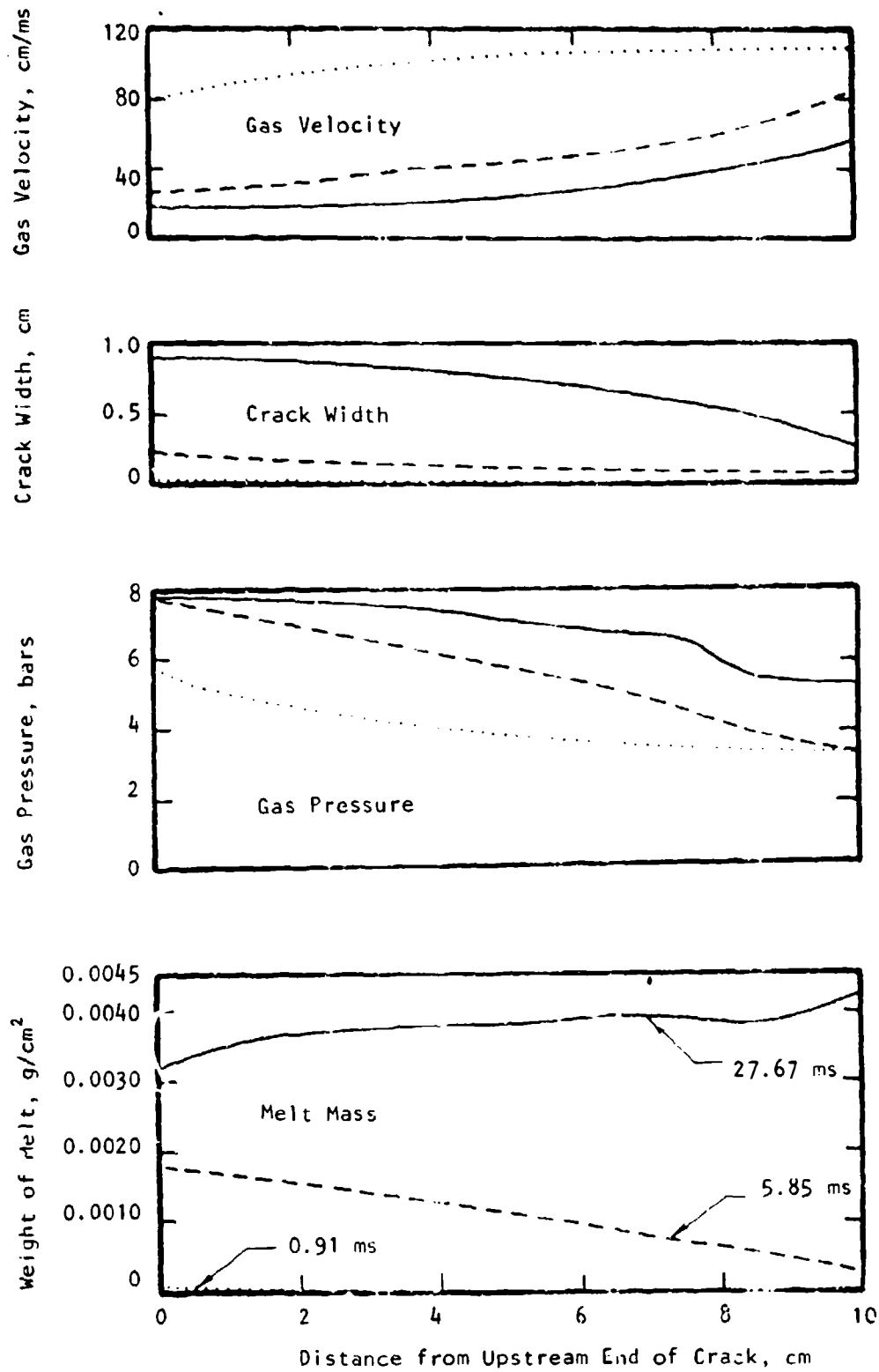


Figure 19. Consequence of sudden exposure to "open crack" to high pressure (8 bars) cavity.

IIT RESEARCH INSTITUTE

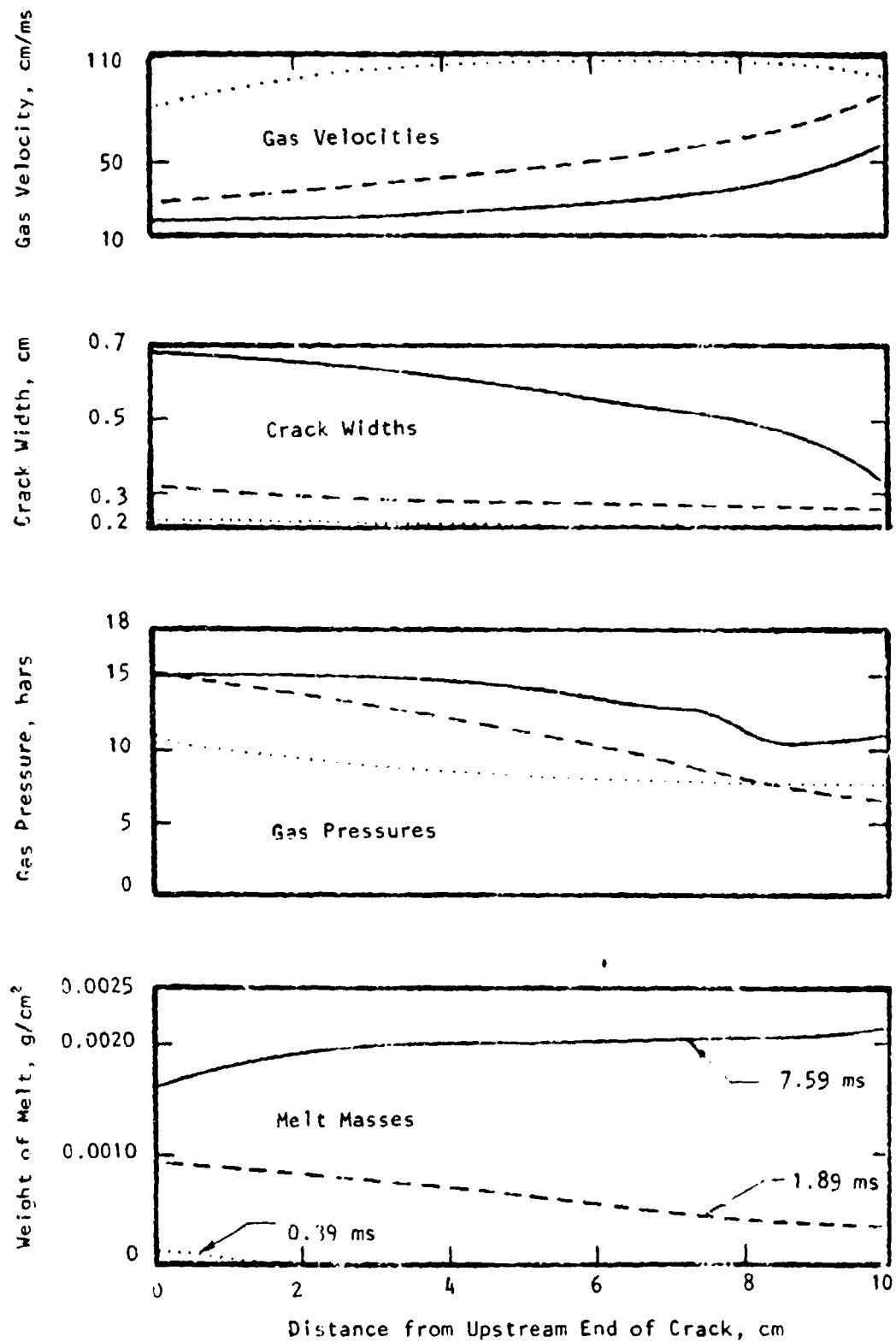


Figure 20. Consequence of sudden exposure of "open crack" to high pressure (16 bars) cavity.

IIT RESEARCH INSTITUTE

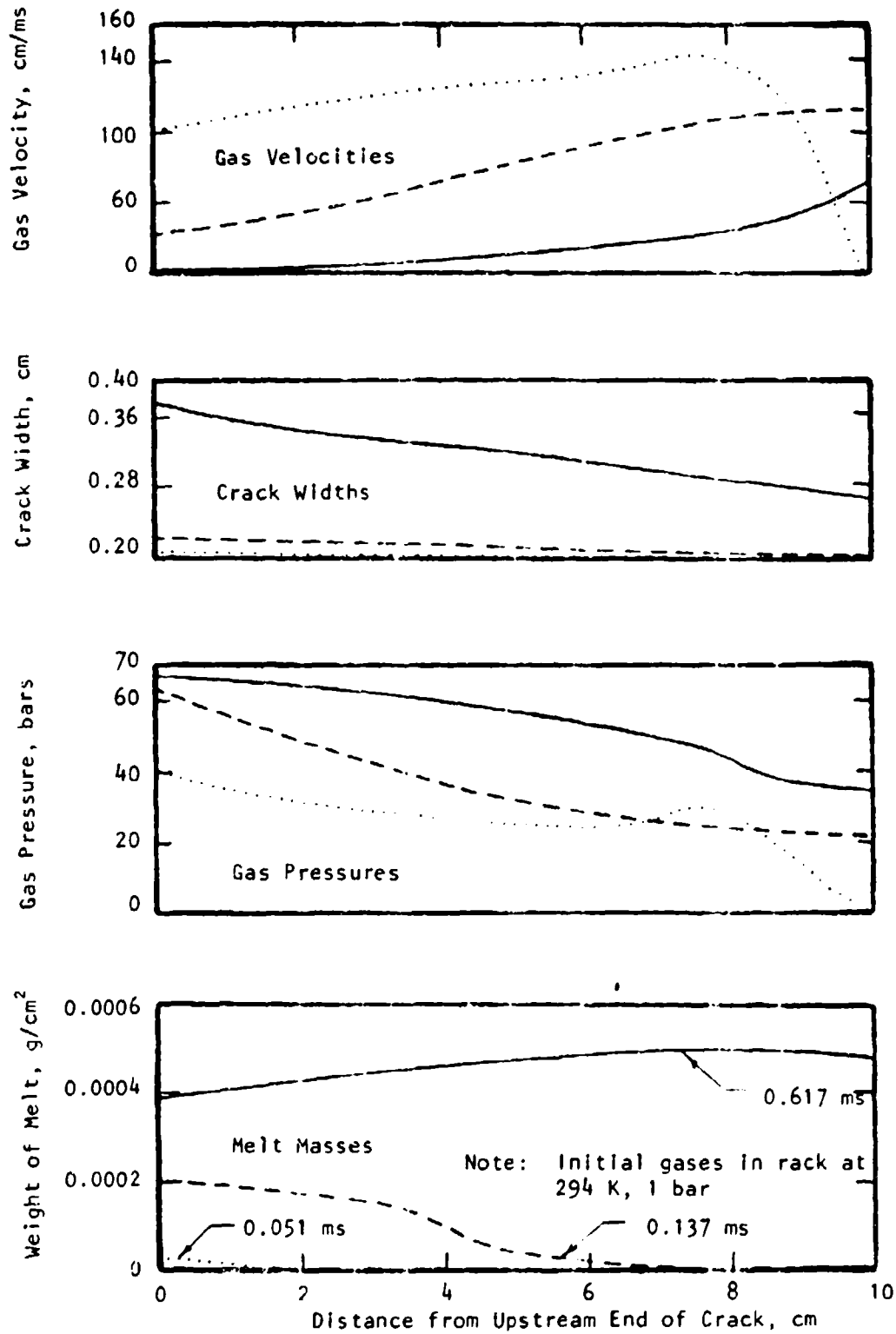


Figure 21. Consequence of sudden exposure of "open crack" to high pressure (68 bars) cavity.

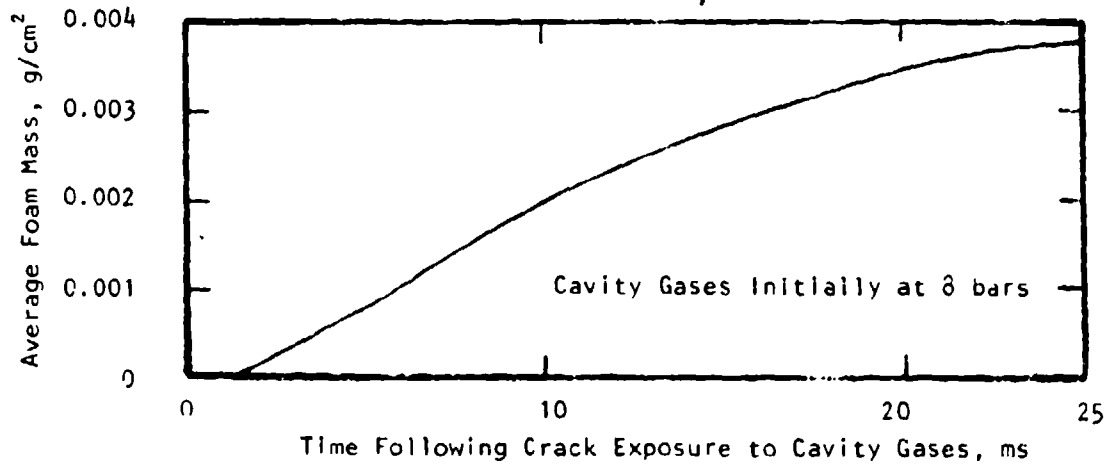
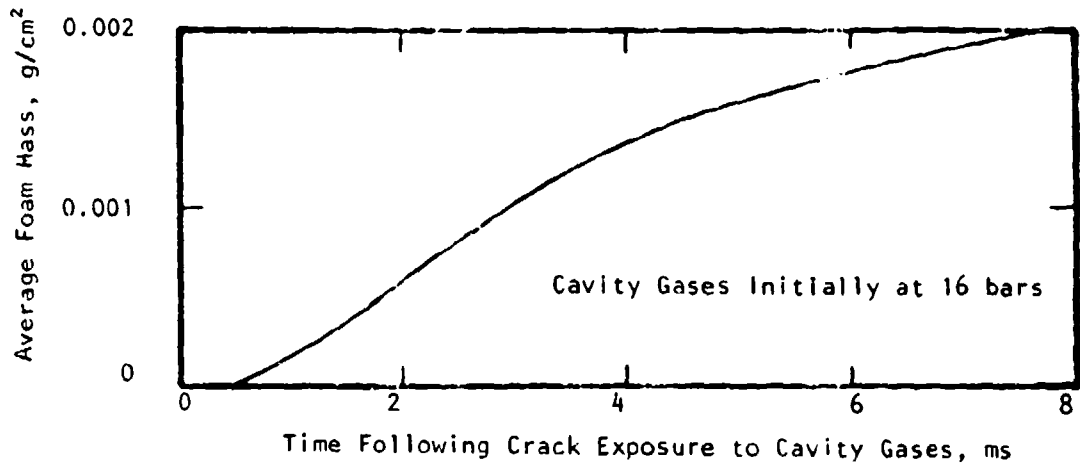
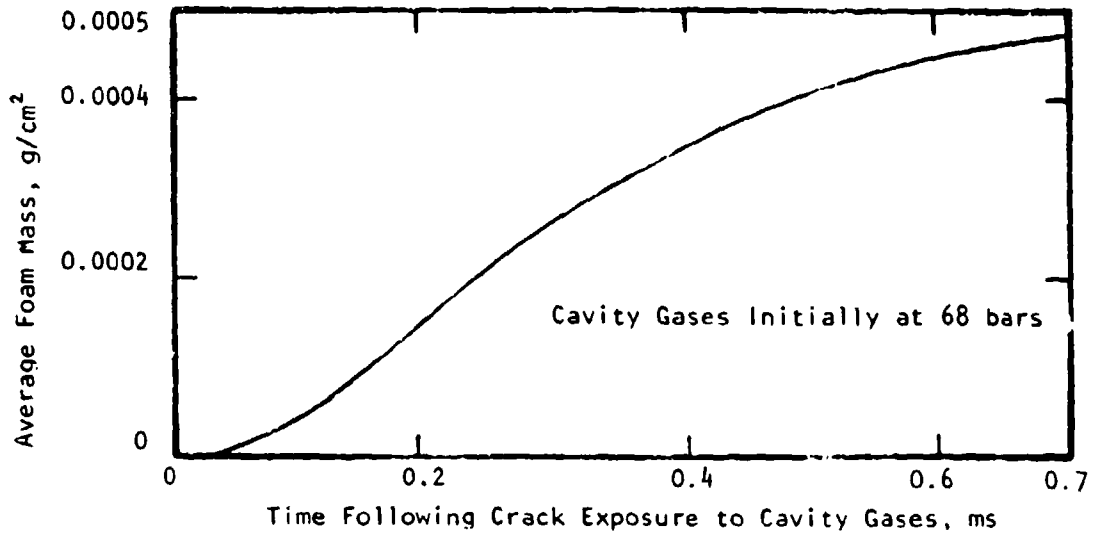


Figure 22. Mean HMX foam mass within "open cracks" versus time.

IIT RESEARCH INSTITUTE

## 5. BURNING PROPELLANT EXPERIMENTS

### 5.1 EXPERIMENTAL PROCEDURE

A series of 18 experiments were conducted with the objective of validating the analytical conclusions described in Section 4. A schematic illustrating essential features of the experimental set-up is presented in Figure 23. The design simulates partial closure of burning-propellant cracks by stress waves. Nomenclature is included in Figure 23 for future reference.

In the experimental set-up of Figure 23, a lead driver is dropped onto the piston assembly which closes the vents as it moves downward. Pressure then rises due to reduction of the void space and increases of the burning rate brought about by increased pressure. A necessary but not sufficient condition for DDT is reductions of the height of the void space to hundredths of a cm or less in order to generate pressures of the order of ten k bars or more.

Ignition was accomplished by placing six 0.5 cm diameter balls of the propellant along with 4 gm of ball powder upon the upper surface of the propellant cylinder located at the bottom of the chamber. The ball powder was ignited by an electrical heater wire. Then the burning ball powder ignited the balls of propellant that ignited the cylinder of propellant. In this regard, ball powder burns too rapidly to ignite the propellant cylinder directly. Propellant balls are more susceptible to ignition than the surface of the propellant cylinder because much of their surface is in the flame zone. Immediately following ignition, the electrical heater wire was withdrawn from the chamber so it would not interfere with subsequent movements of the piston.

Following ignition, the propellant was allowed to burn for 25 sec to achieve steady burning. Steady burning is desired in that it is easier to characterize than transient burning. Then the driver was released forcing the piston assembly into the chamber. The nominal clearance between the bearing surfaces of the piston and chamber was only 0.001 in. to deter gas escape. Various lubricants were used to maintain piston velocities.

IIIT RESEARCH INSTITUTE

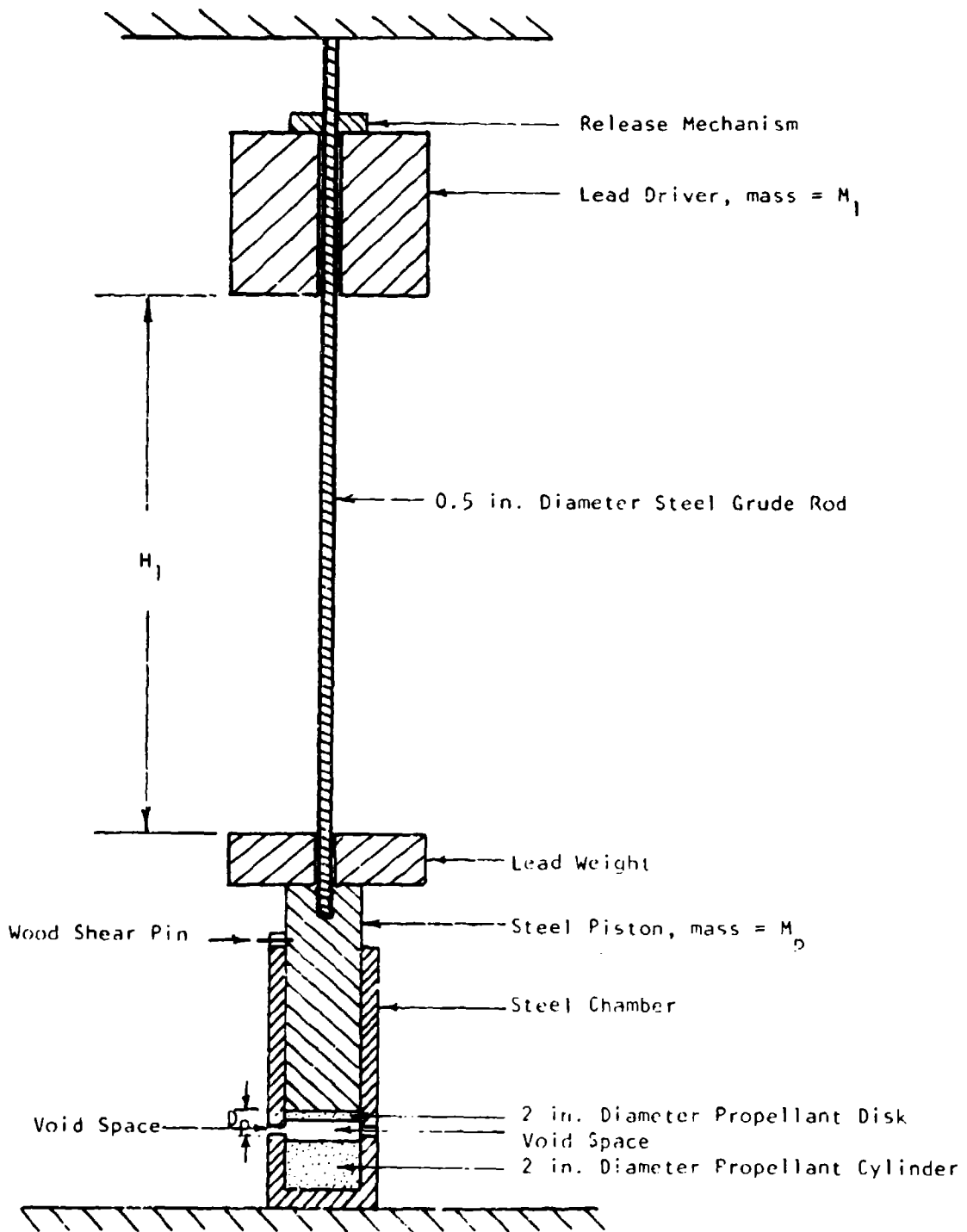


Figure 23. Schematic of experimental setup.

Closest approach of the burning propellant surfaces (or minimum height of the void space) was determined by attaching a metal pin to the lower face of the piston. This pin extended through any propellant disk attached to the piston so the pin would indent the propellant cylinder. Such indentations would be preserved by sudden extinguishment of the burning provided the explosion did not destroy the propellant cylinder. Extinguishment, of course, is caused by reduction in the propellant heating brought about by sudden pressure relief, and by inadequate heat stored in the propellant to maintain burning at ambient pressure.

In the remainder of this section, we shall describe the experiments and analysis used to interpret the experimental results.

## 5.2 ANALYSIS

Three important factors affect the response of the burning propellant. The first is increases of the heat fluxes brought about by pressure rises. This aspect of the problem is described in Section 2.1.1. The second factor is velocities of the piston assembly and driver following impact. Impacts were assumed ideal in which energy and momentum is conserved. Resultant velocities  $V_p$  and  $V_d$  of the piston assembly and driver, respectively, are

$$V_p = [2 M_d V_{do} + (M_p - M_d) V_{po}] / [M_d + M_p] \quad (33)$$

$$V_d = [2 M_p V_{po} + (M_d - M_p) V_{do}] / [M_d + M_p] \quad (34)$$

where  $M_p$  and  $M_d$  represent masses of the piston assembly and driver, respectively, while  $V_{po}$  and  $V_{do}$  represent their velocities immediately prior to impact. The above equations not only apply to the initial impact wherein  $V_{po} = 0$ , but also to any subsequent impacts.

The third and last feature of the experiments has to do with drag forces imparted the moving piston by lubricants and contaminant produced by the burning. These drag forces are assumed to vary linearly with the piston velocity so that

$$M_d \frac{dV_p}{dt} = M_p g - A_d d V_p - A_p \Delta P g \quad (35)$$

where  $A_d$  and  $A_p$  represent the areas of the bearing surface and face of the piston, respectively, while  $d$  and  $g$  represent the drag coefficient and acceleration of gravity, respectively. Pressure rises per unit area are represented by  $\Delta P$ . Preliminary estimates of the drag coefficients  $d$  were determined prior to the burning propellant experiments by measuring the terminal velocity  $\bar{V}_p$  of the piston and applying the applicable terms of Equation 35 to yield

$$d = M_p g / (A_d \bar{V}_p) \quad (36)$$

Actual  $d$  values were estimates by use of a computer code that accounts for each of the above phenomena. Evaluation was made by trial and error until predicted closure of the void space agreed with measurements. Drag coefficients were along appreciably higher than preliminary estimates due to contamination and/or loss of lubricant.

### 5.3 EXPERIMENTAL RESULTS

A composite propellant containing appreciable HMX was selected due to the lack of apparatus to press pure HMX cylinders of the large sizes desired. The propellant samples were manufactured by the Jet Propulsion Laboratory (AFJPL) in California. The AFJPL specifications indicated that the composite propellant contained:

PEG	6.250 percent
CAB	0.250
N-100	12.500
TEGON	12.500
HMXa	40.000
HMXe	25.000
MNA	1.000
ZRC	1.000
CARBON	0.500
TPB	0.025
MALIC,	
ANHY.	0.025
	<hr/>
	100.000 percent

According to AFJPL, the resultant propellant cylinders were of poor quality. They were very oily, stuck to anything they touched, and did not hold their

IIT RESEARCH INSTITUTE

shape when removed from their molds. In order to achieve firm propellant cylinders, the propellant was wrapped in highly absorbent paper to remove the excess oil. Then the propellant was pressed into desired shapes to eliminate any voids. In doing so, the propellant specimens incurred a weight loss of approximately 7 percent.

Eighteen experiments were conducted using the experimental set-up illustrated by Figure 23. The first two of the eighteen experiments, namely Nos. 1 and 2, were used to develop the ignition system described earlier in Section 5.1. Table 4 summarizes the remaining experiments. Nomenclature is presented in Figure 23. The experiments differed according to the:

- height and weight of the driver
- weight of piston assembly
- presence of propellant disk on piston
- location of propellant surfaces with respect to vent holes
- type of lubricant used on bearing surfaces

In tests 3 through 8 the bearing surfaces were coated with a 0.002 in. film of silicone grease (prior to inserting piston into chamber), and the driver weights and heights were progressively increased in an attempt to increase the order of the explosion by improving closure of the void space. Test 4 was lost due to failure of the driver release mechanism. Tests 6 and 7 produced the most severe explosion driving the 101 lb driver/piston against the reinforced concrete ceiling of the test facility. The explosion was clearly not a detonation. In fact the only damage to the chamber and piston was caused by the falling driver and piston assembly. Test 8 yielded the least severe explosion of the 6 tests. In fact there were two minor explosions. The first explosion was due to venting caused by the piston being driven above the vents by the pressure rise. The second explosion was caused by the driver driving the piston downward pass the vent holes a second time.

The greatest closure or smallest height of the void space obtained in tests 3 through 8 was 0.8 cm in test 7. All other closures were in excess of 1.0 cm. Such void space heights are much too great to achieve DDT. Initially, the lack of closure was attributed solely to burning propellant particles becoming wedged between the piston and chamber after being embedded in the lubricant.

As a consequence, it was decided to conduct test 9 with no lubricant whatsoever. It may be observed that closure was not improved. In fact,  $\bar{S}_x$  increased to 1.5 cm. Residues found on the chamber walls after the test prevented a clean piston from being pushed through the chamber by hand.

At this point, it was decided to sprinkle powdered graphite upon the silicone grease film used in tests 3 through 8. It was hoped that the powdered graphite would deter combustion products from sticking to the silicone grease. This lubricant was used in tests 10 and 11 without success. Drag coefficients  $d$  were essentially the same as those obtained using the silicone grease without powdered graphite. Improved closure (0.6 and 0.7 cm) of the void space was attributed to increased driver weight and height along with a greater piston assembly mass. Even though the closure was about an order of magnitude less than desired, the explosions of test 10 was sufficiently intense to propel 209 lbs against the facility's concrete ceiling with considerable force. The guide rod shown in Figure 23 was driven into the concrete to a depth of 1 inch. Remainder of the rod was bent much like a pretzel. Energy needed to propel the piston/driver against the ceiling exceeded 35 percent of the energy stored in the foam layer.

In tests 12 and 13, it was decided to discard the use of silicone grease in favor of powdered graphite wetted with silicone oil for purposes of integrity. Drag coefficients were higher than those found earlier; explosions were less severe and closure was not significantly improved from tests 10 and 11. The latter is in spite of greater driver heights. It is suspected that much of the lubricant was swept away by the flow of combustion products.

The best lubricant found involved using an extremely thin layer of silicone grease to hold the graphite particles. The thin silicone grease film was formed by first applying the grease to the piston and chamber walls, and then inserting the piston into the chamber to remove excess grease. This process was repeated until the piston fell freely through the chamber. Then powdered graphite was sprinkled upon those lubricant surfaces that subsequently will be exposed to the hot combustion products. This lubricant was first used in test 14. Two reasons may be advanced for the improved lubrication. These are greater resistance of the film to the flow of combustion gases, and a reduction of the likelihood of particles being embedded in the thin film of

silicone grease. These reasons are of course, conjectural. The above lubricant was used in each of the remaining tests.

In test 15, the masses of the driver and piston assembly were increased appreciably, and the height  $S_x$  of the void space (distance between bottom of vent holes to surface of burning propellant cylinder at time of driver release) was reduced. This test was particularly discouraging in that there was no improvement in closure and the driver/piston assembly was thrown less than 1 ft upward.

Two possibilities remained for the inadequate closure. The first is thermal distortion of the exposed chamber walls; and the second is much more rapid consumption of the foam layer than anticipated by analysis. Test 16 was used to check the former hypothesis. The sole difference with test 15 was a 0.020 in. reduction of the piston's diameter so the piston would hopefully not be slowed or stopped by distortions of the heated chamber walls. In this regard, the exposed chamber walls absorbed an average heat flux of 4 cal/cm<sup>2</sup>-sec, based upon thermal measurements. The essentially identical results of tests 15 and 16 discounts thermal distortions of the chamber walls as the prime cause of poor closure. A further test of the hypothesis was achieved by redesigning the set-up of Figure 23 as illustrated by Figure 24. In this set-up, the chamber walls are thermally protected by attaching a steel sleeve to the piston with the propellant contained within the sleeve. The clearance between the sleeve and piston was increased from its normal value of 0.001 in. to 0.004 in. to counter any thermal expansion of the sleeve. This device was used in test 17. The lack of improved closure suggests thermally-induced distortion was not the cause of piston stoppage.

At this point, it concluded that lack of closure was due to the production of higher than anticipated gas pressures while the piston was moving downward. Two possible causes are ejection of molten HMX and particulates from the foam layer into the combustion zone, or a more rapid increase in the rate of internal heating than predicted by  $\rho Q_s r_f$ . Both would speed gasification of the foam layer and hence accelerate pressure rises. Unfortunately, elaborate instrumentation needed to test this hypothesis were not included in the scope of work and could not be afforded by existing funds. Instead, it was decided to vent some of the gas during closure, and determine--whether or not closure

IIT RESEARCH INSTITUTE

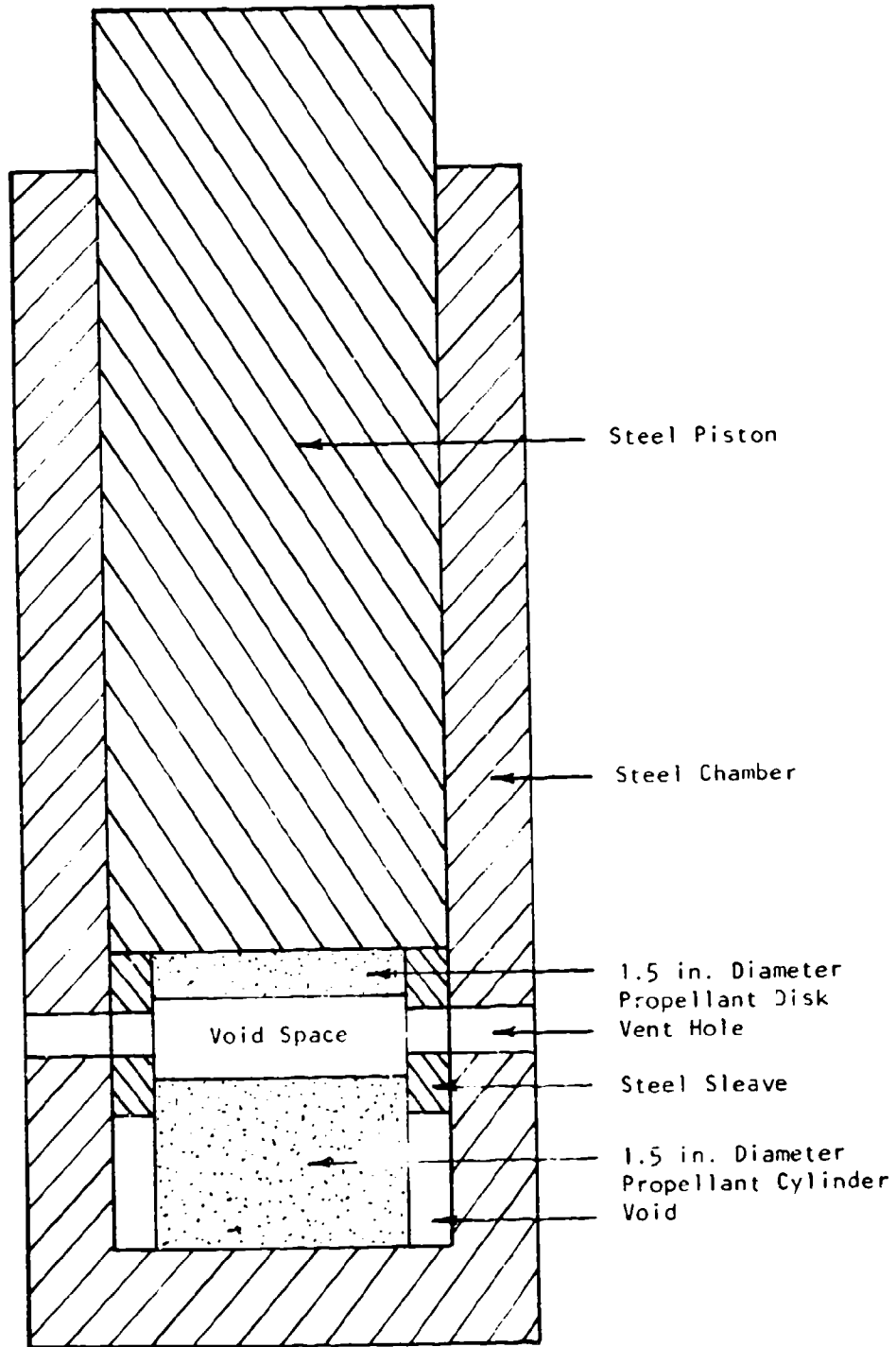


Figure 24. Modified piston and chamber used in Test 17.

IIT RESEARCH INSTITUTE

is improved sufficient to cause DDT. The additional vent was provided in the final test, namely No. 18. An illustration indicating provisions for the additional venting is presented in Figure 25. Here a single 0.25 in. diameter vent hole was located beneath the surface of the propellant cylinder with a passage way cut in the propellant. Vent size was purely a guess lacking information regarding how much gas must be allowed to escape to achieve desired closures of the order of hundredths of a cm or less.

Remaining features of test 18 are summarized in Table 4 along with experimental results. This test produced two low-order explosions very similar to that produced in test 8. The composite weight of 275 lbs of the driver and piston assembly rose less than 1 ft. Closure, however, improved from a previous low of 0.6 cm to 0.3 cm. Unfortunately, the resultant closure was roughly an order of magnitude larger than predicted for DDT by analysis. Nevertheless, the improved closure was sufficient to indicate that the foam mass is consumed much faster than expected. At this point in time, further testing was suspended due to the lack of propellant.

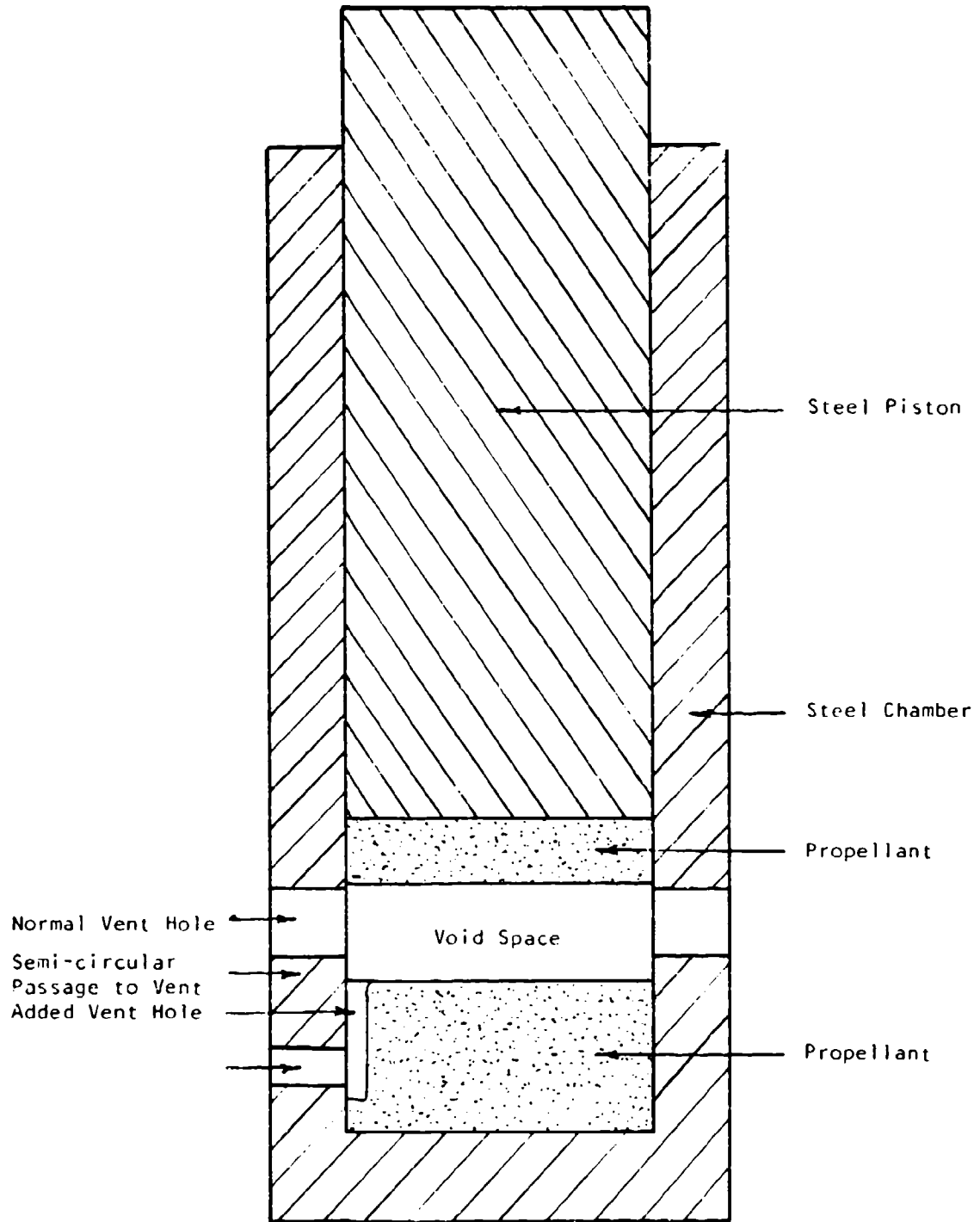


Figure 25. Modified chamber used in Test 18.

TABLE 4. SUMMARY OF TEST RESULTS

Test No.	Number of Propellant Specimens*	M <sub>d</sub> <sup>†</sup> lbs	M <sub>p</sub> <sup>†</sup> lbs	S <sub>x</sub> <sup>†</sup> cm	D <sub>p</sub> <sup>†</sup> cm	H <sub>d</sub> <sup>†</sup> ft	Lubricant <sup>†</sup>	S <sub>x</sub> <sup>‡</sup> cm	He, # ft	d, lbs/cm -sec	Comments
3	2	64	5	1.3	2.8	1.0	1	1.2	4.3	42	Explosion
4	2	64	5	1.3	4.0	1.0	1	--	--	--	Driver didn't drop
5	2	64	5	1.3	4.0	1.0	1	1.2	3.6	32	Explosion
6	2	96	5	1.9	4.0	2.0	1	1.5	>5.0	50	Explosion
7	1	96	5	1.6	2.8	3.1	1	0.8	>5.0	52	Explosion
8	2	150	5	1.6	2.8	3.1	1	--	1.0	--	Double explosion
9	2	108	128	1.6	2.8	2.6	2	1.5	1.9	136	Explosion
10	1	108	101	2.3	1.7	2.8	3	0.6	>5.0	31	Explosion
11	1	108	39	1.7	2.0	3.7	3	0.7	3.7	47	Explosion
12	2	108	155	1.2	2.8	4.0	4	0.7	1.0	92	Explosion
13	1	108	155	1.5	2.8	4.0	4	0.7	1.0	94	Explosion
14	1	54	32	2.2	2.5	1.1	5	0.6	3.6	10	Explosion
15	2	207	191	0.8	2.5	3.2	5	0.6	1.0	11	Explosion
16	2	207	191	0.8	2.5	3.2	5	0.6	1.0	10	Explosion
17	2	180	191	0.8	2.5	3.2	5	0.7	1.0	9	Explosion
18	2	180	95	0.6	1.6	4.2	5	0.3	1.0	--	Double explosion

\*Two propellant specimens conforms to set-up shown by Figure 23; one propellant specimen indicates omission of propellant disk on piston.

†Distance between bottom of vent holes and surface of burning propellant at time of driver release.

‡Lubricant No. 1 consisted of a 0.002 in. thick film of silicone grease; lubricant No. 2 involved bare surfaces; Lubricant No. 3 involved a 0.002 in. grease covered with powdered graphite; lubricant No. 5 involved a 0.001 in. thick film of silicone grease covered with powdered graphite.

#Minimum height of void space during test.

He Height at which driver/piston assembly were blown upward by the explosion. Heights in excess of 5 ft indicate collision with reinforced concrete ceiling of test facility.

## 6. SUMMARY/CONCLUSIONS

### 6.1 ANALYSES

This study concludes that burning HMX melts and forms a melt on a foam layer over the burning surface. During steady burning, this layer progressively decreases with increased pressure. The primary threat of DDT or HMX based propellants lies in the relatively high thermal energy content of its melt. When triggered into dynamic burning, the melt will rapidly gasify. In restricted spaces such as cracks, its gasification will generate pronounced pressure transients. In this regard, stress waves can trigger rapid gasification of the melt layer by partially collapsing cracks. Such stress waves originate when cracks propagate into relatively high-pressure cavities. Subsequently, their amplitude may be increased by reflection of the stress wave by stiff media such as a motor case.

The effect of stress waves is two fold. The first is to raise the gas pressure by reducing the void volume and thereby increase the rate of heat transfer into the burning in an propellant. In turn the increased heat fluxes accelerate the burning in an exponential fashion. The second effect of stress waves is to restrain crack expansion while the pressures always peak before decaying. When sufficiently strong stress waves act upon burning-propellant cracks with adequate melt (depends upon stress wave), pressure rises of the order of tens of kbars can be generated within a fraction of a  $\mu\text{sec}$  (See Section 4). This statement is conservative in that it neglects ejection of melt and/or particulates into the hot combustion gases or other processes that apparently speed consumption of the melt (See Section 5.3). Step-wise pressure waves with amplitudes of the order of tens of Kbars are known to initiate a composite propellant containing HMX in impact experiments.<sup>5</sup>

One can conceive of three situations in which adequate melt layers needed for DDT can develop. These are:

1. burning in cracks or debonds at near-ambient pressures wherein melt layers are greatest

2. sustained low rates of heating (less than that associated with burning or 1 bar of pressure) of unignited propellant surfaces,
3. accumulation of flowing melt within cracks

Of the three only the third appears plausible. In this regard, Item 1 is highly unlikely in that it requires burning under conditions of sustained near-ambient pressures. Moreover, Item 2 appears unlikely in that it is difficult to comprehend how low rates of heating could be sustained long enough to develop substantial melt.

Item 3 seems most likely because of the appreciable velocities of gases flowing into cracks from high-pressure cavities (i.e. of the order of hundreds of meters/sec), and the relatively slow rate of gasification of newly melted HMX (i.e. more than an order of magnitude slower than molten HMX during burning). Melt will accumulate if sufficient molten HMX is moved over the crack surfaces by the gas flows rather remaining stagnant or being swept into the gas stream. Questions regarding the latter remain to be resolved. If melt flows over the crack surfaces, then the cooler most recent melt can mix with hotter melt in the crack. The result would be a lowering of the latter's temperature and hence its rate of gasification. By this process, substantial melt may accumulate even though the propellant is burning at high pressures wherein the melt layer is normally very thin. Only by this process, does it appear possible to generate the amounts of melt needed for DDT when a single crack or debond is present.

Appreciably less melt is required for DDT when several burning propellant cracks are present. The latter is because the consequence of stress waves acting upon a burning-propellant crack are stress waves of greater amplitude. By the process progressively stronger stress waves can be generated as they move from one burning crack to other similarly oriented burning cracks. Transient gas pressures will progressively increase in successive cracks and reach their peaks in shorter and shorter times. In this regard, rapid pressure-rises are an important requirement for DDT as well as high-amplitude pressures of the order cited earlier. That is because the pressure waves must develop extremely steep fronts to cause detonation. At pressures in excess of roughly 10 kbar, higher pressure portions of the wave will eventually catch up with the lower pressure portions of the wave provided sufficient propellant is present. That is why rapid pressure rises are important.

IIT RESEARCH INSTITUTE

## 6.2 EXPERIMENTS

### 6.2.1 Melt Layer

The mass of the melt or foam present during steady burning of the HMX-based composite propellant was determined at ambient pressure. Its purpose was two fold; namely to determine whether or not there is sufficient melt to produce DDT experimentally and to gain a better appreciation of the validity of the substantial melt predicted for pure HMX at 1 bar (See Figure 4).

The determinations involved calorimetric measurements of the total heat content in burning propellant specimens, and thermocouple measurements of the heat content in the solid propellant. From these measurements the heat content of the melt was obtained and divided by the enthalpy of pure HMX at its reaction temperature to estimate the mass of the melt layer. It was found to be in substantial agreement with that predicted for pure HMX. Computer runs indicated it was adequate to produce DDT by the experimental design described in Section 5 of this report.

### 6.2.2 DDT Experiments

A total of eighteen experiments were conducted in an attempt to initiate a burning HMX based propellant. They involved partial closure of the void space above burning propellant in a manner analogous to that produced by stress waves acting upon burning propellant cracks. The latter was achieved by driving a piston into a chamber containing a burning cylinder of the propellant.

In each experiment, partial closure of the void space over the burning propellant cylinder resulted in blowing the piston and driver weights out of the chamber. Detonation did not occur. Lack of detonation was attributed to inadequate closure of the void space predicted for DDT. There are three possible causes of the lack of adequate closure. These are:

- excessive drag on piston caused by contaminants being weighed between piston and chamber walls
- thermal deformation of chamber walls exposure to combustion gases
- more rapid consumption of melt or foam layer than anticipated theoretically

Several materials were used to lubricate the bearing surfaces. Initial lubricants were not satisfactory in that the piston was slowed by passage of combustion products into the 0.001 clearance between the piston and chamber. Subsequently, closure was improved using a film of silicon grease of thickness less than 0.001 in. over which produced graphite was sprinkled. The possibility of piston stoppage due to thermal deformation of the chamber walls was assessed by increasing the piston/chamber clearance several fold. Lack of closure improvement suggested thermal distortion was the cause of the problems. From these results, it appears that inadequate closure was due to extremely rapid consumption of the melt or foam layer. This conclusion is consistent with a two-fold reduction of the void space when a vent hole was provided to lessen the pressure rise. Two possibilities may be advanced of for extremely rapid burning. The first is blow off of melt and particulate into the hot gas stream wherein they are most rapidly gasified. The second is inadequacy of the expression  $\rho Q_s r_f$  used to described the internal heating. This expression implies a constant quantity of the heat is transferred to the foam layer per unit mass of gas evolved. Residence times of the gases in the foam will affect the extent to which the gases decompose in the foam and hence the amount of heat transferred to the foam. In highly dynamic burning under consideration, order of magnitude variations of residence time may be expected---first due to order of magnitude changes in the amount of foam present, and second due to reductions of gas bubbles brought about by rising pressures.

The above conclusions pertaining to consumption of the melt layer do not alter the conclusion presented in the report in regard to DDT. Instead they make DDT More likely than anticipated by speeding gasification of the foam provided adequate crack close is achieved.

### 6.2.3 Recommendations

Based upon conclusions drawn from Section 6.2.2, appreciably higher piston speeds and/or smaller void-volume heights are needed to validate our DDT theory. It is anticipated that piston speeds at least several times greater than those used herein should be used depending upon the mass of the piston

and its appendages. Driving the piston with gas pressure would provide a controlled versatile means for developing the necessary momentum. In addition it is desirable to reduce the initial void space.

The above device is also amenable to experiments with which to assess how substantial melt layers are consumed during accelerated burning. Here pressure transducers would be needed along with means to determine the void space dynamically. A comparison of the dynamic pressures with analytic predictions would serve to indicate the adequacy of existing burn theories and means for improvement thus predictions capability.

While the above requirements are rather costly, it is believed that they should shed considerable light on DDT. Because of the extremely dynamic burn conditions, they would also severely test existing theories of how such propellants burn dynamically.

## APPENDIX A

### METHOD FOR PREDICTING TRANSIENT TEMPERATURE IN SOLID-PHASE OF PROPELLANTS

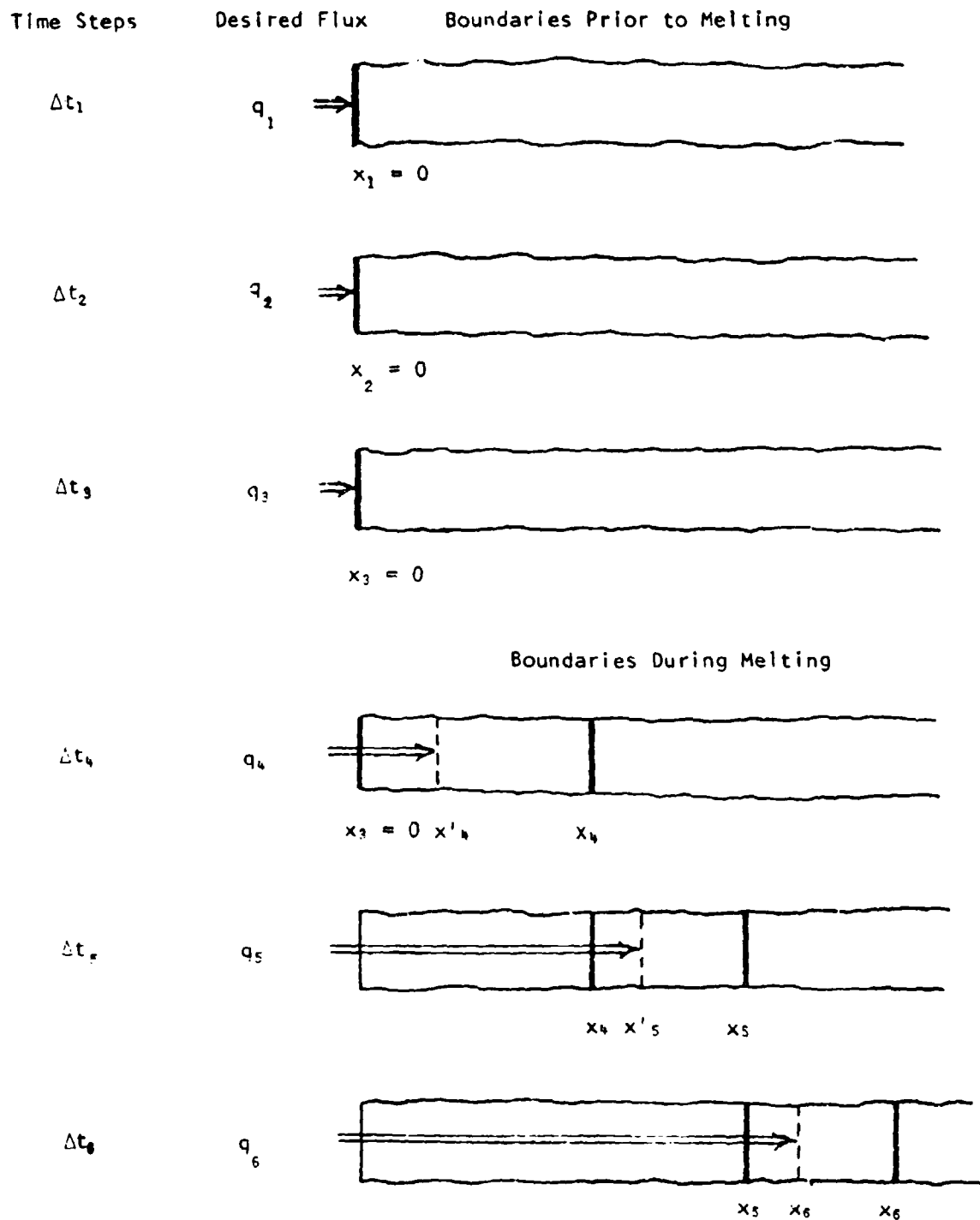
In order to predict dynamic burning of propellants, it is necessary to compute the propellant temperatures under rapidly changing pressures and conditions. In this regard, finite difference methods requires periodic refinement of various spacial increments when the burning becomes extremely dynamic. As a consequence such methods are not computationally efficient in dealing with problems in which the temperature gradients within the propellant become extremely pronounced.

In view of the above, a method of sources and sinks was developed. It predicts transient temperatures within solid propellants at desired depths and times. The method may be applied to burning propellants with or without a melt or foam layer on the propellant's surface.<sup>o</sup>

#### 1. DESCRIPTION OF METHOD

In this method, the propellant is assumed to be semi-infinite in that heat penetrates only relatively shallow depths during burning. The computational method utilizes a fixed cartesian coordinate system in which the melt or burn interface is considered to move in a step-wise fashion with respect to time as shown in Figure A-1. As will be shown later, mass removal is accounted for by adjustment of the heat fluxes.

Prior to the start of melting or burning the "moving boundary" is of course stationary. During subsequent time steps  $\Delta t_i$ , the interface is considered to move from depth  $x_{i-1}$  to  $x_i$ . Time average heat fluxes crossing the moving solid-propellant boundary during  $\Delta t_i$  are represented by  $q_i$ . These fluxes are evaluated from the boundary conditions at the moving boundary, and vary with the propellant, and pressures and temperatures to which it is subjected. Each flux  $q_i$  or more precisely  $q_i'$  is located at particular depth that yields the same quantity of heat entering the propellant at  $x_i$  during



Desired Fluxes  $q_i$  Differ From Applied Fluxes  $q_j$

Figure A-1. Schematic of computational procedure.

IIT RESEARCH INSTITUTE

$\Delta t_i$  as would be produced by the moving boundary. Means for determining the appropriate depth are described in Section 1.2 of this appendix.

In this discussion to follow, the subscript  $i$  designates values of  $q$ ,  $t$  and  $x$  associated with prior time steps while the subscript  $j$  indicates values for the most recent time step  $\Delta t_j$ . First we shall discuss means for achieving the given flux  $q_j$  at the desired depth  $x_j'$ .

### 1.1 APPLIED HEAT FLUXES

The consequence of applying fluxes at a depth  $x_j'$  during  $\Delta t_j$  is to create conductive fluxes  $q_{i,j}$  at the depth  $x_j'$  during the most recent time step  $\Delta t_j$ . These conductive fluxes must be eliminated to account for propellant removal.

Therefore in order to produce a desired flux  $q_j$  at  $x_j'$ , it is necessary to apply a flux  $q_j'$  equal to the difference between  $q_j$  and the undesirable conductive flux. To illustrate the above mathematically we shall represent the undesirable time-average conductive flux produced at  $x_j'$  during  $\Delta t_j$  by each of the prior fluxes  $q_i'$  and  $q_{i,j}$ . Thus, the time-average flux  $q_j'$  to be applied at  $x_j'$  during  $\Delta t_j$  is

$$q_j' = q_j - \sum_{i=1}^{j-1} q_{i,j} \quad (A-1)$$

Clearly one must know  $q_{i,j}$  in order to determine the flux  $q_j'$  that needs to be applied at  $x_j$  to achieve the desired flux  $q_j$ . For this purpose, consider the temperature rises produced within a semi-infinite body of uniform initial temperature by flux  $q_j'$  of constant magnitude applied at a depth  $x_j'$  for all times to starting at  $t_{j-1}$ . The temperature rises beneath  $x_j'$  are given by:<sup>9</sup>

$$C q_j' \sqrt{t - t_{j-1}} \operatorname{ierfc} \frac{x - x_j}{2\sqrt{\alpha(t - t_{j-1})}} \quad (A-2)$$

where  $C = 2/\sqrt{k\rho C_p}$  and  $t \geq t_{j-1} = \Delta t_1 + \Delta t_2 \dots \Delta t_{j-1}$ . Equation A-2 applies to the most recent flux  $q_j'$ . In order to determine the temperature rises produced by prior fluxes  $q_i'$ , one must recognize that temperature rises

produced by a series of constant fluxes are additive. Replacing the subscript  $j$  in the above expression by  $i$  yields the temperature rise produced by the flux  $q_i'$  applied for all times  $t$  greater than  $t_{i-1}$ . Replacing  $t_{i-1}$  by  $t_i$  yields the temperature rise produced by the same flux when it is applied for all times  $t$  greater than  $t_i$ . Subtracting the latter temperature rises from the form yields the temperature rises produced by  $q_i'$  applied over the time step from  $t_{i-1}$  to  $t_i$ . The result is given below:

$$C q_i' \left[ \sqrt{t - t_{i-1}} \operatorname{ierfc} \frac{x - x_i'}{2 \sqrt{\alpha(t - t_{i-1})}} - \sqrt{t - t_i} \operatorname{ierfc} \frac{x - x_i'}{2 \sqrt{\alpha(t - t_i)}} \right] \quad (\text{A-3})$$

Here  $x \geq x_i'$  and  $t > t_i$ .

Multiplying the above expression by the negative value of the propellant's thermal conductivity  $K$  and differentiating with respect to  $x$  yields the time-dependent fluxes at  $x$  presented below

$$q_i' \left[ \operatorname{erfc} \frac{x - x_i'}{2 \sqrt{\alpha(t - t_{i-1})}} - \operatorname{erfc} \frac{x - x_i'}{2 \sqrt{\alpha(t - t_i)}} \right] \quad (\text{A-4})$$

The subscript  $i$  ranges from 1 to  $j - 1$ .

To find the time-average fluxes  $q_{ij}$  at  $x_j'$  over the time step  $\Delta t_j$ , we shall replace  $x$  and  $t$  of Equation A-4 by  $x_j'$  and  $t_{j-1} + \tau$ , respectively. The integral of the result over the time step divided by  $\Delta t_j$  yields the desired time-average flux  $q_{ij}$  presented below:

$$q_{ij} = \frac{q_i'}{\Delta t_j} \int_0^{t_j} \left[ \operatorname{erfc} \frac{x_j' - x_i'}{2 \sqrt{\alpha(t_{j-1} - t_{i-1} + \tau)}} - \operatorname{erfc} \frac{x_j' - x_i'}{2 \sqrt{\alpha(t_{j-1} - t_i + \tau)}} \right] d\tau \quad (\text{A-5})$$

As one would expect  $q_{ij}$  is zero if the propellant interface does not recede, i.e.,  $x_j' = x_i' = 0$ . Performing the integration of Equation A-5 yields:

$$q_{ij} = \frac{q_i'}{t_j} [F(y_1) - F(y_2) - F(y_3) + F(y_4)] \quad (A-6)$$

Where the function F is expressed below in terms of the normal distribution function represented by N.

$$F(y) = -\frac{\operatorname{erfc} y}{y^2} + y^2 \sqrt{\pi} \exp(-y^2) + 4 N(\sqrt{2}y)$$

and  $y_1, y_2, y_3,$  and  $y_4$  are

$$y_1 = (x_j' - x_i')/2 \sqrt{\alpha(t_{j-1} - t_{i-1})}$$

$$y_2 = (x_j' - x_i')/2 \sqrt{\alpha(t_{j-1} - t_{i-1} + \Delta t_j)}$$

$$y_3 = (x_j' - x_i')/2 \sqrt{\alpha(t_{j-1} - t_i)}$$

$$y_4 = (x_j' - x_i')/2 \sqrt{\alpha(t_{j-1} - t_i + \Delta t_j)}$$

Substituting  $q_{ij}$  into Equation A-1 yields the flux  $q_j'$  that must be applied at  $x_j'$  during  $\Delta t_j$  in order to achieve the net desired flux  $q_j$ . Means for defining the depth  $x_j'$  are described in the following section.

## 1.2 DEPTHS AT WHICH FLUXES ARE APPLIED

The depth  $x_j'$  at which  $q_j'$  is applied affects the heat transfer into the propellant at the depth  $x_j'$ . Location of the depth  $x_j'$  becomes more critical as the size of the spacial increment  $\Delta x_j$  increases. For optimal utility, it is desirable that the method be capable of using relatively large  $\Delta x_j$  wherein the depth  $x_j'$  is important. The desired depth  $x_j'$  may be defined in terms of the fraction  $\xi$  of the displacement  $\Delta x_j$  during  $\Delta t_j$  as follows:

$$x_j' = x_{j-1} + \xi (x_j - x_{j-1}) = x_{j-1} + \xi \Delta x_j \quad (A-7)$$

The factor  $\xi$  varies with the acceleration of the interface and the thermal conduction parameter  $\beta$  described below:

$$\beta = \Delta x_j / (2 \sqrt{\alpha \Delta t_j}) \quad (A-8)$$

Two sets of calculations were used to determine the above dependence.

First a given displacement  $\Delta x_j$  was subdivided into small increments wherein the location of the applied times ceased to be important. Then the quantity of heat passing the depth  $x_j$  during  $\Delta t_j$  was computed by summing the time-dependent fluxes predicted by Equation A-4. It is this quantity of heat that should be effected by the correct  $\xi$  value using the single spacial increment  $\Delta x_j$ .

The final set of calculations involved varying  $\xi$  with the single increment  $\Delta x_j$  until the heat entering the depth  $x_j$  during  $\Delta t_j$  equaled that predicted above using extremely fine spacial and temporal increments. Results are presented in Table A-1.

TABLE A-1.  $\xi$  VALUES

Changes of Rate of Melting During Time Step $\Delta t_j$ , percent	$\xi$ Values (dimensionless)		
	$\beta = 0.04$	$\beta = 0.08$	$\beta = 0.12$
-80	0.289	0.295	0.300
-60	0.321	0.325	0.329
-40	0.322	0.335	0.339
-20	0.336	0.339	0.341
0	0.335	0.337	0.341
40	0.334	0.336	0.338
80	0.329	0.331	0.332
150	0.319	0.320	0.321
300	0.297	0.299	0.300
600	0.270	0.270	0.270

### 1.3 TEMPERATURE/FLUX PREDICTIONS

Temperature rises produced by the heat fluxes  $q_j'$  and  $q_i'$  at depths  $x_j'$  and  $x_i'$  over time steps  $\Delta t_j$  and  $\Delta t_i$  are given by Equations A-2 and A-3 respectively. Values for  $q_j'$  or  $q_i'$  are determined from Equations A-1 and A-5 while the depths  $x_j'$  and  $x_i'$  are found as described by the previous section.

IIT RESEARCH INSTITUTE

In that the temperature contributions are additive, the temperature of the surface of the solid propellant at the melt or burning interface at the end of the time step  $\Delta t_j$  is given by Equation A-8.

$$T(x_j) = C \sum_{i=1}^{j-1} q_i' \left[ \sqrt{t_j - t_{i-1}} \operatorname{ierfc} \frac{x_j - x_i'}{2 \sqrt{\alpha(t_j - t_{i-1})}} - \sqrt{t_j - t_i} \operatorname{ierfc} \frac{x_j - x_i'}{2 \sqrt{\alpha(t_j - t_i)}} \right] + C \sqrt{\Delta t_j} q_j' \operatorname{ierfc} \frac{x_j - x_j'}{2 \sqrt{\alpha \Delta t_j}} + T_0 \quad (\text{A-8})$$

For propellants that melt,  $T(x_j)$  equals the melt temperature  $T_m$  once melting starts.

The heat flux entering the solid propellant at  $x_j$ ,  $t_j$ , namely

$$\sum_{i=1}^{j-1} q_i' \left[ \operatorname{erfc} \frac{x_j - x_i'}{2 \sqrt{\alpha(t_j - t_{i-1})}} - \operatorname{erfc} \frac{x_j - x_i'}{2 \sqrt{\alpha(t_j - t_i)}} \right] + q_j' \operatorname{erfc} \frac{x_j - x_{j-1}'}{2 \sqrt{\alpha(t_j - t_{j-1})}} \quad (\text{A-9})$$

equals the flux supplied externally when the propellant is not melting. When propellants melt, it is necessary to combine the fluxes heat flux expressed above with expressions describing the external and internal generated heating of the melt layer to arrive at the temperature of the melt and its rate of gasification. The latter expressions are presented in Section 2.

## 2. VALIDATION OF METHOD

### 2.1 PROPELLANT WITH FOAM LAYER

Here we are concerned with checking the method by assessing how well dynamic burning approaches known steady burning under fixed external conditions.

IIT RESEARCH INSTITUTE

Initially, the propellant is considered at a uniform ambient temperature. Thereafter the propellant is exposed to a constant heat flux equal to that present during steady burning associated with a preselected constant pressure. Dynamic calculations were then conducted until the changes of the burn velocities, foam temperatures, and foam masses were insignificant. These results are presented in Table A-2 under the columns titled Model Predictions. Values predicted by Equations 13 and 14 are in the columns titled Analytical Predictions.

It may be observed that the model predictions are in good agreement with the analytical predictions. They indicate that the cummulation of errors by the numerical calculations is relatively small.

#### Propellant Without Foam Layer

In this case validation was achieved by comparing the regression rate predictions with those obtained by Kooker using finite differences. The calculations involved the KTSS combustion model.<sup>4</sup> Initially, Kooker<sup>10</sup> considered the solid propellant burns at a steady regression rate. Thereafter the pressure  $\bar{P}$  (dimensionless) is considered to increase as follows

$$\bar{P} = 1 + 2.5 (1 - \exp(-2.5 \bar{t})) \quad (A-10)$$

where  $\bar{t}$  represents the dimensionless time.

The consequences of increased pressure is increased regression rates. Figures A-2 and A-3 present the results of Kooker<sup>10</sup> following the increase of pressure described by Equation A-10. In these figures, N and M are pressure and temperature rise exponents describing steady and nonsteady burning rates, respectively. H is proportional to the internal heating. Our results are presented by dots.

It may be observed that our regression rate predictions are in reasonably good agreement with those obtained by Kooker<sup>10</sup> considering both methods are numerical. Number of time steps used to generate the IITRI results of Figures A-2 and A-3 were 73 and 188, respectively, and involved execution times of 5 and 37 seconds on a 1109 computer.

TABLE A-2. COMPARISON OF MODEL PREDICTIONS WITH STEADY-STATE ANALYTICAL PREDICTIONS

Pressure, bars	Steady Burn Velocities, cm/sec		Foam Temperatures, °K		Foam Mass, g/cm <sup>2</sup>	
	Analytical Predictions*	Model Predictions	Analytical† Predictions	Model Predictions	Analytical† Predictions	Model Predictions
1	0.030	0.030	600.8	601.3	0.03760	0.03570
10	0.217	0.216	653.2	653.9	0.00738	0.00702
32	0.591	0.599	688.5	688.7	0.00250	0.00242
50	0.867	0.861	702.5	703.3	0.00162	0.00154
100	1.574	1.560	727.1	728.1	0.00080	0.00075

\*From Equation 2

†From Equation 15

‡From Equations 15 and 16

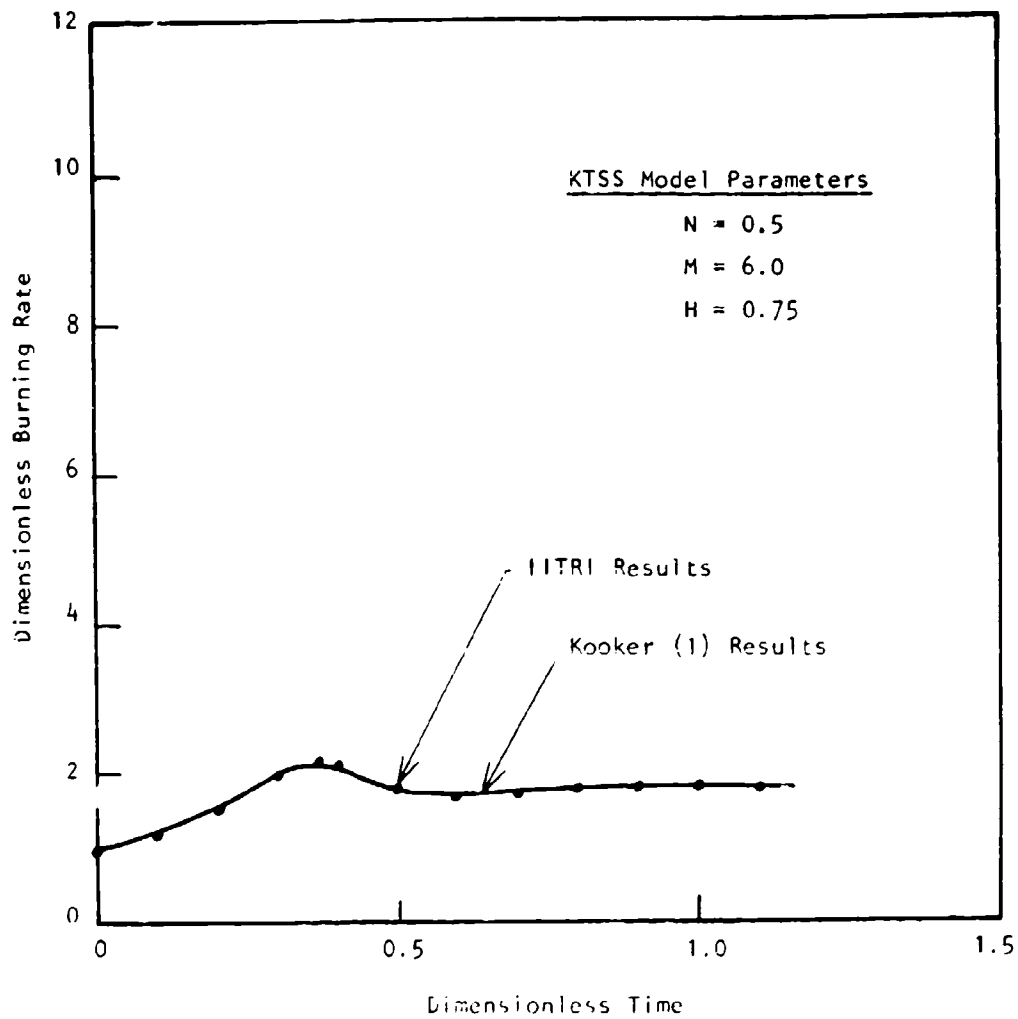


Figure A-2. Validation of IITRI method with  $H = 0.75$ .

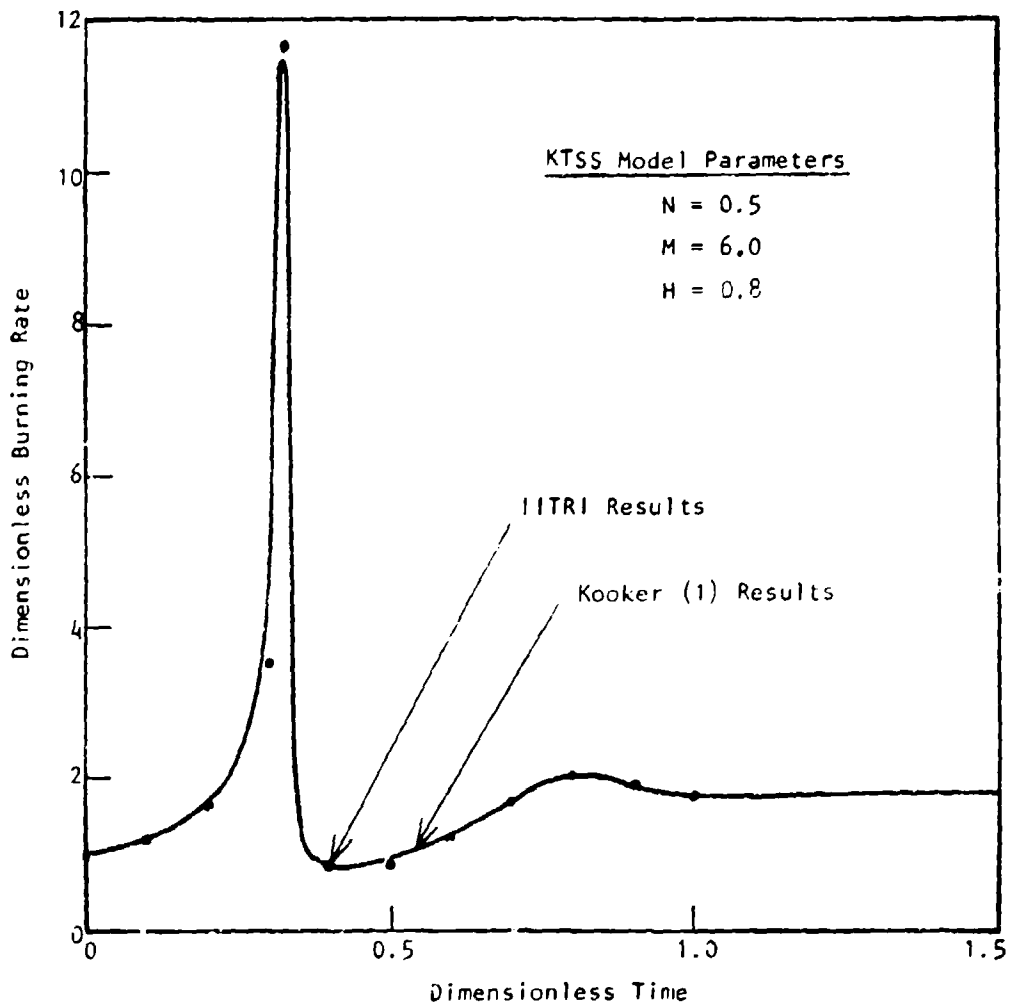


Figure A-3. Validation of IITRI method with  $H = 0.3$ .

## APPENDIX B

### DETERMINATION OF CONSTANTS $c_1$ AND $c_2$ FOR HEAT-TRANSFER COEFFICIENT $h$

Here we shall determine the constants  $c_1$  and  $c_2$  of Equation 7 by use of estimated foam masses during steady burning of HMX. To this end, two equations must be solved for  $c_1$  and  $c_2$ .

The first equation is based upon Equations 6 and 7 for steady burning as follows:

$$\bar{q}_p = c_1 (\exp(-E/\bar{T}_f(P)))^{c_2} (\bar{T}_f - T_m) \quad (B-1)$$

To support steady burning,  $\bar{q}_p$  must also satisfy

$$\bar{q}_p = \rho \bar{r}_f [C_p (T_m - T_0) + Q_m], \quad (B-2)$$

Equating the above expressions for  $\bar{q}_p$  and using Equation 13 yields

$$c_1 (\exp(-E/\bar{T}_f(P)))^{c_2} (\bar{T}_f - T_m) = \rho a P^n (C_p (T_m - T_0) + Q_m) \quad (B-3)$$

Equation B-3 represents the first of the two equations.

The second equation is obtained from Equations 13 and 14 for steady velocities  $\bar{r}_f$ . It is given by

$$\rho a P^n = \bar{M}_f(P) Z \exp(-E/\bar{T}_f(P)) \quad (B-4)$$

At any given pressure  $P$ , all of the parameters of Equations B-3 and B-4 are known except for the constants  $c_1$  and  $c_2$ , and the foam mass  $\bar{M}_f$  and temperature  $\bar{T}_f$  at the given pressure. To determine the constants  $c_1$  and  $c_2$  it is necessary to know the melt mass  $\bar{M}_f(P)$  at two pressures  $P$ . In this regard, Boggs<sup>1</sup> has photographed the "frozen" HMX foam layer following extinguishment of the burning by rapid pressure relief. Bogg's photographs indicate that the steady-state foam thickness at 34 bars is roughly 25  $\mu$ m

IIT RESEARCH INSTITUTE

thick; at 68 bars it appears to be about half as thick as that at 34 bars of pressure.

Assuming that the density of the "frozen foam" is half the density (1.9 g/cm<sup>3</sup>) of solid high-density HMX propellant yields

$$\bar{M}_f(34) = 0.0024 \text{ g/cm}^2 \quad (\text{B-5})$$

$$\bar{M}_f(68) = 0.0012 \text{ g/cm}^2 \quad (\text{B-6})$$

At this point, one may raise a question regarding the correspondence between the mass of "frozen" foam with the foam mass present during steady burning. In other words, how much does the foam mass change following pressure relief due to further outgassing and melting?

The one-dimensional model (foam) was used to resolve the above question. It indicated that the foam mass at 34 bars will decrease by 13.4 percent during pressure relief while the foam mass at 68 bars will decrease by 19.4 percent. The somewhat greater reduction (percentagewise) of the foam mass present at 68 bars is due to its higher temperature. The result is more rapid mass loss of initially smaller amounts of foam.

While the above mass losses are significant, they are probably small compared to errors in estimating the thickness and density of the "frozen" foam. For this reason, the foam masses presented by Figure 4 shall not be corrected until better measurements of the "frozen" foam mass are available. Substituting each pair of  $\bar{M}_f$ , P values of Equations B-5 and B-6 into Equation B-4 and solving for  $\bar{T}_f(P)$  with the propellant properties given in Appendix F yields

$$\bar{T}_f(34) = 689.5^\circ\text{K} \quad (\text{B-7})$$

$$\bar{T}_f(68) = 713.0^\circ\text{K} \quad (\text{B-8})$$

Substituting the above  $T_f$ ,  $P$  values into Equation B-3 yields two equations involving the two unknowns  $c_1$  and  $c_2$ .

$$c_1 = 7.6 \cdot 10^5 \text{ cal/cm}^2\text{-sec-}^\circ\text{K} \quad (\text{B-9})$$

$$c_2 = 0.338 \text{ (dimensionless)} \quad (\text{B-10})$$

## APPENDIX C

### IGNITION CRITERIA

Ignition refers to the start of propellant burning. Knowledge of when ignition occurs is important in that the heat flux undergoes rapid change following ignition.

Ignition represents a complex phenomenon resulting in exponential temperature rises of the evolved reaction gases caused by exothermic decomposition. Ignition is a function of a number of factors foremost of which are:

- temperature, composition and flow rates of the gases evolved by the heated propellant, and
- physical and thermal environment into which the gaseous products are discharged.

Fortunately, as will be seen later in this appendix, one need not conduct detailed analyses of each of the above phenomena to approximate ignition times. Nevertheless one should be aware of the phenomena in designing experiments with which to establish ignition criteria for the propellant/conditions of interest.

At present, ignition criteria are based upon propellant temperature, or combinations of a constant incident flux and duration.<sup>1,2</sup> The former criterion is of greater value in that it applies to time-dependent heat fluxes. Ignition is predicted when the temperature of the propellant's surface or at some propellant depth exceeds a critical temperature.

In the remainder of this section we shall examine the effect of disregarding gas evolution upon the ignition time. Before doing so it should be noted that a one-to-one correspondence does not exist between foam (or surface) temperature and rates of gas evolution.

Table C-1 presents predicted foam temperatures following exposure of HMX to specified incident heat fluxes. Internal heating is also provided for even though it is not specified in the table. The initial temperature of the propellant is 294°K. Foam or propellant surface temperatures are specified

at times at which the gas evolution rates equal specific fractions  $\delta$  of the steady burning rate of 0.03 cm/sec at 1 atmosphere of pressure.

TABLE C-1. PREDICTED FOAM TEMPERATURES AND REGRESSION RATES OF HEATED HMX

Incident Heat Flux* cal/cm <sup>2</sup> -sec	Temperature T <sub>f</sub> yielding to specified fraction $\delta$ of the steady burning rate, K <sup>†</sup>				
	$\delta = 0$	$\delta = 0.1$	$\delta = 0.5$	$\delta = 0.9$	$\delta = 1.0$
0.5	555.0 (211.44)	565.6 (237.19)	580.9 (239.33)	587.7 (239.58)	588.9 (239.60)
0.1	555.0 (52.86)	570.30 (61.99)	585.9 (64.45)	589.1 (64.71)	592.3 (64.74)
2.0	555.0 (13.25)	579.0 (16.50)	588.9 (18.25)	594.9 (18.50)	596.1 (18.53)
10.0	555.0 (0.529)	603.5 (0.668)	607.8 (0.875)	611.6 (0.959)	612.4 (0.974)
30.0	555.0 (0.0587)	629.1 (0.0697)	630.4 (0.0902)	631.8 (0.01031)	632.2 (0.1057)
100.0	555.0 (0.00529)	665.6 (0.00577)	664.5 (0.00681)	664.5 (0.00760)	664.6 (0.00770)

\*Incident heat fluxes are from some external heat source

†Times of occurrence given in parentheses in seconds.

First it should be observed that more time is needed to initiate melting than the remaining time needed to achieve steady-state rates of gasification ( $\delta = 1.0$ ). The latter is due to rapid decomposition of HMX at and above its high melt temperature.

From Table C-1 it may be observed that an ignition criterion based solely upon a given temperature implies that ignition occurs with differing rates of gas release. The latter reemphasizes the question raised earlier regarding the significance of the differing rates of gas evolution upon the ignition time.

In order to perform the above assessment we shall assume that the critical ignition temperature lies between the melt temperature of 555 K and the lowest temperature cited in Table C-1 for  $\delta = 1$ . A  $\delta$  value of 1 is chosen since it corresponds to a regression rate equal to the steady burning rate. Based on the above assumptions, the critical temperature lies between 555.0 and 588.9 K.

Applying the above temperature range to Table C-1 indicates that the ignition time is between 211.4 and 239.6 sec when the incident flux is 0.5 cal/cm<sup>2</sup>-sec; and between 0.00559 and a linearly interpolated value of 0.00544 sec when the incident flux is 100 cal/cm<sup>2</sup>-sec. Notice that the above times differ by only 13.3 and 2.8 percent for the two fluxes. These results suggest that ignition temperature provides a reasonably accurate means for predicting ignition at least for HMX. Rates of gas evolution are of secondary importance.

For the present we shall assume that the ignition temperature of HMX equals the mean temperature (572°K) associated with the range of temperatures cited earlier. Ignition times  $t_i$  required to achieve a foam temperature of 572°K may be determined from Table F-1 as a function of  $q$ . They are given approximately by

$$t_i = 59/q^2 \quad (C-1)$$

where  $t_i$  is in seconds when  $q$  is in cal/cm<sup>2</sup>-sec. Experimental results presented in reference 12 indicate that the exponent <sup>2</sup> of Equation F-1 can vary from about 1.6 to 2.0 depending upon the propellant. Most propellants involve coefficients only a fraction of the coefficient 59 presented by Equation F-1. The relatively large coefficient is attributed to the high melt temperature of HMX and the fact that much of the "ignition time" is expended in initiating melting. In this regard, times to initiate melting are proportional to the square of the difference between the melt temperature and the initial temperature of the propellant.<sup>9</sup>

## APPENDIX D

### DYNAMIC REGRESSION RATES OF PROPELLANTS HAVING NO FOAM LAYER

Dynamic regression rates of completely solid propellants are usually predicted in terms of the surface temperature of the propellant.<sup>3</sup> No account is made for propellant temperatures beneath the surface or of the mass of propellant involved at elevated temperatures. Clearly the greater the amount of propellant at elevated temperatures, the greater the rate of gasification should be. It is with this reason that the following analysis is conducted.

To account for variations in the propellant temperature as a function of depth, dynamic regression rates are predicted by integrating the Arrhenius relationship as follows:

$$r_f = z \int_0^{\infty} \exp(-E/(T(x) + T_0)) dx \quad (D-1)$$

where  $x$  represents depth beneath the burn surface at time  $t$ . Due to the presence of pronounced temperature gradients during burning, Equation D-1 need only be integrated over shallow depths.

A simpler more approximate expression for  $r$  may be achieved by approximating the temperature rises by

$$T(x) = T(0) \exp(-C_3 x) \quad (D-2)$$

where  $C_3$  is given by

$$C_3 = q/(KT(0)) \quad (D-3)$$

Substituting  $T(x)$  of Equation D-2 into Equation D-1, and integrating by parts with the neglect of second-order terms yields

$$r_f \sim \frac{KZ}{q\bar{E}} \exp(-\bar{E}/(T(o) + T_o)) (T(o) + T_o)^2 \quad (D-4)$$

It may be observed that the above expression differs in form from that conventionally used.<sup>3</sup> Usually the exponential function is multiplied by a constant. Here it includes the variable factor  $(T(o) + T_o)^2/q$  to account for variations in the depths of heated propellant.

In order to use Equation D-4, it is necessary to determine the time-dependent surface temperature  $T(o)$  of the propellant as well as the flux  $q$ . The flux  $q$  equals  $q_f$  given by Equations 11 or 12 depending upon whether or not there is a cross flow. The surface temperature  $T(o)$  may be calculated in terms of time-dependent fluxes  $q$  following the procedure described in Appendix A.

## APPENDIX E

### FLUID DYNAMICS AND STRESS WAVES

This appendix presents means used to predict gas flows withing cracks, and the generation and effect of stress wave upon cracks.

#### 1. FLUID DYNAMICS

##### 1.1 BASIC EQUATIONS

The equations of fluid dynamics are written with respect to the Eulerian frame of reference in which the independent variables are the distance,  $x$ , along the crack and the time,  $t$ . These equations represent the conservation of mass, momentum, and energy. The present gas dynamic model includes the effects of inertia, wall friction, mechanical wall response, and mass and energy addition. Heat transfer effects are incorporated into the energy addition term.

The conservation laws can be developed by considering a control surface enclosing an element of volume of length,  $dx$ . This control surface is illustrated in Figure E-1. The conservation laws state that the time rate of change of the entity considered, within the control volume must equal the net flux of this entity through the control surface, plus any related boundary contributions such as mass or energy addition, work done at the boundary, or boundary forces. The area of the flow channel,  $A$ , is one of dependent variables to be considered. However, in view of the fact that the lateral extent of a crack is very wide compared to its width  $C_w$ . We shall set the lateral extent of the flow channel equal to unity so that cross-section area  $A$  of the channel is:

$$A = 1 \cdot C_w \quad (E-1)$$

It should be noted that although this variable has the dimensions of length, a dimensional check of the following equations will imply that it should have

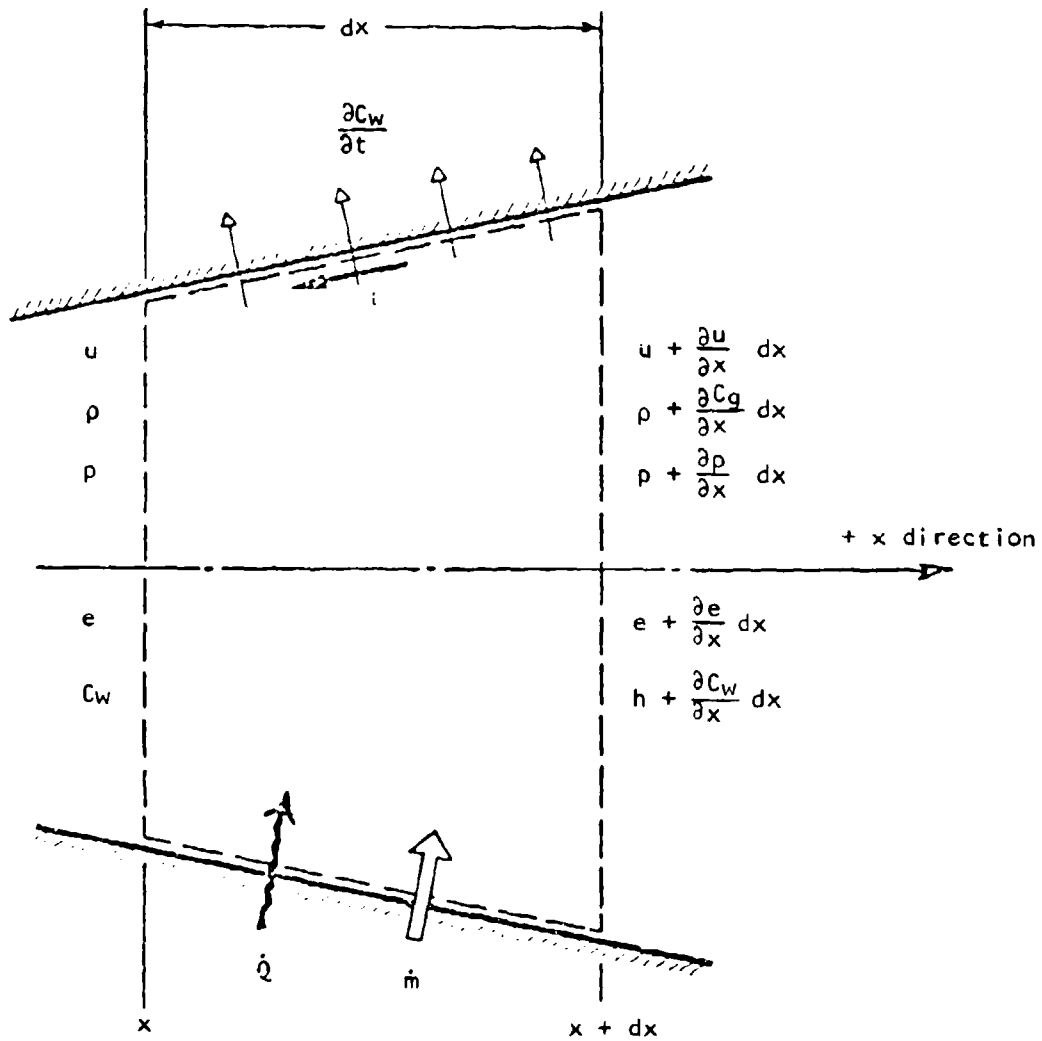


Figure E-1. Control surface for flow channel.

the dimensions of length squared. This is the case when it represents the area of the flow channel.

The three conservation equations are:

Mass

$$\frac{\partial \rho_g}{\partial t} + \rho_g \frac{\partial u}{\partial x} + u \frac{\partial \rho_g}{\partial x} = \frac{\dot{m}}{C_w} - \frac{\rho_g u}{C_w} \frac{\partial C_w}{\partial x} - \frac{\rho_g}{C_w} \frac{\partial C_w}{\partial t} \quad (E-2)$$

where:

$\rho_g$  = gas density

$u$  = gas velocity

$\dot{m}$  = mass addition per unit length per unit time

The wall motion (velocity) is given by  $(\partial C_w / \partial t)$  (see Figure E-1)

Momentum

$$\frac{\partial u}{\partial t} + u \frac{\partial u}{\partial x} + \frac{1}{\rho_g} \frac{\partial P}{\partial x} = - \frac{2\tau}{\rho_g C_w} - \frac{u\dot{m}}{\rho_g C_w} \quad (E-3)$$

where  $\tau$  = wall shearing stress. The wall shearing stress can be expressed in terms of the conventional pipe friction coefficient,  $F$ , defined by:

$$F = \frac{\tau}{\frac{1}{2} \rho_g u^2} \quad (E-4)$$

Furthermore this stress acts in a direction opposite to the fluid motion. The momentum equation can then be reformulated as:

$$\frac{\partial u}{\partial t} + u \frac{\partial u}{\partial x} + \frac{1}{\rho_g} \frac{\partial P}{\partial x} = - F \frac{u|u|}{C_w} - \frac{u\dot{m}}{\rho_g C_w} \quad (E-5)$$

The coefficient  $F$  is assumed to be constant at a nominal value because its value and dependence are uncertain for this complex flow environment.

Energy

$$\frac{\partial e_T}{\partial t} + u \frac{\partial e_T}{\partial x} + \frac{1}{\rho_g} \frac{\partial}{\partial x} (P u) = \frac{\dot{Q}}{\rho_g C_w} - \frac{P u}{\rho_g C_w} \frac{\partial C_w}{\partial x} - \frac{P}{\rho_g C_w} \frac{\partial C_w}{\partial t} \frac{e_T \dot{m}}{\rho_g C_w} \quad (E-6)$$

IIT RESEARCH INSTITUTE

where  $\dot{Q}$  = energy addition per unit length per unit time and  $e_T$  = specific total energy.

The specific total energy is given by:

$$e_T = e + \frac{1}{2}u^2 \quad (E-7)$$

where  $e$  = specific internal energy

Equations E-2, E-5, and E-6 have been arranged so that the terms which define the contributions of the special effects are grouped on the right hand side of the equal sign. When the sum of the terms of the right hand side are set equal to zero the conventional gas dynamic equations for the nonsteady flow in a constant area channel are obtained. These reduced equations will be used to establish the numerical method.

## 1.2 EQUATION OF STATE

The equation of state which has been selected initially for the propellant reaction products is that of a perfect gas. This equation of state is considered to be adequate for the initial phases of the investigation, but eventually a better formulation must be established.

The equation of the state of the gas is the following:

$$P (1/\rho_g - b) = RT \quad (E-8)$$

where  $R$  = gas constant and  $T$  = absolute temperature of the gas.

Furthermore, the specific heats at constant pressure and at constant volume are both constant. The internal energy  $e$  is given by:

$$e = P (1/\rho_g - b)/(\gamma - 1) \quad (E-9)$$

where  $\gamma$  = ratio of specific heats.

The sound velocity of the gas,  $c$ , is given as:

$$c = \sqrt{\frac{\gamma P}{\rho_g}} \quad (E-10)$$

IIT RESEARCH INSTITUTE

The values of the gas constant, the two specific heats and the ratio of specific heats are subject to some uncertainty. The following values have been selected for the gas constant and the ratio of specific heats for the reaction products

$$R = 3228 \text{ (cm}^2/\text{°C)}$$

$$\gamma = 1.2$$

### 1.3 FLOW CONFIGURATIONS AND BOUNDARY CONDITIONS

The solutions of the above field equations are subject to the initial conditions within the crack and to boundary conditions at both the upstream and downstream end of the flow channel. The initial conditions are those of a gas at rest ( $u(x) = 0$ ) and at some pressure  $p_0$ , an temperature,  $T_0$ . The initial height,  $C_{w0}(x)$  of the channel is also specified, however no initial wall motion is permitted (i.e.,  $(\partial C_{w0}/\partial t) = 0$ ). The propellant mass in the vicinity of the crack is thus in mechanical equilibrium with the initial pressure field within the crack.

Two basic crack configurations are treated. These are illustrated in Figure E-2. They consist of a high pressure cavity connected to the upstream end ( $x = 0$ ) of a crack of length,  $L_c$ , together with one of two downstream end conditions. One configuration has a simple closed end while the other configuration consists of a connection to a low pressure cavity. The high pressure cavity contains a gas at a pressure  $p_c$  and temperature  $T_c$ , both of which are held constant with respect to time. The gas pressure within the low pressure cavity is held constant at the level of the initial gas pressure within the crack (i.e.,  $P_0$ ) and only outflow is permitted.

The boundary conditions at the high pressure cavity end will depend upon whether the gas flow is into (inflow) or out of the crack (outflow). These boundary conditions are illustrated in the Hodograph plane of Figure E-3. The cavity State,  $S_c$ , (a rest state) is the appropriate reference state. When the pressure is low relative to the cavity pressure at the downstream end of the crack inflow may occur. If inflow does occur, the cavity gas will flow into the crack after first expanding isentropically (at constant energy) in the vicinity of the inlet. This expansion process will accelerate the gas and lower both the pressure and the sound velocity. The flow Mach number,  $M$

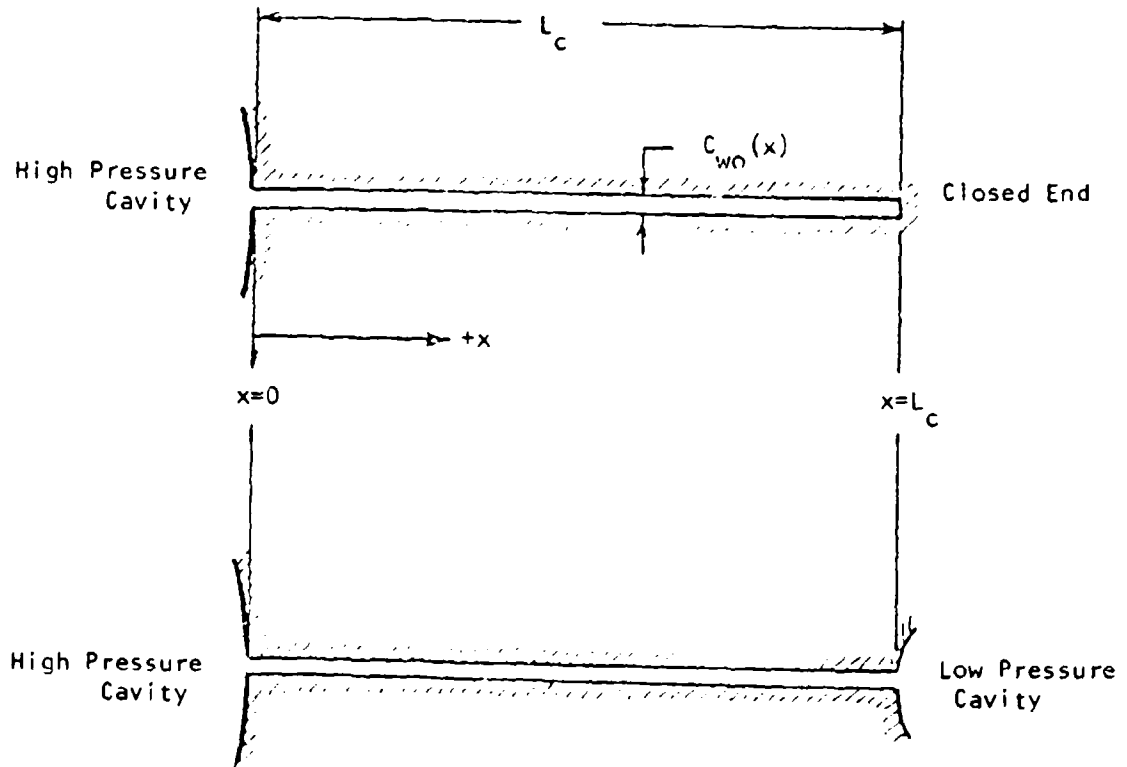


Figure E-2. Basic crack configurations.

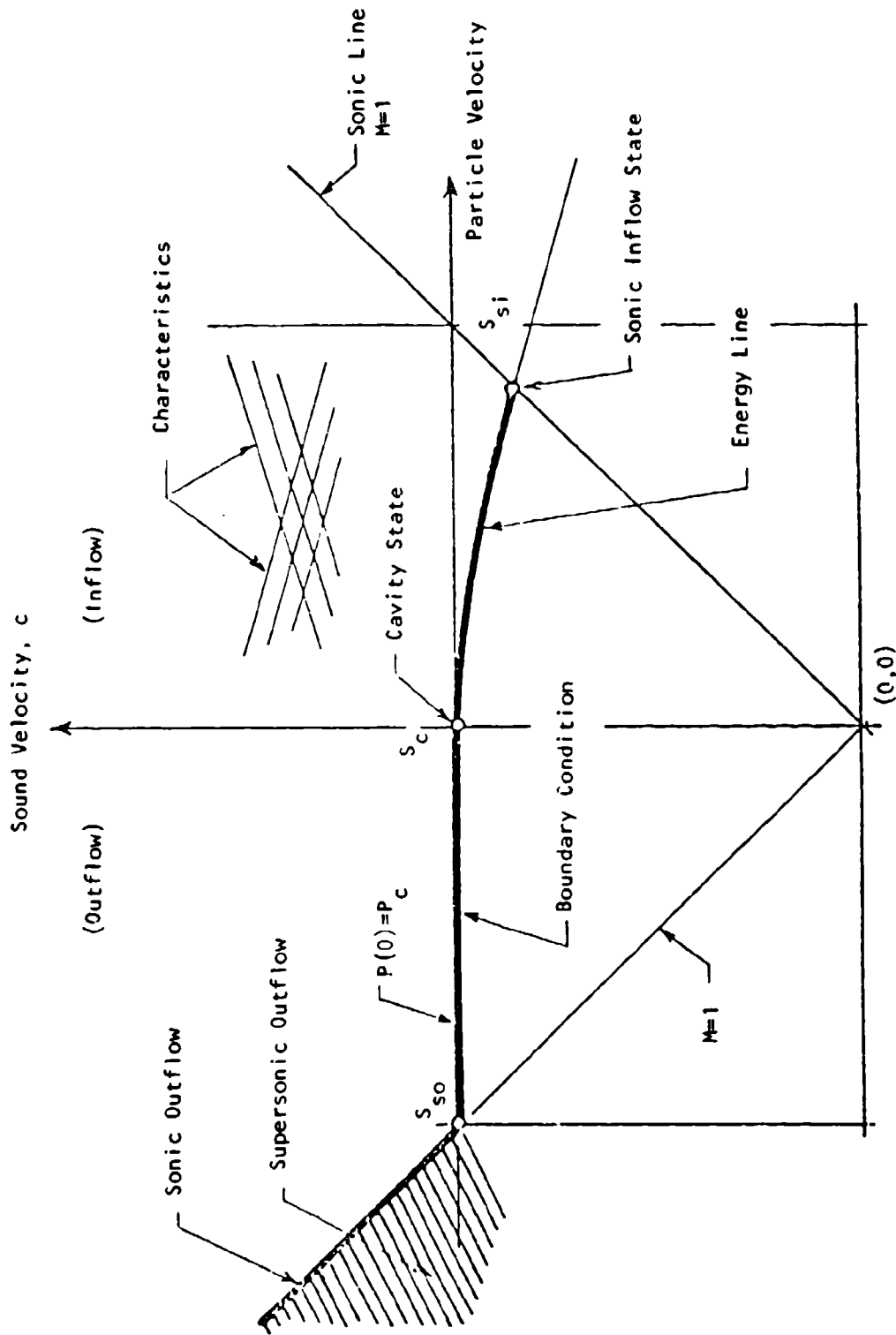


Figure E-3. Hodograph plane - boundary conditions at cavity end.

( $M \equiv u/c$ ) will increase until it reaches a state which is in equilibrium with the internal flow at the boundary provided it does not exceed a value of unity. At that critical point no further expansion can occur since, in effect, no further information regarding any additional expansion can be communicated back to the cavity. Any additional expansion, if it can occur, will occur as a non-steady expansion within the crack. The field equation will provide for the solution of this additional expansion. Thus the permissible boundary conditions at the downstream end of the crack under inflow conditions will be those states associated with the energy line bounded by the cavity State,  $S_c$ , at one end and the sonic inflow State  $S_{S_i}$  at the other end. The energy line is defined by

$$c_c^2 = c^2 + \left(\frac{\gamma - 1}{2}\right) u^2 \quad (E-11)$$

If subsonic outflow occurs the pressure at the upstream end of the crack will be equal to the cavity pressure,  $P_c$  (see Figure E-3). However, if the flow becomes sonic or supersonic then the pressure can change to any value such that the boundary state within the crack lies in the supersonic outflow region bounded by the sonic outflow line. This region is illustrated in Figure E-3.

The same boundary conditions apply at the low pressure cavity end of the crack when this configuration is used, however the present model does not permit inflow to occur. Some model modifications in this area may be needed however, they will be influenced by the physical model associated with this low pressure cavity, such as for example a cavity filling process with a subsequent buildup of pressure and temperature within the finite volume cavity.

The boundary condition for the closed end is a simple one of no flow (i.e.,  $u(L_c) \equiv 0$ ). The current model does permit the crack length to be extended arbitrarily whenever this configuration is used. Whenever the crack is extended, the new portion is filled with a rest gas at the initial pressure and temperature ( $P_0, T_0$ ) and the closed end boundary condition is applied to the new closed end location. This crack extension is, in effect, an instantaneous crack extension.

## 1.4 NUMERICAL PROCEDURE

The numerical solution technique employed in the gas dynamic model of the present study is, in its reduced form, a rather conventional Eulerian method of the FLIC (fluid in cell) type. This method was originally developed at the Los Alamos Scientific Laboratory.

The numerical solution of the foregoing equations proceeds from the initial conditions specified in a forward stepping time wise manner subject to the numerical solution to the field equations, auxilliary, time wise inputs, and the appropriate boundary conditions. An artificial viscous pressure term,  $q$ , is added to the thermodynamic pressure during the computations when the flow is subsonic and the compression rate is positive. This contributes to the suppression of flow discontinuities and to the computational stability in regions of subsonic flow.

### 1.4.1 The Computing Mesh

A one-dimensional mesh of uniform length  $\Delta x$ , cells is established. Each cell is identified by an indice,  $i$ , corresponding to its center. Thus the boundaries of the  $i$ th cell are at the location  $i \pm \frac{1}{2}$ . Increasing  $i$  corresponds to increasing  $x$ . The selection of uniform cell length is an initial convenience. If subsequent results indicate that one portion of the crack requires substantially greater resolution in the space variable,  $x$ , than do other portions then variable length cells can be introduced with little additional complications.

The values of the dependent variables are associated with the cell centers with the exception of the pseudoviscous terms which are computed at the cell boundaries. Assuming that all properties are known for each cell at some time  $t^n$ , the computational procedure is to determine the state in each cell at a later time  $t^{n+1} = t^n + \Delta t$ . The time step  $\Delta t$  is restricted in magnitude by conditions required for stability of the computations. The resulting space time grid network is illustrated in Figure E-4.

### 1.4.2 Stability Formulation

There are several stability type conditions that over investigators have found applicable with this type numerical technique. One such, restriction is that  $(u_{\max} \Delta t / \Delta x) < 1$ . If fluid particles were explicitly treated in the

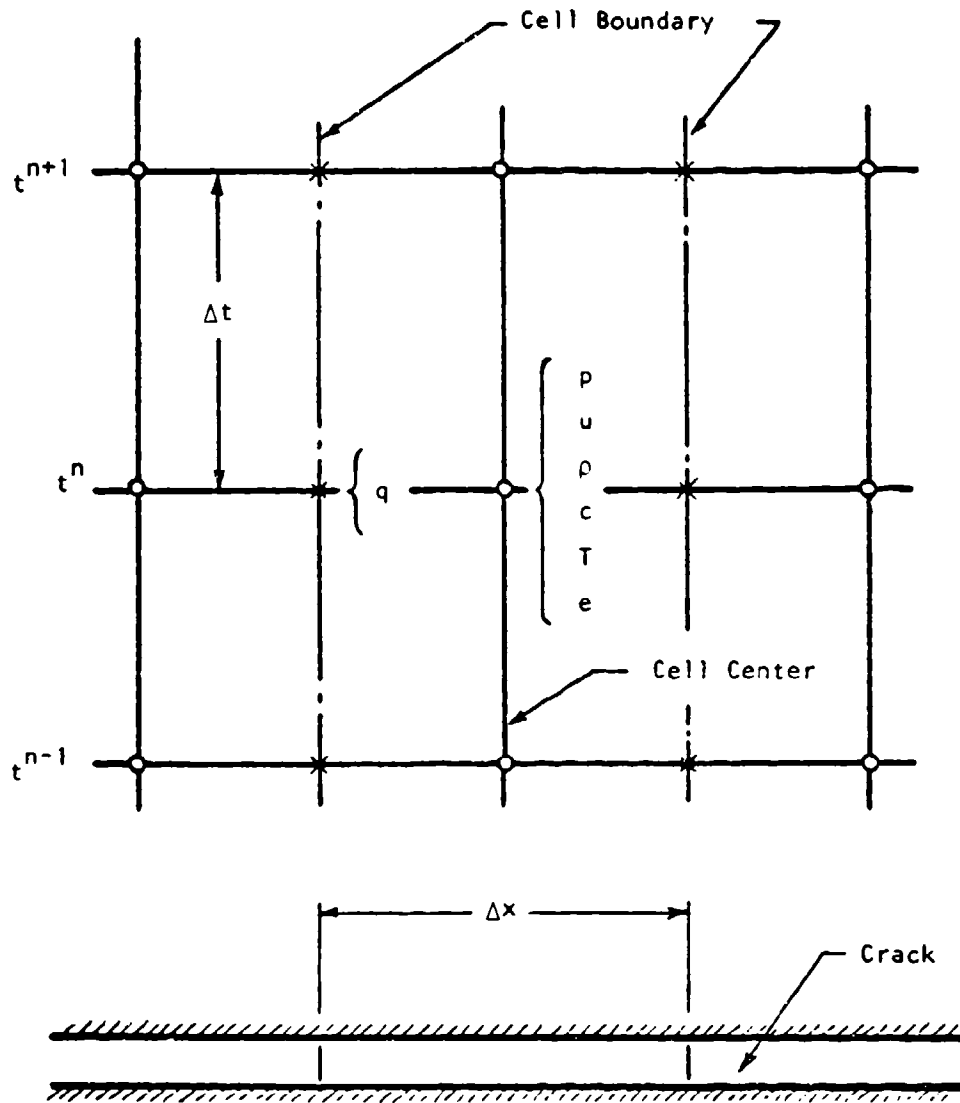


Figure E-4. One dimensional eulerian space time mesh.

computation, this criterion would prevent a particle from crossing a complete cell during one time step. In the pure Eulerian scheme the interpretation is made that the transport terms are calculated more accurately with corresponding improved averaging of the numerical fluctuations. A second restriction is the familiar Courant condition,  $c\Delta t/\Delta x < 1$ , which limits the propagation of fluctuations in the subsonic flow regions. Another source of instability is the computation of negative internal energies in the cell due primarily to the treatment of boundary conditions, but also from inherent numerical fluctuations. For a fluid obeying the ideal gas relation, the criterion that prevents negative internal energies is that  $4(\gamma - 1) u_{\max} \Delta t/\Delta x < 1$ . These stability criteria can be written as

$$\Delta t < \min \left( \frac{\Delta x}{u_i} \right), \text{ over } i \quad (\text{E-12})$$

$$\Delta t < \min \left( \frac{\Delta x}{c_i} \right), \text{ over } i \quad (\text{E-13})$$

$$\Delta t < 0.625 \min \left( \frac{\Delta x}{u_i} \right), \text{ over } i \quad (\text{E-14})$$

A simple stability criteria which satisfies all of the foregoing requirements is

$$\Delta t = \frac{1}{2} \min \left( \frac{\Delta x}{\max(u_i, c_i)} \right), \text{ over } i \quad (\text{E-15})$$

where the factor  $\frac{1}{2}$  is chosen to reflect the typical severity with which the inequalities (E-12) to (E-14) are generally applied. More details regarding the computations procedure are described in Appendix B of Reference 14.

## 2. GENERATION AND EFFECTS OF STRESS WAVES

The flow of high pressure gases into cracks within an adjacent propellant mass and any subsequent burning of these propellant surfaces will create a time varying pressure environment with the cracks. The surrounding propellant mass, which was originally in mechanical equilibrium with a low pressure distribution within the crack will respond to these new mechanical loads. It is the purpose of this appendix to describe several mechanical

IIT RESEARCH INSTITUTE

response models which have been used in conjunction with the gas dynamic model described in Section 1 of this appendix. One response model treats the early phases of the mechanical response when stress waves radiate from the crack and the crack is in a growth phase. The second model tests, in a simple fashion, the interaction of these radiating waves with the confining shell structure and their subsequent interaction with the crack. Under these conditions the crack growth will generally be arrested and may ultimately lead to partial or complete crack collapse.

## 2.1 MECHANICAL PROPERTIES OF THE PROPELLANT

The propellant response to the transient pressure loads within a crack will be that associated with the generation and propagation of stress waves in the propellant mass. The mechanical properties of most propellant materials are quite complex in that they are generally nonlinear, rate sensitive, and hysteretic in nature. Any simple mechanical response model cannot deal effectively with these types of complex behavior characteristics; however their impact upon the subject problem is not considered to be important. Rather it should be sufficient to model in some simple way the gross compressibility characteristics of the material. Thus the material will be viewed initially as a simple linear isotropic elastic material which does not yield or fail in any manner under the imposed stresses.

An elastic material will support two basic types of stress waves, i.e., dilatation and shear waves. These waves will propagate at the following speeds.

Dilatation Wave Speed,  $c_d$

$$c_d = \sqrt{\frac{E'}{\rho}} \sqrt{\frac{(1-\tau)}{(1-2\tau)(1+\tau)}} \quad (E-16)$$

Shear Wave Speed,  $c_s$

$$c_s = \sqrt{\frac{E}{\rho}} \sqrt{\frac{1}{2(1+\tau)}} \quad (E-17)$$

where:

$E'$  = Young's modulus

$\tau$  = Poisson's ratio

$\rho$  = density

The ratio of these two wave speeds is dependent only upon Poisson's ratio, viz:

$$\frac{c_s}{c_d} = \sqrt{\frac{1 - 2\tau}{2(1 - \tau)}} \quad (E-18)$$

The influence of Poisson's ratio is not great until it exceeds a value of about 0.45 and then it primarily affects the dilatation wave speed. The effective wave speed  $c^* = \sqrt{E'/\rho}$  is the most significant parameter. Since Poisson's ratio may be in the broad range of from 0.2 to 0.4 the dilatation wave speed will be approximately 1.2  $c^*$  while the shear wave speed will be approximately 0.6  $c^*$ . Thus the wave speed ratio will be approximately 0.5. The density of the propellants are well known and a nominal value of 1.5 g/cm<sup>3</sup> is used in the mechanical response models. A nominal value of 250 cm/ms was selected for the effective wave speed. This corresponds to a value of approximately 10<sup>6</sup> psi for Young's modulus and yields dilatation and shear wave speeds of 300 cm/ms (approximately 10,000 fps) and 150 cm/ms respectively.

## 2.2 INITIAL RESPONSE MODEL

During the entry phase of the gas flow into the crack a shock wave is generated which propagates at a speed (depending upon a number of parameters) of approximately 150 cm/ms. The pressure distribution behind this shock wave is relatively uniform. Weak disturbances (i.e., sound waves) propagate at the local sound speed relative to the gas. The sound speed is generally in the approximate range of from 50 to 100 cm/ms while the particle velocity is in the range of from -50 to 100 cm/ms. Thus these disturbances will propagate, on the average, at an absolute velocity of about 100 cm/ms. These considerations lead us to the following approximate inequality,

$$|(u \pm c)| < U \approx c_s < c_d \quad (E-19)$$

where:

- U = shock velocity in the gas
- $\mu$  = particle velocity in the gas
- c = sound velocity in the gas

Thus the wave system illustrated in Figure E-5 should exist initially. While this wave system is quite complex, many of the waves should be weak and need not be considered. This is especially true for the outrunning waves. The primary motion of the propellant mass will be in a direction normal to the crack, causing the crack width to increase locally. For this reason, a very simple, one dimension wave propagation (plane strain) model has been selected with which to define the response of the propellant adjacent to the crack. The momentum equation for this case is of the form

$$\Delta\tau = (\rho_g c_d) \quad (E-20)$$

where:

- $\Delta\tau$  = change in stress at the crack boundary
- $\Delta\mu$  = change in velocity at the crack boundary

The change in the stress at a given location along the crack is identical to the change in the corresponding gas pressure. Thus the wall velocity  $\dot{W}$  used in the gas dynamic model is given for the  $i$ th cell as

$$\dot{W}_i = (\rho c_d) (P_i - P_0) \quad (E-21)$$

where:

- $\rho c_d$  = shock impedance ( $\approx 450$  bars-ms/cm)
- $P_i$  = gas pressure
- $P_0$  = initial gas pressure

This expression was modified to include some contribution from the adjacent cells ( $i-1$ , and  $i+1$ ). In this manner some influence of the spreading nature of the propagation within the propellant mass was included, at least in a crude manner.

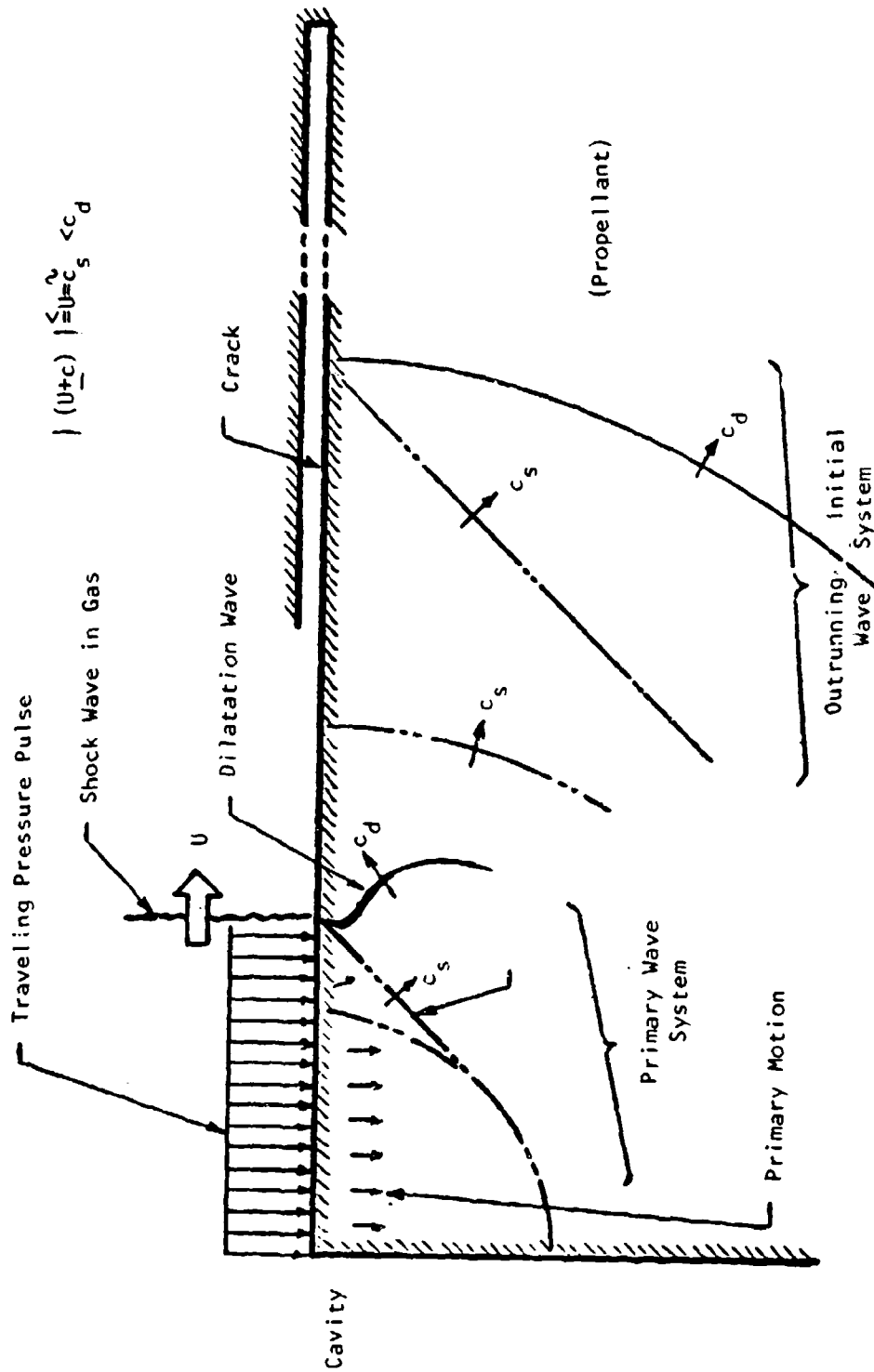


Figure E-5. Stress wave system in propellant during initial transient.

### 2.3 INFLUENCE OF REMOTE BOUNDARIES

The stress wave which radiates away from the crack will eventually react with the remote boundaries of the propellant mass, reflect and return, in some modified form, to the crack. These reflected waves will also influence the response crack walls. This type of wave system is illustrated in part a of Figure E-6. The nature of reflected wave system will be very complex and varied. For this reason a number of idealized reflection models will have to be established to define the configurations and conditions of interest.

As an initial attempt to treat the influence of the remote boundaries of the propellant mass one idealized model was established. This model is shown in part b of Figure E-6. It is designed to introduce the ultimate confining influence of a cased mass of propellant. A radiative stress field,  $\Delta P_r$ , which is the integrated or averaged value of the current local stress field along the entire crack is defined and assumed to propagate, under the conditions of the plane strain, into the propellant mass. These stress waves interact with the remote boundary after a delay time corresponding to a boundary/crack separation distance,  $L_e$ . The case is treated as a spring supported mass characterized by its inertia (weight per unit area) and stiffness (breathing mode of the case). The reflected wave system,  $\Delta P_s$  is evaluated from this case boundary interaction and applied uniformly along the crack after the appropriate delay period. This reflected wave system then interacts locally with the crack boundary such that the wall velocity changes according to the following momentum consideration

$$\dot{\Delta W}_i = -2\Delta P_s / (\rho c_s) \quad (E-22)$$

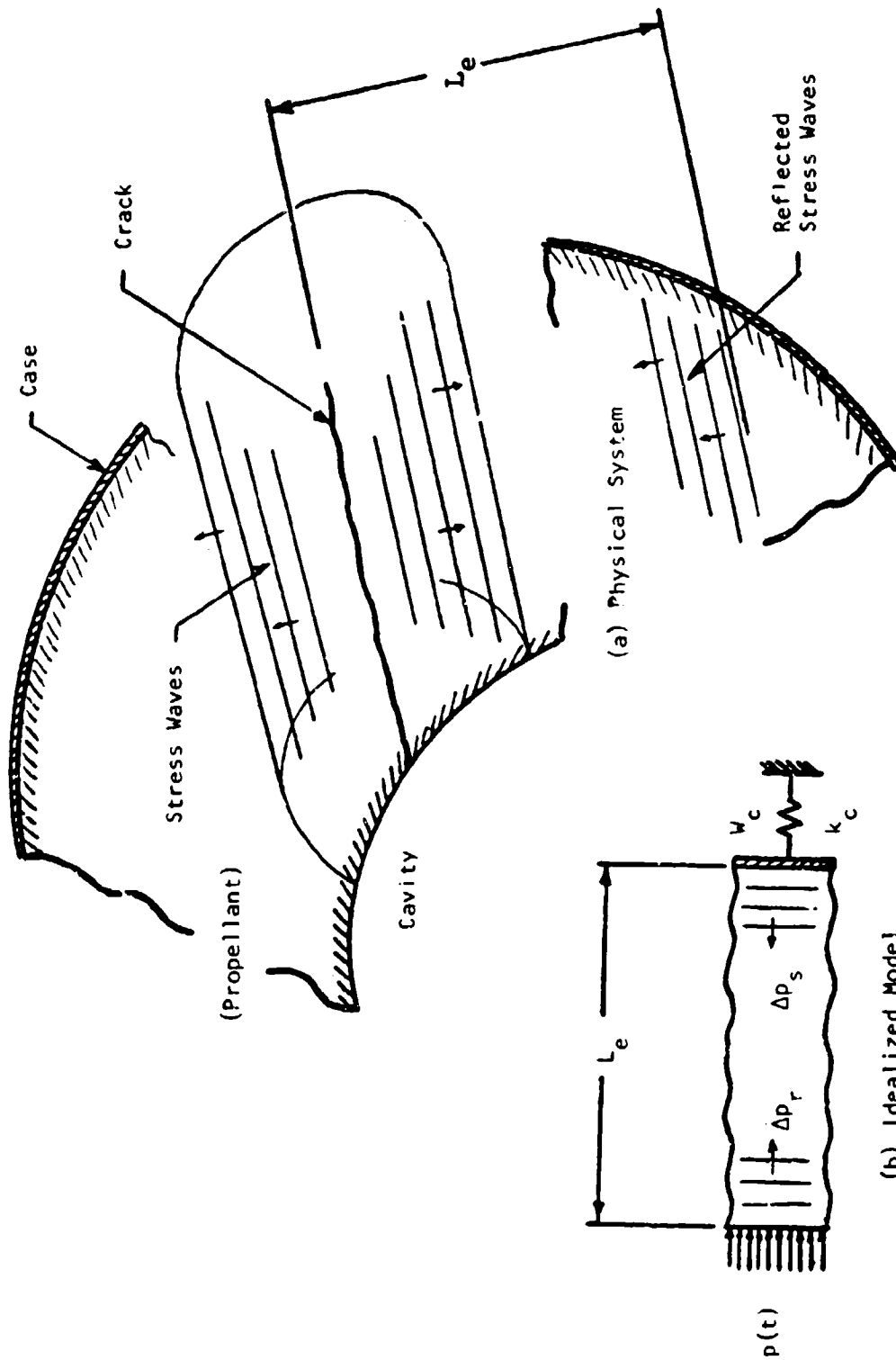


Figure E-6. Influence of remote boundaries on mechanical response.

**APPENDIX F**  
**NOMENCLATURE AND HMX PROPERTY DATA**

This appendix described variables used in this report as well as the values used for the properties of HMX and its reaction gases.

**1. NOMENCLATURE**

Nomenclature is presented below. In the report, bars over the parameters indicate steady-state values while the subscript 0 indicates initial values or values immediately prior to the event under consideration.

- a            rate of steady burning at ambient pressure, cm/sec.
- A            area of flow channel, cm (see Appendix E for description of units).
- $A_d$         bearing area between piston and chamber, cm<sup>2</sup>.
- $A_p$         area of piston face, cm<sup>2</sup>.
- B            constant used to evaluate erosive heating.
- c            sound speed, cm/msec.
- $c_d$         dilatation wave speed, cm/msec.
- $c_s$         shear wave speed, cm/msec.
- C            constant given by  $2 \sqrt{K\rho C_p}$ , cm<sup>2</sup> °K (sec)<sup>0.5</sup>/cal.
- $C_g$         specific heat of gases evolved by propellant at constant pressure, cal/g-°K.
- $C_m$         specific heat of molten propellant, cal/g-°K.
- $C_p$         specific heat of solid propellant, cal/g-°K.
- $C_w$         crack width, cm.
- $c_1, c_2$     constants used to describe heat-transfer coefficient  $h$  where  $h = c_1 [Z \exp(-E/T_f)]^{c_2}$
- d            drag coefficient
- $D_p$         piston travel needed to close vent holes, cm.
- $\ell$          internal energy of combustion gases, cal/g.
- E            activation energy of propellant divided by gas constant, °K.
- $E^1$         Young's modulus, psi.
- f            rates of crack area to that of planar surface, dimensionless.
- F            conventional pipe friction coefficient.
- g            acceleration of gravity.

IIT RESEARCH INSTITUTE

$h$	heat-transfer coefficient, cal/cm <sup>2</sup> -sec-°K.
$h_c$	convective heat-transfer coefficient, cal/cm <sup>2</sup> -sec-°K.
$i$	subscript indicating value.
$I$	mechanical impedance of solid propellant, equals $I_0 + 0.002P$ , bars-sec/cm.
$I_0$	see $I$ .
$j$	subscript indicating value of parameter during time step $t_j$ .
$K$	thermal conductivity of solid propellant, cal/cm-sec-°K.
$L$	indepth crack distance, cm.
$m$	mass, g.
$M_d$	mass of driver, lbs.
$M_f$	mass of unit area of foam layer, g/cm <sup>2</sup> .
$M_g$	mass of combustion gases.
$M_p$	mass of piston assembly, lbs.
$M_w$	molecular weight of reaction gases, g/mole.
$n$	exponent of pressure $P$ used to describe steady burning rate $\bar{r}_f$ .
$P$	pressure, bars or k bars.
$P_{max}$	maximum value of $P$ achieved, k bars.
$P_r$	Prandth number, dimensionless.
$\Delta P$	amplitude of incident stress wave, bars.
$q$	heat flux entering solid propellant, cal/cm <sup>2</sup> -sec.
$q_f$	rate of heating of unit area of foam, cal/cm <sup>2</sup> -sec.
$q_j^1$	heat flux applied at depth $x_j^1$ during time step $\Delta t_j$ , cal/cm <sup>2</sup> -sec.
$q_p$	heat flux from foam to melt interface, cal/cm <sup>2</sup> -sec.
$q_{t,j}$	mean conductive heat flux $q_j$ , cal/cm <sup>2</sup> -sec.
$Q_f$	sensible heat per unit mass of foam, cal/g.
$Q_m$	latent heat of fusion of propellant, cal/g.
$Q_r$	reaction heat of propellant, cal/g.
$Q_s$	heat generated within foam per unit mass of evolved propellant gas, cal/g.
$r$	rate of melting of propellant, cm/sec.
$r_f$	rate of propellant burning, cm/sec.
$R$	gas constant, cm/°K.
$t$	time, sec.
$\Delta t_j$	$j$ th time step, sec.

IIT RESEARCH INSTITUTE

$u$	gas velocity, cm/msec.
$v$	shock velocity, cm/msec.
$T_f$	temperature of foam or propellant surface, °K.
$T_g$	temperature of combustion gas, °K.
$T_m$	melt temperature of propellant, °K.
$T_o$	initial temperature of propellant, °K.
$V_d$	velocity of driver, cm/sec.
$V_p$	velocity of piston, cm/sec.
$\dot{W}_1$	velocity of crack wall exposed to incident stress wave, cm/sec.
$\dot{W}_2$	velocity of crash wall not exposed to incident stress wave, cm/sec.
$x$	distance, cm.
$x_j$	depth of melt interface at end of time step $\Delta t_j$ , cm.
$x_j^1$	depth at which flux $q_j^1$ is applied during time step $\Delta t_j$ , cm.
$Z$	frequency factor associated with propellant, 1/sec.
$\alpha$	thermal diffusivity of propellant, cm <sup>2</sup> /sec.
$\beta$	dimensionless term used to determine time steps used to calculate propellant temperature.
$\gamma$	ratio of specific heats of combustion gases, dimensionless.
$\mu$	particle velocity of gas, cm/msec.
$\xi$	factor used to determine depths $x_j^1$ at which fluxes $q_j^1$ are applied, dimensionless.
$\rho$	density of solid propellant, g/cm <sup>3</sup> .
$\rho_q$	density of combustion gases, g/cm <sup>3</sup> .
$\tau$	Poisson's ratio.

## 2. HMX PROPERTY DATA

Properties for HMX propellant and evolved gases are presented in Table F-1.

TABLE F-1. PROPERTIES OF HMX PROPELLANT AND GASES

Parameter	Value	Source
Constants a, n of Equation (2)	a = 0.030 cm/sec n = 0.86 (dimensionless)	Reference 7 Reference 7
Constants c <sub>1</sub> , c <sub>2</sub> of Equation (9)	c <sub>1</sub> = 7.6 · 10 <sup>5</sup> cal/cm <sup>2</sup> -sec-°K	See Appendix B
C <sub>g</sub>	c <sub>2</sub> = 0.338 (dimensionless) 0.5 cal/g-°K	See Appendix B Assumed
C <sub>p</sub>	0.4 cal/g-°K	Reference 1
C <sub>m</sub>	0.5 cal/g-°K	Reference 1
f	1.5 (dimensionless)	Assumed
E	27,000°K	Reference 13
K	0.0013 cal/cm-sec-°K	Assumed
Q <sub>m</sub>	50 cal/g	Reference 1
Q <sub>r</sub>	3517 cm/°K	Assumed
R	3517 cm/°K	Assumed
T <sub>m</sub>	555°K	Reference 1
Z	0.5 10 <sup>20</sup> /sec	Reference 13
ρ	1.9 g/cm	Reference 7
γ	1.2	Assumed

## REFERENCES

1. Takata, A.N., W. Wulff, et al., *Study of the Behavior of Systems Containing High Explosives when Subject to Fire (U)*, DASA Report 1833, July, 1966.
2. Takata, A.N., *Vulnerability of Nuclear Weapons Systems to Fire---Studies of Burning Explosives*, DASA Report 1417, December 1963.
3. Kuo, K.K., A.T. Chen, and T.R. Davis, *Transient Flame Spreading and Combustion Processes Inside a Solid Propellant Crack*, The Pennsylvania State University, University Park, Pennsylvania, 1977.
4. Krier, H., J.S. Tien, W.A. Siregnamo, and M. Summerfeld, *Nonsteady Burning Phenomena of Solid Propellants: Theory and Experiments*, AIAA J 6 (2), February, 1968.
5. King, M.K., *A Modification of the Composite Propellant Burning Model of Lenoir and Robillard*, *Combustion and Flame* 24, pp 365-368, 1975.
6. de Longuville, Y., C. Fanguignon, H. Mowlard, *Initiation of Several Condensed Explosives by a Given Duration Shock Wave*, Sixth Symposium (International) on Detonation, pp 16-24.
7. Beckstead, M.W., R.L. Derr, and C.F. Price, *The Combustion of Solid Monopropellants and Composite Propellants*, 13th Symposium (International) on Combustion, pp 1047-1056, 1971.
8. Takata, A.N., and A. Widemann, *Initiation Mechanisms of Solid Rocket Propellant Detonation*, 14th JANNAF Combustion Meeting, Chemical Propulsion Information Agency Publication, 292, December, 1977.
9. Carslaw, H.S., and J.C. Jaeger, *Conduction of Heat in Solids*, Oxford Press, 2nd ed., 1959.
10. Kooker, D.E., and C.W. Nelson, *Numerical Solution of Three Solid Propellant Combustion Models during Gas Pressure Transient*, 12th JANNAF Combustion Meeting, CPIA Publication, 273, pp 173-198, December, 1975.
11. Boggs, T.L., C.F. Price, D.E. Zurn, R.L. Derr, and E.J. Dibble, *The Self-Deflagration of Cyclotetramethylenedinitramine (HMX)*, AIAA/SAE 13th Propulsion Conference, July 1977.
12. Nelson, C.W., *On Calculating Ignition of a Propellant Bed*, Memorandum Report ARBAL-MR-02864, U.S. Army Research and Development Command, Ballistic Research Laboratory, September, 1978.

REFERENCES, continued

13. Tomlinson, W.R., Jr., *Properties of Explosives of Military*, Picatinny Arsenal, Technical Report 1740, April 1958.
14. Takata, A.N., and A.H. Wiedermann, *Initiation Mechanisms of Solid Rocket Propellant Detonation*, First Interim Report for AFOSR, August 1976.